

**HIGH TEMPERATURE OXIDATION BEHAVIOR OF Mo-Si-B BASE ALLOYS**

by

David Andrew Helmick

BS, University of Pittsburgh, 1997

MEng, Rensselaer Polytechnic Institute, 1999

Submitted to the Graduate Faculty of  
the School of Engineering in partial fulfillment  
of the requirements for the degree of  
Doctor of Philosophy

University of Pittsburgh

2003

UNIVERSITY OF PITTSBURGH

SCHOOL OF ENGINEERING

This dissertation was presented

by

David Andrew Helmick

It was defended on

July 29, 2003

and approved by

Michael R. Lovell, Associate Professor, Mechanical Engineering

Ian Nettleship, Associate Professor, Materials Science and Engineering

Jörg M. K. Wiezorek, Assistant Professor, Materials Science and Engineering

Gerald H. Meier, Professor, Materials Science and Engineering  
Dissertation Director

Frederick S. Pettit, Professor, Materials Science and Engineering  
Dissertation Director

## ABSTRACT

### HIGH TEMPERATURE OXIDATION BEHAVIOR OF Mo-Si-B BASE ALLOYS

David Andrew Helmick, PhD

University of Pittsburgh, 2003

Molybdenum base alloys with the addition of small amounts of silicon (2 – 4.5 wt%) and boron (~1 wt%) can form a passivating layer protecting the alloy from further rapid oxidation. When such molybdenum base alloys are exposed to oxidizing environments at high temperatures, a borosilicate glass layer can form that will reduce the transport of oxygen to the alloy for further oxidation. Oxidation is then controlled by the diffusion through the borosilicate glass layer. The focus of this research was to study the mechanisms, thermodynamics and kinetics of Mo-Si-B base alloy high temperature oxidation. The base alloy has a composition of Mo-3Si-1B (wt%) and was studied in a variety of gas environments as well as a range of temperatures in order to elucidate the critical factors that allow it to develop a protective borosilicate glass layer. The borosilicate glass layer is protective when no continuous channels exist in the layer extending from the gas interface to the alloy interface. The borosilicate layer that develops is believed to contain channels at early stages and the elimination of the channels is obtained by appropriate control of the temperature and gas flow conditions whereby  $\text{MoO}_3$  is removed via vaporization while the borosilicate viscosity is not increased due to loss of  $\text{B}_2\text{O}_3$ . Once the borosilicate layer is continuous and free of channels, subsequent oxidation occurs by inward diffusion of oxygen and the outward diffusion of molybdenum through this layer with

vaporization of  $\text{MoO}_3$  occurring at the gas borosilicate layer interface and the formation of  $\text{MoO}_2$  and additional borosilicate occurring at the alloy  $\text{MoO}_2$  interface.

## **ACKNOWLEDGMENTS**

First and foremost, I would like to thank my advisors, Dr. F. S. Pettit and Dr. G. H. Meier for their unwavering support and guidance in this research. The invaluable suggestions provided by the committed members are also gratefully acknowledged.

I would like to thank all my High Temperature Oxidation colleagues for their encouragement throughout my stay at the University of Pittsburgh. Thanks are also due to the faculty and staff of the Materials Science and Engineering Department for their constant support. A special thanks goes to Earle Hewitt for his technical expertise and friendship. He will be sorely missed by the university and by me.

The financial support provided by Pratt & Whiney is gratefully acknowledged.

I would like to thank my parents and all my family members for believing in me and constantly supporting me in this challenging endeavor. Finally, I would like to thank my wife, Crystal, for her love and patience and being with me through the most critical stages of this research.

## TABLE OF CONTENTS

1.0 INTRODUCTION .....	1
2.0 BACKGROUND .....	3
2.1 Oxidation of Metals .....	3
2.1.1 Parabolic Rate Law .....	3
2.1.2 Linear Rate Law.....	4
2.1.3 Combined Parabolic and Linear Rate Laws for Volatile Oxides.....	5
2.2 Molybdenum .....	5
2.3 Oxidation of Molybdenum.....	6
2.4 Oxidation of Silicon.....	9
2.5 Oxidation of Boron .....	10
2.6 Oxidation of MoSi <sub>2</sub> .....	12
2.7 Oxidation of Mo <sub>5</sub> Si <sub>3</sub> Base Alloys .....	13
2.8 Borosilicate Glass Properties .....	14
2.9 Mo-Si-B Oxidation .....	15
3.0 RESEARCH OBJECTIVES .....	16
4.0 EXPERIMENTAL APPROACH.....	17
4.1 Molybdenum Base Alloy .....	17
4.2 Experimental Techniques.....	18
4.2.1 Scanning Electron Microscopy Techniques.....	19
4.2.2 Thermogravimetric Analysis .....	21

4.2.3 Cold Finger Technique .....	21
4.2.4 Sample Preparation .....	22
5.0 RESULTS AND DISCUSSION .....	24
5.1 Relevant Phase Diagrams and Thermodynamic Data.....	25
5.2 Development of the Borosilicate Layer on Mo-3Si-1B.....	26
5.3 Transport Processes in Continuous Borosilicate Layers on Mo-3Si-1B .....	32
5.4 The Effect of Temperature.....	36
5.5 The Effect of Gas Composition and Gas Flow Rate.....	37
5.6 The Effect of Alloy Composition .....	47
6.0 CONCLUDING REMARKS.....	50
BIBLIOGRAPHY.....	143

## LIST OF TABLES

Table 1: Tabulation of selected properties of molybdenum at room temperature. ....	52
Table 2: Comparison of the effects of temperature and gas environment on the development of a protective borosilicate layer (C), or a borosilicate layer containing channels (X). ....	53

## LIST OF FIGURES

Figure 2.3.1: Volatile species diagram for molybdenum at 1100K.....	54
Figure 2.3.2: Volatile species diagram for molybdenum at 1350K ( $p_{\text{H}_2\text{O}} = 0.1\text{atm}$ ).....	54
Figure 2.4.1: Volatile species diagram for silicon at 1350K ( $p_{\text{H}_2\text{O}} = 0.1\text{atm}$ ). .....	55
Figure 2.5.1: Volatile species diagram for boron at 1100K.....	56
Figure 2.5.2: Volatile species diagram for boron at 1350K ( $p_{\text{H}_2\text{O}} = 0.1\text{atm}$ ).....	56
Figure 2.8.1: Borosilicate glass viscosity as a function of composition at $\sim 1760^\circ\text{C}$ .....	57
Figure 2.8.2: Borosilicate glass (25 mol% $\text{B}_2\text{O}_3$ ) viscosity as a function of temperature <sup>51</sup> . .....	58
Figure 4.1: Micrograph showing the three phases in Mo-3Si-1B.....	59
Figure 4.2: Molybdenum rich corner of the Mo-Si-B isothermal ternary phase diagram at $1600^\circ\text{C}$ with Mo-3Si-1B composition identified.....	59
Figure 5.1.1: $\text{SiO}_2\text{-B}_2\text{O}_3$ phase diagram.....	61
Figure 5.1.2: Mo-O phase diagram (the sequence of phases should be $\text{Mo}_9\text{O}_{24}$ , $\text{Mo}_4\text{O}_{11}$ , $\text{Mo}_8\text{O}_{23}$ , $\text{MoO}_3$ rather than as indicated in this diagram). .....	61
Figure 5.2.1: Weight change versus time data for the oxidation of Mo-3Si-1B exposed in static laboratory air at the temperature indicated (continuous borosilicate layer free from channels). .....	62
Figure 5.2.2: Weight change versus time data for the oxidation of Mo-3Si-1B exposed at $1100^\circ\text{C}$ in dry air flowing at 10cm/sec (borosilicate layer containing unsealed channels). .	62
Figure 5.2.3: Backscattered electron micrograph showing the surface of the borosilicate layer on Mo-3Si-1B after five hours exposure at $816^\circ\text{C}$ in static laboratory air. ....	63
Figure 5.2.4: Backscattered electron micrograph showing the cross-sectional view of the specimen described in Figure 5.2.3. The borosilicate layer is continuous and a layer of $\text{MoO}_2$ is evident on the alloy beneath the borosilicate layer. ....	63

- Figure 5.2.5: Surface micrograph and cross-section of Mo-3Si-1B alloy exposed at 1100°C in dry air flowing at 10cm/sec for one hour. Channels exist within the borosilicate layer..... 64
- Figure 5.2.6: Backscattered electron micrograph showing the cross-section of Mo-3Si-1B specimen exposed at 816°C in dry air flowing at 1cm/sec for one hour. Channels in the borosilicate are evident and the walls of these channels contain balls of liquid MoO<sub>3</sub>..... 65
- Figure 5.2.7: Backscattered electron micrographs that show the borosilicate layer development on Mo-3Si-1B as a function of time after exposure at 1000°C in static laboratory air. .... 66
- Figure 5.2.8: Backscattered electron micrographs showing the cross-sectional views of Mo-3Si-1B exposed at 1000°C in static laboratory air as a function of exposure time. These specimens were plated with nickel prior to metallographic preparation. .... 67
- Figure 5.2.9: Backscattered electron micrographs that show characteristics of the borosilicate layer formed on Mo-3Si-1B. In (a), channels exist in the borosilicate layer and the attack of the alloy is more extensive in the vicinity of these channels. In (b), all of the channels have sealed but the borosilicate layer is thicker in those areas where the channels had caused more extensive attack..... 68
- Figure 5.2.10: Mo-3Si-1B exposed at 816°C in dry air flowing at 1cm/sec. Open channels are evident at the trailing edge of the specimen whereas the channels are sealed near the center of the specimen. (Ref. Shiela Woodard)..... 69
- Figure 5.2.11: Cross-sectional views of the specimen described in Figure 5.2.10. (a) buckle in the borosilicate layer near the center of the specimen. (b) a section near the leading edge of the specimen showing spherical pores. (c) a cross-section near the trailing edge showing unsealed channels, spherical pores, and balls of MoO<sub>3</sub>. .... 71
- Figure 5.2.12: Weight change versus time data for the oxidation of Mo-3Si-1B exposed at 1000°C in argon flowing at 10cm/sec..... 72
- Figure 5.2.13: Backscattered electron micrographs of Mo-3Si-1B exposed at 1000°C in argon flowing at 10cm/sec for (a) 2 hours and (b) 18 hours. .... 73
- Figure 5.2.14: Weight change versus time data for Mo-3Si-1B exposed at 1000°C in dry air flowing at 1cm/sec for one hour followed by an exposure at 700°C in dry air flowing at 1cm/sec for an additional 20 hours with the specimen remaining in situ. .... 74
- Figure 5.2.15: Surface photographs of Mo-3Si-1B exposed at (a) 1000°C in dry air flowing at 1cm/sec for one hour (pretreatment) and (b) 1000°C in dry air flowing at 1cm/sec for one hour (pretreatment) followed by an exposure at 700°C in dry air flowing at 1cm/sec for 20 hours with the specimen in situ..... 75
- Figure 5.2.16: Backscattered electron micrographs of Mo-3Si-1B exposed at (a) 1000°C in dry air flowing at 1cm/sec for one hour (pretreatment) and (b) 1000°C in dry air flowing at

1cm/sec for one hour (pretreatment) followed by an exposure at 700°C in dry air flowing at 1cm/sec for 20 hours with the specimen in situ.....	76
Figure 5.2.17: Backscattered electron micrograph of the borosilicate layer on Mo-3Si-1B exposed at (a) 1000°C in dry air flowing at 1cm/sec for 20 hours and (b) 1000°C in dry air flowing at 1cm/sec for one hour (pretreatment) followed by an exposure at 700°C in dry air flowing at 1cm/sec for 20 hours with the specimen in situ.....	77
Figure 5.2.18: Sketches illustrating schematically the development of the borosilicate layer on the three phases in the Mo-3Si-1B upon exposure to air at temperatures of 816°C and higher .....	78
Figure 5.2.19: Backscattered electron micrograph showing the Mo-3Si-1B alloy after seven days in static laboratory air at 1000°C. Particles of alloy covered with MoO <sub>2</sub> are evident in the borosilicate and borosilicate can be seen to have developed beneath the layer of MoO <sub>2</sub> .....	79
Figure 5.3.1: Backscattered electron cross-sectional micrograph taken through a channel in a layer of the borosilicate. Spheres of MoO <sub>3</sub> can be seen on the walls of the channel. In the borosilicate adjacent to the channel, only MoO <sub>2</sub> on particles of the alloy are evident. ....	80
Figure 5.3.2: Schematic diagram to show a possible mechanism for transport through the borosilicate layer on Mo-3Si-1B along with formation of MoO <sub>2</sub> and vaporization of MoO <sub>3</sub> and B <sub>2</sub> O <sub>3</sub> .....	81
Figure 5.3.3: Schematic showing the variation of the activity of molybdenum, and the activity of oxygen across a borosilicate layer on Mo-3Si-1B assuming that the activity of MoO <sub>2</sub> throughout the borosilicate layer is constant. ....	82
Figure 5.3.4: Backscattered electron micrograph of the surface of a borosilicate layer formed upon Mo-3Si-1B after one hour in dry flowing air (10cm/sec) at 1100°C. Spheres of MoO <sub>3</sub> are present in the borosilicate just beneath the borosilicate-gas interface. ....	83
Figure 5.3.5: Mo-3Si-1B pretreated at 1000°C in dry air flowing at 1cm/sec for one hour followed by additional exposures under the same conditions, along with the weight of the MoO <sub>3</sub> deposition and the calculated Mo weight associated with additional exposures. ....	84
Figure 5.4.1: Weight change versus the square root of time data for the oxidation of Mo-3Si-1B exposed at 700°C in dry air flowing at 1cm/sec and oxygen flowing at 10cm/sec. The results show that these data conform to a parabolic rate law and weight gains rather than weight losses are observed.....	85
Figure 5.4.2: Weight change versus time data for the oxidation of Mo-3Si-1B exposed at 700°C in dry air flowing at 1cm/sec. For these long oxidation times, weight losses eventually occur.....	86

Figure 5.4.3: Optical macrograph of Mo-3Si-1B specimen after 160 hours of oxidation where the weight change versus time data are presented in Figure 5.4.2.....	87
Figure 5.4.4: Backscattered electron micrograph of the oxide scale formed on Mo-3Si-1B after exposure at 700°C for one hour in dry air flowing at 1cm/sec. Calculation of the thickness of the oxide using the weight change data in Figure 5.4.1 gives an oxide thickness of 16.5µm whereas the actual thickness is 42µm. There must have been a weight loss of 3.83mg/cm <sup>2</sup> .....	88
Figure 5.5.1: Weight change versus time data for the oxidation of two specimens of Mo-3Si-1B exposed to identical conditions (816°C in dry air flowing at 10cm/sec).....	89
Figure 5.5.2: Weight change versus time data for the oxidation of two specimens of Mo-3Si-1B exposed to identical conditions (816°C in dry air flowing at 1cm/sec).....	90
Figure 5.5.3: Comparison of weight change versus time data for the oxidation of forged and cast specimens exposed to identical conditions (816°C in dry air flowing at 10cm/sec). .....	91
Figure 5.5.4: Comparison of weight change versus time data for the oxidation of forged and cast specimens exposed to identical conditions (1100°C in dry air flowing at 1cm/sec). .....	92
Figure 5.5.5: Weight change versus time data for the oxidation of Mo-3Si-1B exposed at 816°C in static laboratory air. ....	93
Figure 5.5.6: Backscattered electron micrographs of the surface and cross-section of Mo-3Si-1B exposed at 816°C in static laboratory air for 5 hours.....	94
Figure 5.5.7: Weight change versus time data for the oxidation of Mo-3Si-1B exposed at 816°C in static dry air. ....	95
Figure 5.5.8: (a) Optical and (b) backscattered electron micrographs of Mo-3Si-1B exposed at 816°C in static dry air for 1 hour. ....	97
Figure 5.5.9: Backscattered electron micrograph of the surface of Mo-3Si-1B exposed at 816°C in static dry air for 5 hours.....	98
Figure 5.5.10: Backscattered electron micrographs of the surface and cross-section of Mo-3Si-1B exposed at 816°C in static oxygen for 1 hour. ....	99
Figure 5.5.11: Weight change versus time data for the oxidation of Mo-3Si-1B exposed at 816°C in dry air flowing at 1cm/sec. ....	100
Figure 5.5.12: Optical macrographs of Mo-3Si-1B exposed at 816°C in dry air flowing at 1cm/sec for 20 hours. ....	101

Figure 5.5.13: Backscattered electron micrographs of the cross-section of Mo-3Si-1B exposed at 816°C in slowly flowing dry air for 20 hours. ....	102
Figure 5.5.14: Weight change versus time data for the oxidation of Mo-3Si-1B exposed at 816°C in air + 0.1atm of H <sub>2</sub> O flowing at 1cm/sec. ....	103
Figure 5.5.15: Optical macrograph of Mo-3Si-1B exposed at 816°C in air + 0.1atm of H <sub>2</sub> O flowing at 1cm/sec for 1 hour. ....	104
Figure 5.5.16: Backscattered electron micrographs of Mo-3Si-1B exposed at 816°C in air + 0.1atm H <sub>2</sub> O flowing at 1cm/sec for 3 hours.....	105
Figure 5.5.17: Weight change versus time data for the oxidation of Mo-3Si-1B exposed at 816°C in dry air flowing at 10cm/sec.....	106
Figure 5.5.18: Optical macrographs of Mo-3Si-1B exposed at 816°C in dry air flowing at 10cm/sec. ....	107
Figure 5.5.19: Optical macrographs of Mo-3Si-1B exposed at 816°C in dry air flowing at 10cm/sec for 20 hours. ....	108
Figure 5.5.20: Backscattered electron micrographs of Mo-3Si-1B exposed at 816°C in dry air flowing at 10cm/sec for 20 hours.....	109
Figure 5.5.21: Weight change versus time for the oxidation of Mo-3Si-1B exposed at 900°C in dry air flowing at 1cm/sec.....	110
Figure 5.5.22: Backscattered electron micrograph of the cross-section of Mo-3Si-1B exposed at 900°C in dry air flowing at 1cm/sec for 1 hour. ....	111
Figure 5.5.23: Weight change versus time for the oxidation of Mo-3Si-1B exposed at 1000°C in static laboratory air. ....	112
Figure 5.5.24: Backscattered electron micrograph of Mo-3Si-1B exposed at 1000°C in static laboratory air for 110 minutes.....	113
Figure 5.5.25: Change of weight versus time for the oxidation of Mo-3Si-1B exposed at 1000°C in dry air flowing at 1cm/sec. ....	114
Figure 5.5.26: Backscattered electron micrograph of the cross-section of Mo-3Si-1B exposed at 1000°C in dry air flowing at 1cm/sec for (a) 2 minutes and (b) 10 minutes. ....	115
Figure 5.5.27: Backscattered electron micrograph of the cross-section of Mo-3Si-1B exposed at 1000°C in dry air flowing at 1cm/sec for (a) 20 minutes, (b) 30 minutes, (c) 1 hour, and (d) 20 hours.....	117

Figure 5.5.28: Backscattered electron micrographs of internal oxidation in Mo-3Si-1B exposed at 1000°C in dry air flowing at 1cm/sec for 20 minutes. ....	118
Figure 5.5.29: Weight change versus time for the oxidation of Mo-3Si-1B exposed at 1000°C in dry air flowing at 10cm/sec.....	119
Figure 5.5.30: Backscattered electron micrographs of Mo-3Si-1B exposed at 1000°C in dry air flowing at 10cm/sec. ....	120
Figure 5.5.31: Weight change versus time for the oxidation of Mo-3Si-1B exposed at 1000°C in oxygen flowing at 10cm/sec. ....	121
Figure 5.5.32: Backscattered micrograph of the cross-section of Mo-3Si-1B exposed at 1000°C in oxygen flowing at 10cm/sec for one hour.....	122
Figure 5.5.33: Weight change versus time for the oxidation of Mo-3Si-1B exposed at 1100°C in static laboratory air. ....	123
Figure 5.5.34: Backscattered electron micrograph of Mo-3Si-1B exposed at 1100°C in static laboratory air for 100 hours. ....	124
Figure 5.5.35: Weight change versus time for the oxidation of Mo-3Si-1B exposed at 1100°C in static dry air.....	125
Figure 5.5.36: Backscattered electron micrographs of Mo-3Si-1B exposed at 1100°C in static dry air for 3 hours. ....	126
Figure 5.5.37: Weight change versus time for the oxidation of Mo-3Si-1B exposed at 1100°C in dry air flowing at 1cm/sec.....	127
Figure 5.5.38: Backscattered electron micrograph of Mo-3Si-1B exposed at 1100°C in dry air flowing at 1cm/sec for 20 hours.....	128
Figure 5.5.39: Weight change versus time for the oxidation of Mo-3Si-1B exposed at 1100°C in air + 0.1atm H <sub>2</sub> O flowing at 1cm/sec.....	129
Figure 5.5.40: Backscattered electron micrographs of Mo-3Si-1B exposed at 1100°C in air + 0.1atm H <sub>2</sub> O flowing at 1cm/sec for 4 hours.....	130
Figure 5.5.41: Weight change versus time for the oxidation of Mo-3Si-1B exposed at 1100°C in dry air flowing at 10cm/sec.....	131
Figure 5.5.42: Backscattered electron micrographs of Mo-3Si-1B exposed at 1100°C in dry air flowing at 10cm/sec for one hour. ....	132

Figure 5.5.43: Weight change versus time data for the oxidation of Mo-3Si-1B exposed at 1100°C in oxygen flowing at 10cm/sec.....	133
Figure 5.6.1: Backscattered electron micrograph of as-processed Mo-3Si-1B. ....	134
Figure 5.6.2: Backscattered electron micrograph of as-processed Mo-5Si-1B. ....	134
Figure 5.6.3: Backscattered electron micrograph of as-processed Mo-7Si-1B. ....	135
Figure 5.6.4: Backscattered electron micrograph of as-processed Mo-8.2Si-1B. ....	135
Figure 5.6.5: Backscattered electron micrograph of as-processed Mo-7.4Si-2B. ....	136
Figure 5.6.6: Backscattered electron micrograph of as-processed Mo-3Si-1B-6Ti. ....	136
Figure 5.6.7: Backscattered electron micrograph of as-processed Mo-3Si-6Ti. ....	137
Figure 5.6.8: Backscattered electron micrograph of as-processed Mo-3Si-1B-0.3Hf.....	137
Figure 5.6.9: Backscattered electron micrograph of as-processed Mo-3Si-1B-1Hf.....	138
Figure 5.6.10: Weight change versus time data for the oxidation of alloys exposed at 816°C in dry air flowing at 1cm/sec.....	139
Figure 5.6.11: Weight change versus time data for the oxidation of alloys exposed at 816°C in dry air flowing at 1cm/sec.....	140
Figure 5.6.12: Weight change versus time data for the oxidation of alloys exposed at 816°C in dry air flowing at 1cm/sec.....	141
Figure 5.6.13: Weight change versus time data for the oxidation of alloys exposed at 816°C in dry air flowing at 1cm/sec.....	142

## 1.0 INTRODUCTION

Superalloys are the current choice of manufacturers for high temperature applications such as turbine engines. These alloys have high strength and oxidation resistance at elevated temperatures, but as technology advances the need for higher operating temperatures arises. Molybdenum base alloys are a possible system to replace superalloys in high temperature applications because of their excellent strength at high temperatures. However, the oxidation characteristics of molybdenum limit its application. At high temperatures, molybdenum oxidizes to form molybdenum trioxide, which is highly volatile. This results in porosity, shrinkage and a non-protective oxide layer that may lead to disintegration of the metal.

Other materials have been considered to replace superalloys in high temperature applications. Each has shortcomings. However in the case of molybdenum base alloys, with the addition of small amounts of silicon (2 – 4.5 wt%) and boron (~1 wt%) a passivating layer can form, protecting the alloy from further rapid oxidation. When such molybdenum base alloys are exposed to oxidizing environments at high temperatures, a borosilicate glass layer can form that will significantly reduce the transport of oxygen. Oxidation is then controlled by the diffusion through the borosilicate layer. The diffusion through the borosilicate must be slow enough to prevent catastrophic failure because, like the alloys in use today, a coating will be applied. The focus of this research was to study the mechanisms, thermodynamics and kinetics of Mo-Si-B oxidation.

Background information will be presented that will provide the necessary information to understand the high temperature oxidation mechanisms of Mo-Si-B. The research objective will then be presented followed by the experimental results. The results will then be discussed and future research will be proposed in order to fully understand the high temperature oxidation behavior of Mo-Si-B.

## **2.0 BACKGROUND**

The background information presented will include a short description of the basic oxidation mechanisms that occur during high temperature oxidation of Mo-Si-B alloys. Then the oxidation behavior of the main components of the alloy will be described followed by background information on oxidation of alloys with similar compositions to the alloy in this study. Finally, properties of the scale formed on Mo-Si-B during oxidation will be discussed.

### **2.1 Oxidation of Metals**

#### **2.1.1 Parabolic Rate Law**

The oxidation kinetics of a metal follows a parabolic rate law<sup>1</sup> when diffusion through the oxide is rate controlling. The parabolic rate law can be expressed as:

$$x \, dx = k' \, dt \tag{1}$$

where  $x$  is the oxide thickness,  $t$  is the time and  $k'$  is the parabolic rate constant. From the above equation it can be seen that the oxide thickness ( $x$ ) will be proportional to the square root of time ( $t$ ). If weight change is measured in the laboratory rather than oxide thickness (which often is the case), the change in weight will also be proportional to the square root of time.

The logarithm of the parabolic rate constant ( $k'$ ) is linearly related to the inverse of temperature. Therefore, if two or more parabolic rate constants are calculated from empirical data, other rate constants at other temperatures can be extrapolated from those data points.

### 2.1.2 Linear Rate Law

When oxidation kinetics of a metal proceeds at a constant rate they are said to follow a linear rate law<sup>1</sup>. The linear rate law can be expressed as:

$$x = k_1 t \quad (2)$$

where  $x$  is the oxide thickness,  $t$  is the time and  $k_1$  is the linear rate constant. From the above equation it can be seen that the change in oxide thickness with time ( $dx/dt$ ) will be a constant. If weight change is measured in the laboratory rather than oxide thickness, the change in weight with time will also be linear.

A linear rate law can also be followed for vaporization. In the case of vaporization of the oxide scale, where vaporization is continually rapid enough to eliminate the oxide layer before it becomes a diffusion barrier, the metal surface recession will be linearly related to time rather than oxide thickness (as well as the mass change).

### 2.1.3 Combined Parabolic and Linear Rate Laws for Volatile Oxides

In the case of a volatile oxide, the oxidation reaction may follow the parabolic rate law discussed earlier but the vaporization of the oxide will follow a linear rate<sup>1</sup>. In this case the change in oxide thickness can be expressed as:

$$\frac{dx}{dt} = \frac{k'}{x} - k_l \quad (3)$$

where  $x$  is the oxide thickness,  $t$  is the time,  $k'$  is the parabolic rate constant for oxidation and  $k_l$  is the linear rate constant for the vaporization of the oxide. From the above equation it can be seen that a steady state constant oxide thickness will develop when the parabolic oxide growth rate equals the linear oxide recession from vaporization (i.e.  $dx/dt = 0$ ). When the oxide reaches its steady state thickness, the metal recession rate will be linear and the weight loss will be linear.

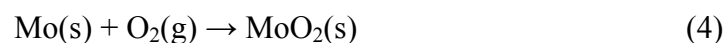
## 2.2 Molybdenum

Molybdenum has a body-centered cubic (bcc) crystal structure and displays the ductile-to-brittle transition behavior typical of such metals<sup>2</sup>. It combines a high melting point (2623°C) with strength retention at high temperatures. Molybdenum also has a high elastic modulus, which makes it attractive for applications that require both high stiffness and low weight. It also has high thermal conductivity, low coefficient of thermal expansion, and low specific heat providing resistance to thermal shock and fatigue. Table 1 is a tabulation of selected properties of molybdenum at room temperature.

## 2.3 Oxidation of Molybdenum

The end product of oxidation of molybdenum at high temperatures and relatively high oxygen partial pressures is well known to be  $\text{MoO}_3$ , which has a melting temperature of  $794^\circ\text{C}$  and is decidedly volatile at temperatures as low as  $700^\circ\text{C}$ <sup>3</sup>. The kinetics of oxidation of a metal that forms a volatile oxide is usually described using a parabolic relationship (Equation 3) between weight change and time. One such metal is chromium<sup>1</sup>. In the case of chromium oxidation, chromium oxide is formed with parabolic kinetics while it vaporizes with linear kinetics. A steady state oxide thickness is formed while the metal recesses in a linear fashion. Molybdenum oxide is volatile, similar to chromium oxide, but at high temperatures (i.e. above  $\sim 800^\circ\text{C}$ ) the oxide vaporizes as soon as it is formed<sup>3</sup> because of its high vapor pressure. Therefore, a steady state oxide thickness is never formed. As a result of this rapid volatilization, other factors, aside from the obvious temperature and oxygen partial pressure effects, heavily contribute to the oxidation kinetics of molybdenum at high temperatures.

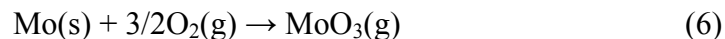
Figure 2.3.1 shows a volatile species diagram for molybdenum at 1100K ( $827^\circ\text{C}$ ). The diagram shows how the vapor pressure of  $\text{MoO}_3$  varies with oxygen pressure as well as the oxygen pressure required to oxidize Mo to  $\text{MoO}_2$  using the following reaction<sup>4</sup>:



and the oxygen pressure required to further oxidize  $\text{MoO}_2$  to  $\text{MoO}_3$  using the following reaction<sup>4</sup>:



The reaction used to calculate the pressure of  $\text{MoO}_3(\text{g})$  over the  $\text{Mo}(\text{s})$  condensed phase is<sup>4</sup>:



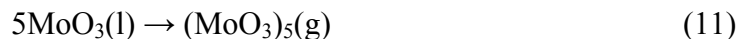
and over the  $\text{MoO}_2(\text{s})$  condensed phase is<sup>4</sup>:



and over the  $\text{MoO}_3(\text{l})$  condensed phase is<sup>4</sup>:



Figure 2.3.2 is a volatile species diagram for molybdenum at 1350K (1077°C). This diagram, once again, shows how the vapor pressure of the vapor species vary with oxygen pressure. The oxygen pressures required to oxidize  $\text{Mo}(\text{s})$  to  $\text{MoO}_2(\text{s})$  and  $\text{MoO}_2(\text{s})$  to  $\text{MoO}_3(\text{l})$  are calculated using (4) and (5), respectively. The vapor pressures of  $\text{MoO}_3(\text{g})$  over the three condensed phases are calculated using reactions (6), (7) and (8). In addition, the vapor pressure of several polymers of  $\text{MoO}_3$  and a hydrated molybdenum oxide over the condensed phase  $\text{MoO}_3(\text{l})$  were plotted on the diagram (calculated at a water vapor pressure of 0.1atm). The reactions used to calculate the vapor pressures of the three polymers of  $\text{MoO}_3$  on the diagram are as follows<sup>5-6</sup>:



and the reaction used to calculate the vapor pressure of the hydrated molybdenum oxide on the diagram is<sup>7-8</sup>:



At 1350K, the vapor species that have the highest vapor pressures are  $(\text{MoO}_3)_3$  and  $(\text{MoO}_3)_4$  both of which have vapor pressure  $\sim 0.5\text{atm}$ .

Since  $\text{MoO}_3$  vaporizes as soon as it is formed at high temperatures, an atmosphere rich in  $\text{MoO}_3(\text{g})$  is formed near the surface of the metal<sup>9,10,11,12,13,14,15,16</sup>. If the partial pressure of the  $\text{MoO}_3(\text{g})$  reaches its saturation pressure, condensed  $\text{MoO}_3$  can form on the surface. This means that the partial pressure of  $\text{MoO}_3(\text{g})$  can control the transport mechanism for oxidation. If the  $\text{MoO}_3(\text{g})$  is permitted to reach its saturation pressure then the transport mechanism will be condensed phase diffusion through the oxide layer on the surface of the metal barring any cracks and pores in the scale. On the other hand, if the partial pressure of  $\text{MoO}_3(\text{g})$  remains below the saturation pressure, the transport mechanism will be gas phase diffusion near the surface of the metal.

By controlling the partial pressure of  $\text{MoO}_3(\text{g})$  near the surface of the metal, the rate of volatilization of  $\text{MoO}_3$  from the surface will be controlled. Bartlett and Williams<sup>11</sup> controlled the partial pressure of  $\text{MoO}_3(\text{g})$  by varying the flow rate of air past the molybdenum specimen. They concluded that rapid gas flow rate increased the volatilization of  $\text{MoO}_3$ , which in turn increased the oxidation rate. Also, they suggested that there is a maximum oxidation rate for molybdenum at a given temperature at which the partial pressure of  $\text{MoO}_3(\text{g})$  is maintained at a low value near the surface of the specimen. These results suggest that the description of oxidation of molybdenum includes boundary layer flow kinetics controlling the transport mechanisms.

## 2.4 Oxidation of Silicon

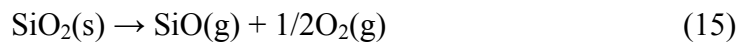
The formation of  $\text{SiO}_2$  on silicon progresses at a very slow parabolic rate indicative of a protective scale in atmospheres containing a substantial pressure of oxygen. At oxygen pressures near the dissociation pressure of  $\text{SiO}_2$  the vapor pressure of the oxide species  $\text{SiO}$  is large enough to create a substantial flux from the surface<sup>1,17,18</sup>. The flux of  $\text{SiO}(\text{g})$  subsequently oxidizes to  $\text{SiO}_2$  forming a non-protective smoke. The formation of the smoke rather than the continuous and protective  $\text{SiO}_2$  scale layer allows the continuous rapid oxidation of the substrate. Figure 2.4.1 shows the volatile species diagram for the Si-O system at 1350K (1077°C) to illustrate this point. The diagram shows how the vapor pressure of  $\text{SiO}$  varies with the oxygen pressure as well as the oxygen pressure required to oxidize  $\text{Si}(\text{s})$  to  $\text{SiO}_2(\text{s})$  using the following reaction<sup>4</sup>:



The reaction used to calculate the pressure of SiO(g) over the Si(s) condensed phase is<sup>4</sup>:



and over the SiO<sub>2</sub>(s) condensed phase is<sup>4</sup>:



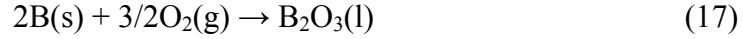
In addition, the vapor pressure of silicon hydroxide (Si(OH)<sub>4</sub>) over the condensed phase SiO<sub>2</sub> is plotted on the diagram (calculated at a water vapor pressure of 0.1atm). The reaction used to calculate the vapor pressures of silicon hydroxide is as follows<sup>19,20,21</sup>:



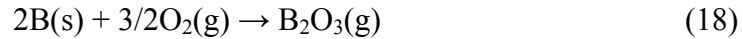
The only data available for the above reaction was obtained at 1600K.

## 2.5 Oxidation of Boron

Figure 2.5.1 shows a volatile species diagram for boron at 1100K (827°C). The diagram shows how the vapor pressure of B<sub>2</sub>O<sub>3</sub> varies with oxygen pressure as well as the oxygen pressure required to oxidize B(s) to B<sub>2</sub>O<sub>3</sub>(l) using the following reaction<sup>4</sup>:



The reaction used to calculate the vapor specie ( $\text{B}_2\text{O}_3\text{(g)}$ ) vapor pressure over the  $\text{B(s)}$  condensed phase is<sup>4</sup>:



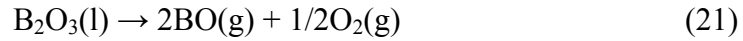
and over the  $\text{B}_2\text{O}_3\text{(l)}$  condensed phase is<sup>4</sup>:



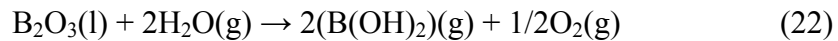
Figure 2.5.2 is a volatile species diagram for boron at 1350K (1077°C). This diagram, once again, shows how the vapor pressure of the vapor species vary with oxygen pressure. The oxygen pressures required to oxidize  $\text{B(s)}$  to  $\text{B}_2\text{O}_3\text{(l)}$  is calculated using reaction (16) and the vapor pressures of  $\text{B}_2\text{O}_3\text{(g)}$  over the two condensed phases are calculated using reactions (17) and (18). In addition, the vapor pressures of  $\text{BO}$  over both condensed phases and the vapor pressure of both dihydroxyborane ( $\text{B(OH)}_2$ ) and boric acid ( $\text{H}_3\text{BO}_3$ ) over the condensed phase  $\text{B}_2\text{O}_3$  were plotted on the diagram (calculated at a water vapor pressure of 0.1atm). The reaction used to calculate the vapor pressure of  $\text{BO}$  over the  $\text{B(s)}$  condensed phase is<sup>4</sup>:



and over the  $\text{B}_2\text{O}_3\text{(l)}$  condensed phase is<sup>4</sup>:



The reactions used to calculate the vapor pressures of dihydroxyborane and boric acid are as follows<sup>4</sup>:



respectively.

## 2.6 Oxidation of MoSi<sub>2</sub>

At room temperature, exposing MoSi<sub>2</sub> to air leads to the formation of a duplex oxide layer of SiO<sub>2</sub> + MoO<sub>3</sub><sup>22</sup>. Berztiss et. al.<sup>23</sup> and others<sup>24</sup> showed that oxidation of MoSi<sub>2</sub> is greatly influenced by the volatility of MoO<sub>3</sub>. At temperatures below 600°C<sup>25</sup>, the volatility of MoO<sub>3</sub> and the slow diffusion of silicon through the substrate prevent a continuous SiO<sub>2</sub> scale from forming. At temperatures above 1000°C, MoO<sub>3</sub> vaporizes and silicon diffusion through the substrate is rapid enough to form a continuous protective SiO<sub>2</sub> layer. At temperatures between 600 and 1000°C, cast MoSi<sub>2</sub> formed a thin oxide layer on the surface as well as internally oxidized

silicon. Small weight changes ( $\pm 1 \text{ mg/cm}^2$ ) are maintained by a near balance between the weight gain from the oxidation of silicon and the volatilization of  $\text{MoO}_3$ .

## 2.7 Oxidation of $\text{Mo}_5\text{Si}_3$ Base Alloys

Meyer et.al.<sup>26,27</sup> and Summers et.al.<sup>28</sup> described the oxidation behavior of  $\text{Mo}_5\text{Si}_3$  base materials for the temperature range of 600 – 1300°C. They observed very poor oxidation resistance for undoped  $\text{Mo}_5\text{Si}_3$ . At 750°C, molybdenum oxide begins to volatilize leaving a porous silica scale with no solid state diffusion barrier. Rapid oxidation and eventual disintegration or pesting was observed at 800°C. Large mass losses controlled by the outward diffusion of  $\text{MoO}_3(\text{g})$  were observed for the temperature range of 900 – 1200°C. The addition of small amounts of boron resulted in a protective scale being formed and parabolic oxidation rate kinetics being observed in the temperature range of 1050 – 1300°C. The oxidation rate decreased by five orders of magnitude at 1200°C with the addition of only 2 wt% boron which also eliminated the pesting at 800°C. The calculated activation energy for oxidation was 134 kJ/mol at 1050 – 1300°C, which compares well to the activation energy of oxygen diffusion in borosilicate glass<sup>26</sup>. The mechanism proposed by this group for the improvement in oxidation resistance is that the boron doping of the intermetallic improves the viscous sintering of the borosilicate glass scale. This process makes it possible for the pores, caused by the volatilization of the molybdenum oxide during the initial stages of oxidation, to be closed. A continuous layer of borosilicate glass results in an oxygen diffusion barrier and a parabolic oxidation rate.

## 2.8 Borosilicate Glass Properties

Sintering experiments conducted in the temperature range of 1000°C to 1390°C by Yan et.al.<sup>29</sup> showed that borosilicate glass sintering kinetics are consistent with the model proposed by Scherer<sup>30,31,32</sup> for the viscous flow sintering mechanism. All sintering models of glass assume that viscous flow is the mass transport mechanism. The reduction of the surface energy is balanced by the energy dissipated in viscous flow during sintering. Kinetic equations can be derived based on this energy balance concept. Scherer derived such a sintering equation with a specific consideration for a cubic array formed by intersecting glass cylinders. Experimental results from Yan et.al. showed negligible sintering at temperatures below 1000°C. For temperatures between 1000°C and 1390°C, the viscosity of SiO<sub>2</sub> glass with 6 wt% B<sub>2</sub>O<sub>3</sub> was observed to range from 9.8X10<sup>9</sup>P at 1000°C to 0.16X10<sup>9</sup>P at 1390°C following an Arrhenius relationship. Also observed was a relation showing that viscosity is not only a function of temperature but composition as well. The values observed by Yan followed the trend of decreasing activation energy with increasing boron content. This was believed to be due to a change in the glass network structure from strongly bonded SiO<sub>4</sub> tetrahedra to an increasing amount of weaker bonded cross links between boroxyl groups<sup>33</sup>. Figure 2.8.1 shows the borosilicate glass viscosity as a function of composition at a constant temperature. As B<sub>2</sub>O<sub>3</sub> content is decreased the viscosity of the borosilicate glass viscosity increases. Figure 2.8.2 shows the borosilicate glass viscosity as a function of temperature at a constant composition. The borosilicate glass viscosity decreases with increasing temperature.

## 2.9 Mo-Si-B Oxidation

Oxidation studies of Mo base alloys rich in Si and B (~10 to 19 wt% Si and ~1 to 2 wt% B) have been performed<sup>26,27</sup>. These studies showed that the addition of B to a Mo-Si alloy can produce a passivating borosilicate layer under high temperature oxidation conditions. The improvement of oxidation resistance provided by the B addition is attributed to the formation of a low viscosity borosilicate glass scale, which flows to form a continuous and protective layer.

Investigations of the oxidation behavior of Mo-Si-B base alloys containing the three phases Mo(ss), Mo<sub>3</sub>Si and T2 have been performed<sup>34,35,36</sup>. These investigations showed that the viscosity of the borosilicate glass layer formed on the surface of the alloy during high temperature oxidation exposures greatly affected the oxidation kinetics. The viscosity of the borosilicate glass was shown to be dependent on the amount of dissolved B<sub>2</sub>O<sub>3</sub>. At intermediate temperatures, the vapor pressure of B<sub>2</sub>O<sub>3</sub> is quite low, forcing the B<sub>2</sub>O<sub>3</sub> to remain in solution and the viscosity to remain low. This low viscosity results in rapid transport through the borosilicate glass scale and increased oxidation kinetics. The investigations also showed that at higher temperatures the vapor pressure of B<sub>2</sub>O<sub>3</sub> is high enough to reduce the amount in solution by volatilization and, consequently, increase the viscosity of the borosilicate glass scale. The increased viscosity, decreases the transport through the scale and decreases the oxidation kinetics. These important investigations showing the effect of oxide volatility on the protectiveness of the scale formed were conducted under static air conditions. If a full understanding of the oxidation behavior of this alloy is to be obtained, conditions that affect the vaporization of the volatile oxides, such as gas flow rate and oxygen partial pressure, must be investigated.

### **3.0 RESEARCH OBJECTIVES**

The objective of this research is to investigate the high temperature oxidation behavior of molybdenum rich Mo-Si-B base alloys. By virtue of the lack of information about this alloy and its oxidation behavior in the literature, baseline general properties must first be determined in order to establish proper methods to study this alloy. Once the general high temperature oxidation behavior of this alloy is determined as well as the experimental methods that will reveal these traits, key contributors to the oxidation behavior of Mo-Si-B base alloys can be established. Armed with this information, experiments can be devised that will make possible the elucidation of these contributors leading towards further understanding of the high temperature oxidation behavior of this alloy.

Molybdenum rich Mo-Si-B base alloys are unique due to the fact that they are a system of alloys that develop a glassy layer for oxidation protection. Because the protective scale is glassy, the development of the layer can be quite different from that of a crystalline layer. Also, transport processes through the glassy scale may also be different from a crystalline scale. Two specific objectives of this research are to understand better the development of the glassy scale and the transport processes applicable to that scale. Furthermore, how development and transport are affected by gas composition and flow rate as well as temperature and alloy composition are objective of this study.

## 4.0 EXPERIMENTAL APPROACH

### 4.1 Molybdenum Base Alloy

The base alloy in this study is molybdenum with 3 weight percent silicon and 1 weight percent boron<sup>37</sup>. Figure 4.1 shows the three phases present in Mo-3Si-1B. From the Mo-Si-B isothermal ternary phase diagram at 1600°C<sup>38</sup> in Figure 4.2, it is clear that the addition of small amounts of Si and B produces a three phase alloy. These three phases include a Mo solid solution (Mo(ss)) phase, a binary intermetallic Mo<sub>3</sub>Si phase and a ternary intermetallic Mo<sub>5</sub>SiB<sub>2</sub> (T2) phase<sup>38,39</sup>. The body-centered cubic Mo(ss) phase has negligible B solubility, but the Si solubility is appreciable at ~3at%. The stoichiometry range of Si in the Mo<sub>3</sub>Si binary intermetallic phase ranges from about 24 at% to about 25 at% and similarly there is negligible B solubility. The range of stoichiometry for Si in the body-centered tetragonal T2 ternary intermetallic phase is from 8 to 13.65 at% and the stoichiometry range for B in the T2 phase is also significant at 23.3 to 32.35 at%<sup>38,40,41</sup>.

Mo-Si-B alloys containing less than about 50vol% Mo(ss) phase have poor room temperature ductility<sup>28,42,43,44</sup> due to the brittle nature of the two intermetallic phases Mo<sub>3</sub>Si and T2. If the volume fraction of the Mo(ss) phase is allowed to approach or exceed about 50vol%, the room temperature toughness becomes high enough for the alloy to be considered for

industrial applications. This favorable room temperature strength is due to a microstructure consisting of a continuous matrix of the more ductile Mo(ss) phase rather than a continuous brittle intermetallic phase.

## 4.2 Experimental Techniques

Pratt and Whitney supplied the material investigated with two preparation procedures. In case one the material is cast and heat-treated at 1871°C for 24 hours in argon gas (and will further be referred to as cast alloy). In case two the material is atomized and consolidated by hot isostatically pressing (HIP). Then it is isothermally forged at 1760°C for a reduction of 80% and finally it is heat treated at 1871°C for 24 hours in an inert gas (and will further be referred to as forged alloy). Test specimens with surface area of 1.0 – 2.5 cm<sup>2</sup> were polished to 600 grit with SiC paper or diamond impregnated disks and ultrasonically cleaned in acetone prior to oxidation. Despite there being two surface preparation methods, the surface conditions were constant throughout the study. Thermogravimetric analyses were conducted in flowing gas using a Cahn 1000 microbalance and a vertical tube furnace utilizing SiC heating elements. The gas flow rate was calibrated by calculating the amount of gas exiting the apparatus through an oil bubbler. The Reynolds number calculated under all flow conditions indicated that flow was laminar. The material proved to be too hard to drill holes for suspension so the specimens were placed in a platinum basket, which was suspended by platinum wire. Static gas experiments were conducted in a horizontal tube furnace. A quartz tube was used in the horizontal furnace to contain the specimen and the gas. Specimens prepared the same way were placed on an alumina boat that was wrapped in platinum wire to exclude any contact of the sample with the alumina. The

specimens were pushed into a pre-heated furnace for a prescribed amount of time and subsequently removed for analysis. For exposures in static laboratory air, the ends of the quartz tube were simply capped with alumina wool. For exposures in static dry air, the ends of the quartz tube were capped with rubber stoppers with one containing a gas inlet and the other containing a gas outlet. The tube was back filled with the bottled gas for no less than 1 hour through an oil bubbler on the outlet. After back filling the tube, the flow of gas was ceased and the tube was slid through the furnace to a point where the specimen was in the hot zone. After the exposure, the specimen in the tube was slid out of the furnace and allowed to cool in the static bottle gas before removal and analysis. For exposures in air plus 0.1atm of water vapor, a similar horizontal tube furnace and quartz tube was used. The inlet bottled dry air was bubbled through water at 46°C, which saturates the air with water. At 46°C, the vapor pressure of water is 0.1atm. The outlet gas was bubbled through water before being vented. The surface and cross-sections of the as-received and oxidized samples were examined using X-ray diffraction (XRD), energy dispersive spectroscopy (EDS), scanning electron microscopy (SEM) and optical microscopy.

#### **4.2.1 Scanning Electron Microscopy Techniques**

Phase identification in this alloy was made difficult by the presence of both very light elements (low atomic number) and very heavy elements (high atomic number). Energy dispersive spectroscopy techniques are unable to measure boron content and the standardless variety are unreliable at measuring oxygen content in the presence of molybdenum. Therefore, to identify the phases in the alloy and in the scale empirical techniques were employed. X-ray diffraction experiments were first conducted in order to identify which phases were present in the

alloy and scale. Once the present phases were known, the backscattered electron detection mode was used on the scanning electron microscope. Backscattered electron detection mainly derives its contrast from atomic number differences. In the case of a Mo-Si-B base alloy, the heaviest element is molybdenum, which would appear bright with respect to the lighter silicon and boron elements. Therefore, a phase that contains more molybdenum would appear brighter. By knowing which phases are present in the alloy from the XRD experiments and noting the contrast differences between each phase, the phases in the alloy can be identified. For example, in the case of the base alloy (Mo-3Si-1B), the three phases Mo(ss), Mo<sub>3</sub>Si and T2 are known to be present from XRD experiments. Under the SEM employing the backscattered electron detector, the phase that appears the brightest will be the Mo(ss) phase by virtue of it containing the greatest amount of the heaviest element (molybdenum) while the phase that appears the darkest is the T2 phase because it contains the least of the heaviest element.

In the case of phase identification in the scale, a slightly different technique was utilized. In this case, standardless energy dispersive spectroscopy was unable to accurately determine the amount of oxygen in the molybdenum oxides. Therefore, determination of the composition of the molybdenum oxides (MoO<sub>2</sub> versus MoO<sub>3</sub>) was not possible, although, differences in oxygen content in the two phases were consistently detectable. Fortunately, at the high temperatures, MoO<sub>2</sub> is solid and MoO<sub>3</sub> is liquid. Upon cooling the alloy from its elevated temperature used during experimental exposure, two distinctive molybdenum oxide morphologies were observed. One is faceted and crystalline in appearance and one is spherical and liquid in appearance. By taking into account the EDS evidence and the morphological evidence, MoO<sub>2</sub> and MoO<sub>3</sub> can be identified. MoO<sub>2</sub> phases are faceted and crystalline looking and contain less oxygen while MoO<sub>3</sub> phases are spherical and liquid appearing and contain more oxygen.

#### **4.2.2 Thermogravimetric Analysis**

Thermogravimetric analyses were conducted in flowing gas using a Cahn 1000 microbalance and a vertical tube furnace utilizing SiC heating elements. The specimens were suspended from the balance in a platinum basket. The specimen and the basket were contained in a tube which lined the furnace and contained the flowing gas. The standard TGA technique under flowing gas conditions flows the gas up past the specimen (from below the furnace to above). Because this alloy forms a volatile oxide ( $\text{MoO}_3$ ) at the experimental temperatures, the flowing gas would sweep the gaseous oxide up through the tube to a position in the tube where the conditions were such that the oxide would condense. By flowing the gas upward, the volatile oxide would condense on the specimen suspension wire affecting the measurements. By reversing the flow direction to downward through the furnace, the volatile oxide would deposit below the specimen not affecting the thermogravimetric analysis.

#### **4.2.3 Cold Finger Technique**

Molybdenum base alloys are known to produce a volatile oxide ( $\text{MoO}_3$ ) and at high temperatures the amount of weight loss of a specimen of this alloy from the vaporization of  $\text{MoO}_3$  can be substantial. In order to approximate the flux of  $\text{MoO}_3(\text{g})$  from the surface of a Mo-Si-B specimen an apparatus was constructed to collect the  $\text{MoO}_3$  when it condensed. The apparatus used a quartz tube through a horizontal tube furnace with dry air flowing through it. In the exit end of the tube a short quartz tube (cold finger) was inserted inside the quartz tube lining the furnace. This short quartz tube was placed in an area at which the  $\text{MoO}_3$  was known to

condense. With this setup, a small specimen could be placed in the hot zone of the furnace and the  $\text{MoO}_3$  that vaporized from its surface would be collected inside the short quartz tube. The change in weight of the short quartz tube is the weight of  $\text{MoO}_3$  vaporized from the surface of the specimen and the weight change of the specimen is the weight of the molybdenum lost to the vaporization (along with any boron lost to the vaporization of  $\text{B}_2\text{O}_3$ ) plus any oxygen pickup by the specimen. Assuming that all of the oxide deposited in the short quartz tube is  $\text{MoO}_3$ , the weight gain of the tube can be multiplied by 0.67 to calculate the amount of molybdenum collected. The difference between the calculated weight of molybdenum collected and the weight change of the specimen will yield the weight of oxygen pickup by the specimen.

#### **4.2.4 Sample Preparation**

For microscopic surface analysis after experimental exposure, specimens were not altered so to observe the surface structure undisturbed. In order to observe the cross-section of an exposed sample several preparation steps were utilized:

1. A nickel plating was applied to the surface of the specimens in order to preserve the edges from deterioration during subsequent metallographic preparation. A Buehler Edgemet Kit was used to plate the specimens. This is an electroless plate process which requires an electrically conductive surface to plate. To aide in the conduction of the surface of the samples, a palladium coating was first sputter coated on the specimen. Despite the addition of the Pd coating, the nickel plating only adhered on specimens that were exposed for very short times producing a non-conductive oxide scale layer that was not continuous. For specimens that were exposed for longer times, this step was omitted.

2. The specimens were placed in Stuers Epofix cold epoxy mount compound.
3. The mounted specimens were then rough ground until an appropriate cross-section was exposed.
4. A Stuers automatic polishing machine was used to fine polish the specimens using a diamond slurry grind media. No etching was done.

## 5.0 RESULTS AND DISCUSSION

In discussing the results obtained for the oxidation of the Mo-3Si-1B alloy, the following procedures will be used. First, some of the phase diagrams and vapor pressures relevant to the various phases that are important to the oxidation of this alloy will be discussed. Then results will be presented to describe how the borosilicate layer develops on the Mo-3Si-1B alloy. A section will follow this with results related to transport processes in continuous borosilicate layers on Mo-3Si-1B. Finally, the effects of temperature, the effects of the gas environment (e.g. flow rate, gas composition) and alloy composition on the development of the borosilicate layer and transport through it will be considered.

Mo-3Si-1B was exposed to a range of conditions in order to determine how the borosilicate layer develops and the transport processes involved. These conditions consist of a range of temperatures (700°C to 1100°C), a range of exposure gas compositions ( $10^{-4}\text{atm} < p_{\text{O}_2} < 1\text{atm}$  and  $0\text{atm} < p_{\text{H}_2\text{O}} < 0.1\text{atm}$ ) and flow rates (static to 10cm/sec). Specimen weight changes were recorded as a function of time under the varying conditions. These weight changes were normalized by dividing by the initial surface area of the specimen. The normalized weight change was then plotted versus time to produce an oxidation kinetics curve. Figure 5.1 shows weight change versus time data for three Mo-3Si-1B specimens exposed at 1000°C in dry air flowing at 1cm/sec. The initial rapid weight loss varies considerably for the three specimens but the final slope of the curves are very repeatable. This is true for most of the exposure conditions and most of the data that will be presented were from multiple experiments.

## 5.1 Relevant Phase Diagrams and Thermodynamic Data

The  $\text{SiO}_2\text{-B}_2\text{O}_3$  quasi-binary phase diagram is present in Figure 5.1.1. There is a eutectic reaction at about  $442^\circ\text{C}$  and 97mol%  $\text{B}_2\text{O}_3$ . The melting point of the liquid phase gradually increases from the eutectic temperature as the  $\text{SiO}_2$  content is increased. The Mo-oxygen binary phase diagram is presented in Figure 5.1.2. The oxide  $\text{MoO}_2$  has a melting temperature above  $2000^\circ\text{C}$ . A number of oxides can exist near the composition  $\text{MoO}_3$ , namely  $\text{Mo}_9\text{O}_{24}$ ,  $\text{Mo}_8\text{O}_{23}$  and  $\text{Mo}_4\text{O}_{11}$ . A eutectic reaction exists between  $\text{Mo}_9\text{O}_{24}$  and  $\text{MoO}_3$  at about  $815^\circ\text{C}$ . All of these compounds have melting temperatures close to this temperature. A liquid phase exists from about  $815^\circ\text{C}$  to about  $1150^\circ\text{C}$ , which is the approximate boiling temperature of  $\text{MoO}_3$ . The composition of this liquid phase varies with temperature but can exist from about  $\text{Mo}_4\text{O}_{11}$  to  $\text{MoO}_3$ . At  $1000^\circ\text{C}$  the oxygen pressure to form  $\text{MoO}_2$  is about  $10^{-15}\text{atm}$ . The oxygen pressure required to convert  $\text{MoO}_2$  to  $\text{MoO}_3$  is about  $6.3 \times 10^{-7}\text{atm}$  at  $1000^\circ\text{C}$ . ( $\text{MoO}_3$  will be used rather than the other oxide phases having compositions close to  $\text{MoO}_3$ ) Volatile species diagrams for the Mo-O, Si-O and B-O systems are presented in Figure 2.3.1, 2.3.2, 2.4.1, 2.5.1 and 2.5.2, respectively for temperatures of 1100K and 1350K. From these diagrams it can be seen that at a constant temperature the oxygen pressure required to form  $\text{SiO}_2$ ,  $\text{B}_2\text{O}_3$ ,  $\text{MoO}_2$  and  $\text{MoO}_3$  progressively increases, and that the major volatile species are the higher oxides of molybdenum. At 1350K ( $1077^\circ\text{C}$ ) the pressures of  $(\text{MoO}_3)_3$  and  $(\text{MoO}_3)_4$  are approximately each at  $\sim 0.5\text{atm}$  and at lower temperatures the sum of the pressures of all of the gaseous oxides of molybdenum is less than one atmosphere. These diagrams also show the pressures of some hydrated species of  $\text{MoO}_3$ ,  $\text{SiO}_2$  and  $\text{B}_2\text{O}_3$ .

## 5.2 Development of the Borosilicate Layer on Mo-3Si-1B

Weight change versus time measurements for the oxidation of Mo-3Si-1B under different conditions are presented in Figure 5.2.1 and 5.2.2. In most cases the weight losses initially are large but with time become less and approach a constant rate of weight loss versus time, Figure 5.2.1. However, in some cases the large weight losses continue and the approach to a constant small rate of weight loss does not occur, Figure 5.2.2. In the cases where a constant small rate of weight loss is approached, the surfaces of the specimens appear to be coated with a continuous borosilicate layer, Figure 5.2.3, and cross-sections of such specimens are consistent with this conclusion, Figure 5.2.4, where the borosilicate layer can be seen above a layer of  $\text{MoO}_2$  on the alloy similar to that observed by Leonard and Vasudevan<sup>45</sup> and Dimiduk<sup>46</sup>. In cases where large weight losses are present, with no approach to a constant rate of small weight loss, the surfaces are covered with borosilicate but the borosilicate contains numerous open channels that extend from the surface of the borosilicate to the alloy, Figure 5.2.5. Along the walls of these channels, particles of alloy are present in the borosilicate and these particles are usually coated with  $\text{MoO}_2$  but the  $\text{MoO}_3$  does not develop in the borosilicate but rather on the walls of the channels as small droplets, Figure 5.2.6.

The surfaces of Mo-3Si-1B were examined as a function of time for specimens exposed in static laboratory air at 1000°C. The surface of a specimen prior to exposure is shown in Figure 5.2.7a where the three phases in this alloy are evident. After one minute, Figure 5.2.7b, the features evident upon the different phases has changed due to oxidation. It appears that a borosilicate melt has formed over the T2 phase. The  $\text{Mo}_3\text{Si}$  phase exhibits dark particles that are  $\text{SiO}_2$ , Figure 5.2.7b, and the Mo solid solution surface can be seen to be at a lower elevation than the other two phases, Figure 5.2.7c. As the time of exposure is increased the borosilicate

gradually develops continuity over the  $\text{Mo}_3\text{Si}$  phase, Figure 5.2.7d, and lastly over the solid solution phase, Figures 5.2.7e and 5.2.7f. However, even after 30 minutes of exposure small channels still exist in the borosilicate layer, Figure 5.2.7e and 5.2.7f (arrows). Features that help describe the development of the borosilicate layer can also be obtained by observing cross-sections of specimens exposed to conditions identical to those in Figure 5.2.7. In Figure 5.2.8a, the reaction products formed over the  $\text{Mo}_3\text{Si}$  and the solid solution phases can be seen. As the  $\text{Mo}_3\text{Si}$  was oxidized the  $\text{MoO}_3$  vaporized very rapidly and the  $\text{SiO}_2$  remains in situ as filaments. The surface of the solid solution phase retreats due to the vaporization of the  $\text{MoO}_3$ . A thin layer of  $\text{MoO}_2$  is evident over both of these two phases. The development of the borosilicate layer over the T2 phase can be seen in Figure 5.2.8b. The nickel backup material (light phase) has penetrated into some of the borosilicate (dark phase). The T2 phase contains about 33at% B and 26at% Si. During oxidation the  $\text{MoO}_3$  vaporizes and the boron and silicon oxidize to rapidly form the liquid borosilicate. With time the borosilicate gradually develops over the  $\text{Mo}_3\text{Si}$  phase and finally over the solid solution phase, but there are channels that extend down through the borosilicate layer, Figure 5.2.8c, Figure 5.2.7e and Figure 5.2.7f. The boron and silicon that form the borosilicate layer come from the individual phases themselves, although there probably is some spreading of the borosilicate from the T2 phase to the other two phases. The channels in the borosilicate are the last to seal. They appear to develop at phase boundaries in the alloy, Figure 5.2.7e. These channels often extend completely through the borosilicate to the  $\text{MoO}_2$  covered alloy, Figures 5.2.5, 5.2.6 and 5.2.9. In locations where the channels take a long amount of time to seal, the alloy has undergone more oxidation as is evident in Figure 5.2.9a. The undercutting action of the channels can result in the borosilicate layer containing substantial

amounts of alloy and  $\text{MoO}_2$ , Figure 5.2.9a. In such cases the borosilicate layer can vary in thickness because it requires time for the channels to seal, Figure 5.2.9b.

The sealing of the channels in the borosilicate is not completely understood and of course, for some conditions they do not seal, Figures 5.2.2 and 5.2.5. The channel provides oxygen whereby  $\text{MoO}_2$  is oxidized to  $\text{MoO}_3$ , and it allows the gaseous  $\text{MoO}_3$  to escape. The sealing of the borosilicate must be dependent upon the borosilicate viscosity, which in turn is affected by the composition of the borosilicate. There is a gas pressure of one atmosphere on the surface of the borosilicate. If the pressure in the channels was greater than one atmosphere this would prevent them from sealing, but the sum of the pressures of the various gaseous species of  $\text{MoO}_3$  do not total one atmosphere until a temperature of approximately  $1100^\circ\text{C}$  is approached.

The pressures of any of the possible vapor species as mentioned above should be less than one atmosphere at temperatures less than  $1100^\circ\text{C}$ . Nevertheless, results have been obtained that suggest possibly otherwise. In Figure 5.2.10 a photograph is presented<sup>47</sup> showing the surface of a specimen of Mo-3Si-1B that was exposed in dry air flowing at 1cm/sec for 50 minutes at  $816^\circ\text{C}$ . It can be seen that a smooth borosilicate layer covers the leading edge of this specimen whereas bubbles in the borosilicate are evident in the middle section of the specimen, and open channels can be seen in the borosilicate at the trailing edge. Micrographs showing the cross-sections through the borosilicate layer are presented in Figure 5.2.11. Spherical pores appear to be in the borosilicate at the leading edge, Figure 5.2.11b. In the center region of the specimen the borosilicate appears to have been pushed up due to a gas pressure that would have to be greater than one atmosphere, Figure 5.2.11a. On the other hand, the coefficients of expansion of the alloy and the borosilicate are such that the borosilicate would be in compression upon cooling, and the borosilicate layer could buckle. The trailing edge cross-section exhibits

channels that extend through the borosilicate, Figures 5.2.10 and 5.2.11c. The results obtained from this experiment certainly show that spherical bubbles are in the borosilicate as well as small spheres of oxide that are believed to be MoO<sub>3</sub>, Figure 5.2.11c (arrows). The observed variation of the borosilicate morphology from the leading edge to the trailing edge, Figure 5.2.10, is believed to be caused by the removal of MoO<sub>3</sub> from the surface of the specimen by the flowing gas. At the trailing edge of the specimen the gas can contain substantial amounts of MoO<sub>3</sub> vapor and so less MoO<sub>3</sub> is removed compared to the leading edge. The removal of MoO<sub>3</sub> from the surface of the specimen is an extremely important factor in the development of a continuous borosilicate layer.

The importance of the removal of MoO<sub>3</sub> from the surface of the specimen in the development of a continuous borosilicate layer is further supported by observing the base alloy exposed in an environment with reduced oxygen pressure. Mo-3Si-1B was exposed at 1000°C in argon flowing at 10cm/sec which has an oxygen partial pressure of approximately 10<sup>-4</sup>atm<sup>48</sup>. Weight change versus time measurements are presented in Figure 5.2.12 showing that the specimen gained weight from the oxidation of the molybdenum, silicon and boron in the alloy but that there was also a weight loss component from the steady state linear weight loss at extended times. The shape of the oxidation kinetics curve indicates that a steady state oxide thickness has developed as opposed to the extremely rapid vaporization of MoO<sub>3</sub> seen at higher oxygen pressures that prevents its development. Surface micrographs, Figure 5.2.13, confirm that molybdenum oxide remains on the surface of the specimen after extended exposure times. The surface micrographs also show that the borosilicate is prevented from becoming continuous by the presence of the condensed molybdenum oxide on the surface of the specimen and the absence of the rapid vaporization of MoO<sub>3</sub>.

Figure 5.2.14 shows the weight change versus time measurements for Mo-3Si-1B initially exposed to a pretreatment at 1000°C in dry air flowing at 1cm/sec for one hour. After the one hour pretreatment, the temperature was reduced from 1000°C to 700°C for 20 additional hours with the specimen in situ and the gas flow conditions remaining constant. The final linear weight loss, Figure 5.2.14, indicates that MoO<sub>3</sub> vaporization is occurring but at such a low temperature the rate of vaporization is reduced. The reduced rate of vaporization is evident from the surface photographs of a specimen exposed to only the pretreatment and the specimen exposed to the above described experiment, Figure 5.2.15. During the exposure at 700°C the specimen developed a large amount of condensed molybdenum oxide. Figure 5.2.16 shows the cross-sections of the specimen exposed only to the pretreatment and the specimen exposed to the above described conditions. The very thick layer of molybdenum oxide compared to the specimen exposed to only the pretreatment proves that the vaporization of MoO<sub>3</sub> is quite slow at 700°C. Also evident from the cross-section, Figure 5.2.16, is that the borosilicate glass layer on the specimen exposed to the pretreatment plus the 700°C exposure is not continuous. The continuity of the borosilicate layer is lost during the 700°C exposure due to the lack of MoO<sub>3</sub> removal, Figure 5.2.16. The lack of MoO<sub>3</sub> removal may be explained by examining the borosilicate layer itself. Figure 5.2.17 shows the cross-sections of the borosilicate layer of a Mo-3Si-1B specimen exposed at 1000°C in dry air flowing at 1cm/sec for 20 hours and the borosilicate layer of the specimen exposed to the above described pretreatment and subsequent exposure at 700°C. The greater amount of MoO<sub>3</sub> (arrows) precipitates in the borosilicate layer of the specimen exposed to the above experiment indicates the borosilicate glass contains more molybdenum than the borosilicate layer on the specimen exposed at only 1000°C. The additional amount of molybdenum in the borosilicate layer may be an indication that the

transport of the molybdenum through the borosilicate glass has been affected in such a manner as to slow the removal of  $\text{MoO}_3$ .

In Figure 5.2.18 a schematic is presented to illustrate the development of the borosilicate layer on the Mo-3Si-1B alloy. During oxidation a borosilicate layer develops rather quickly over the T2 phase, Figure 5.2.18a and 5.2.18b, because the  $\text{MoO}_3$  formed leaves rapidly as a gas and the  $\text{B}_2\text{O}_3$  and  $\text{SiO}_2$  react to form a liquid borosilicate layer. The  $\text{Mo}_3\text{Si}$  phase forms filaments of  $\text{SiO}_2$  because the  $\text{MoO}_3$  vaporizes leaving the  $\text{SiO}_2$  behind, Figure 5.2.18b. The molybdenum solid solution phase has large amounts of molybdenum removed with very little borosilicate formed and consequently its surface retreats. A thin layer of  $\text{MoO}_2$  is formed over all of the phases. Its thickness depends on how rapidly the  $\text{MoO}_3$  phase forms. Evidently the oxygen activity in the borosilicate near the alloy is sufficient to form  $\text{MoO}_2$  but not  $\text{MoO}_3$ . It is also important to note that the oxygen pressure at the  $\text{MoO}_2$  alloy interface is sufficient to oxidize both silicon and boron (see Figure 2.3.1, 2.3.2, 2.4.1, 2.5.1 and 2.5.2). Consequently, beneath the  $\text{MoO}_2$ , oxides of both silicon and boron develop and accumulate as the  $\text{MoO}_2$  is converted to  $\text{MoO}_3$ . As shown in Figure 5.2.19, the borosilicate has been observed beneath the  $\text{MoO}_2$  layer. As the  $\text{MoO}_2$  is converted to  $\text{MoO}_3$ , borosilicate gradually accumulates over both the molybdenum solid solution and  $\text{Mo}_3\text{Si}$  phases, and eventually becomes continuous but can contain channels, Figure 5.2.18c and 5.2.18d. The more rapidly  $\text{MoO}_3$  can be removed from the surface of the specimen, the sooner the borosilicate develops continuity.

There are a number of questions that remain unanswered with regard to the development of the a continuous layer of borosilicate on Mo-3Si-1B. The channels that exist in the borosilicate become sealed for some conditions but not for others. At present it appears that the pressures in these channels do not appear to be greater than one atmosphere. Consequently, as

the borosilicate becomes thicker it would be expected that they would seal. At present it appears the lack of sealing may be associated with the viscosity of the borosilicate. High  $\text{MoO}_3$  concentrations may cause the viscosity of the borosilicate to be increased. Also, these channels always contain small spheres of  $\text{MoO}_3$ . These spheres may prevent the channels from sealing. In cases where the oxidizing gas flows over the surface, these spheres may be removed and the channels may seal. Upon sealing some gas may be entrapped as well as a few spheres of  $\text{MoO}_3$  may remain and also become entrapped. Such processes could account for the spherical voids and spheres of  $\text{MoO}_3$  observed in some borosilicate layers, Figure 5.2.11 and 5.2.17. Also, the microstructure of the alloy at the surface will also affect the scale development based simply on the fact that each phase initially develops a different scale and forms continuity at different times.

### **5.3 Transport Processes in Continuous Borosilicate Layers on Mo-3Si-1B**

In those cases where the borosilicate becomes continuous, the oxidation rate of the Mo-3Si-1B is believed to be controlled by diffusion through the borosilicate layer. The weight change versus time curves depend on temperature, the gas composition and the gas flow rate, but as the borosilicate begins to develop continuity the rate of weight loss decreases abruptly, Figure 5.2.1. However, it appears even when the borosilicate is continuous small weight losses still persist. The borosilicate layer is always on top of a layer of  $\text{MoO}_2$ , but the thickness can vary over the surface of the specimen, Figure 5.2.4 and 5.2.9b, and particles of alloy with some  $\text{MoO}_2$  can be located in the borosilicate layer, Figure 5.2.19. The variation in thickness of the borosilicate is caused by the fact that it does not develop continuity at the same time at all

locations on the specimen surfaces. The alloy particles and MoO<sub>2</sub> in the borosilicate are present because before the channels in the borosilicate are sealed, the alloy is undercut such that portions of alloy remain in the borosilicate. Furthermore, as the channels collapse to seal, some of the MoO<sub>3</sub> spheres on the walls of the channels, Figure 5.2.6 and 5.3.1, become entrapped in the borosilicate and voids can also be incorporated into the borosilicate as entrapped gases, Figure 5.2.11b.

Transport through the borosilicate may be achieved via ions but it is difficult to specify what these ions may be, because complex species between B, Mo, Si and oxygen are possible. It is also possible that transport through the borosilicate could involve atoms or molecules because such species have been proposed for transport in SiO<sub>2</sub><sup>49</sup>. It is reasonable to propose that oxygen moves inward through the borosilicate and that molybdenum moves outward. A schematic of the various processes taking place is presented in Figure 5.3.2, where the various species are identified via the neutral atoms. This seems reasonable since even though the actual species are ionic, well defined activities of the neutral species could be defined. If it is assumed that the borosilicate layer is saturated with MoO<sub>2</sub> and that the Mo and oxygen activities vary across the borosilicate layer as determined by the expression:

$$a_{Mo}a_O^2 = K_{24} \quad (24)$$

the  $a_{Mo}$  and  $a_O$  would vary across the borosilicate as indicated schematically in Figure 5.3.3. The exact shape of these two curves would depend upon actual transport rates of oxygen and molybdenum through the borosilicate layer. The activity of MoO<sub>3</sub> through the borosilicate layer can be defined by the expression:

$$a_{MoO_3} = K_{25}a_O \quad (25)$$

and since the activity of oxygen increases in the direction of the borosilicate layer gas interface the activity of MoO<sub>3</sub> would also increase in this direction as indicated in Figure 5.3.3. In equation (25) the value of K<sub>25</sub> is determined by temperature, but at all temperatures as the oxygen pressure becomes sufficient to form pure MoO<sub>3</sub>, the activity of MoO<sub>3</sub> must approach one. In the borosilicate, many oxidized specimens of Mo-3Si-1B contain small spheres of MoO<sub>3</sub> just beneath the surface of the borosilicate layer near the gas interface, Figure 5.3.4. Such results indicate that the activity of MoO<sub>3</sub> approaches unity just beneath the borosilicate gas interface due to vaporization of MoO<sub>3</sub>, Figure 5.3.3.

In order to approximate the flux of MoO<sub>3</sub>(g) from the surface of a Mo-3Si-1B specimen with a continuous borosilicate layer an apparatus was constructed to collect the MoO<sub>3</sub> when it condenses. The apparatus used a quartz tube through a horizontal tube furnace with dry air flowing at 1cm/sec through it. In the exit end of the tube a short quartz tube was inserted inside the quartz tube lining the furnace. This short quartz tube was placed in an area at which the MoO<sub>3</sub> was known to deposit. With this setup, a small specimen could be placed in the hot zone of the furnace and the MoO<sub>3</sub> that is removed from it can be collected inside a short quartz tube. The change in weight of the short quartz tube is the weight of the MoO<sub>3</sub> removed from the specimen and the weight change of the specimen is the weight of the molybdenum lost to the vaporization of the MoO<sub>3</sub> plus any oxygen pickup by the specimen. This experiment was carried out using a specimen that was first exposed at 1000°C in dry air flowing at 1cm/sec for one hour in order to develop a continuous borosilicate layer free of channels. This specimen was then placed in the above described apparatus at 1000°C in dry air flowing at 1cm/sec for multiple 2.5 hour cycles.

The weight change of the specimen and the short quartz tube ( $\text{MoO}_3$  curve) are plotted versus exposure time in Figure 5.3.5. The weight change associated with the pretreatment (first hour) is omitted in order to compare the subsequent weight changes. In addition, the weight of Mo collected in the short quartz tube is calculated from its weight change (molybdenum makes up about 66.7% of the weight of  $\text{MoO}_3$ ). By comparing the weight loss of the specimen to the calculated weight of the molybdenum collected, it is clear that  $\text{MoO}_3$  continues to vaporize despite the borosilicate layer being continuous. Furthermore, the calculated weight of molybdenum collected is slightly greater than the weight loss of the specimen indicating additional oxygen pickup by the alloy. From this experiment, one definite conclusion can be made, under these conditions despite the continuous borosilicate layer free of channels  $\text{MoO}_3$  continues to vaporize from the surface of Mo-3Si-1B at a considerable rate. The other conclusion that can be made is that this alloy also continues to gain weight from the further oxidation.

In summary, transport through borosilicate is proposed to take place by the outward diffusion of molybdenum and the inward diffusion of oxygen, Figure 5.3.2. At the borosilicate gas interface,  $\text{MoO}_3$  and  $\text{B}_2\text{O}_3$  are lost to the gas and oxygen is incorporated into the borosilicate. At the  $\text{MoO}_2$  borosilicate interface,  $\text{MoO}_2$  is formed and some oxygen is available to form  $\text{B}_2\text{O}_3$  and  $\text{SiO}_2$ . As the  $\text{MoO}_2$  alloy interface moves inward these oxides are incorporated into the  $\text{MoO}_2$ . Finally as the  $\text{MoO}_2$  dissolves into the borosilicate, the  $\text{B}_2\text{O}_3$  and  $\text{SiO}_2$  are incorporated into the borosilicate layer.

## 5.4 The Effect of Temperature

At a temperature of 700°C a continuous borosilicate layer does not develop on the surface of Mo-3Si1B alloy. The initial weight changes are positive and can be approximated by a parabolic rate expression, Figure 5.4.1, but eventually weight losses are observed, Figure 5.4.2. Oxide scale cracking, as shown in Figure 5.4.3, affects the shape of the curve in Figure 5.4.1. The oxide scale is composed primarily of MoO<sub>2</sub> and MoO<sub>3</sub>, Figure 5.4.4. Even when the weight changes are positive, Figure 5.4.1, there is significant vaporization of MoO<sub>3</sub> since the thickness of the oxide scale, Figure 5.4.4, is larger than the calculated thickness in terms of the measured final weight change. This would imply that the measured weight change is being affected by weight losses due to vaporization of MoO<sub>3</sub>. As discussed in previous sections, adequate removal of MoO<sub>3</sub> from the surface of Mo-3Si-1B alloys permits the development of a continuous borosilicate layer. At 700°C, MoO<sub>3</sub> does not vaporize quickly enough for the borosilicate to develop on the alloy.

As the temperature is increased to 816°C and above, continuous borosilicate layers can be developed on the Mo-3Si-1B alloy as well as borosilicate layers permeated with channels. The type of borosilicate layer that develops depends not only on the temperature but also on the gas composition and gas flow rate. The effect of gas composition and gas flow rate will be discussed in the subsequent section.

## 5.5 The Effect of Gas Composition and Gas Flow Rate

The development of the borosilicate layer is affected by the gas composition and gas flow rate. In Table 2 the conditions for which continuous and protective borosilicate layers were observed, as well as cases where such condition was not achieved, are tabulated. As indicated in the table, the weight change at which the borosilicate layer becomes continuous is indicated in black and the slope after sealing is indicated in red. When the absolute value of the slope is greater than about  $2.2\text{mg}/\text{cm}^2\text{sec}$  it was assumed that open channels must have been present in the borosilicate layer. This value is derived by observation of the surface of exposed specimens. Specimens with slopes greater than  $2.2\text{mg}/\text{cm}^2\text{sec}$  were observed to contain channels through the borosilicate layer. The conditions of static air and  $1000^\circ\text{C}$  appear to be most favorable for the borosilicate to develop continuity. Continuous or discontinuous layers of borosilicate develop for other conditions identified in Table 2.

Development of the borosilicate glass layer is affected not only by the gas composition and gas flow rate that it is exposed to but by other factors as well. These factors were not studied in this research but the effects that they have on the high temperature oxidation behavior of Mo-Si-B base alloys is apparent from the lack of reproducibility of the oxidation kinetics data collected. In Figures 5.5.1 and 5.5.2, weight change versus time measurements are presented for specimens tested under identical conditions. The curves have similar shapes but the magnitude of the weight losses vary significantly. This is because the borosilicate layer has not sealed and the number and size of the channels in the borosilicate are not the same. Results obtained for cast and for forged Mo-3Si-1B are presented in Figure 5.5.3 and more dramatically

in Figure 5.5.4. In this case, the curves show the possible difference in oxidation behavior caused by the use of differing fabrication techniques.

In discussing the effect of gas composition and gas flow rate the following procedures will be used. Results from each of the experimental temperatures will be presented followed by discussion of the effect of gas composition and gas flow rate at that temperature. This is concluded by a summary of the general effect of gas composition and gas flow rate for all experimental temperatures.

Figure 5.5.5 shows the weight change versus time measurements for Mo-3Si-1B exposed at 816°C in static laboratory air. Rapid initial weight loss is followed by small linear weight loss indicative of a continuous borosilicate layer. Surface and cross-sectional micrographs, Figure 5.5.6, confirm that the borosilicate layer contains no channels. Figure 5.5.7 shows the weight change versus time measurements for Mo-3Si-1B exposed at 816°C in static dry air. Rapid initial weight loss is followed by small linear weight loss indicative of a continuous borosilicate layer. The initial weight loss under static dry air conditions is larger and continues for more time than the initial rapid weight loss in static laboratory air. Surface micrographs taken at one hour of exposure time at 816°C in static dry air, Figure 5.5.8, show that the borosilicate layer has not developed continuity. It is evident at longer exposure times, Figure 5.5.9, that a continuous borosilicate layer does develop. Mo-3Si-1B was exposed to static oxygen using the same apparatus as the static dry air experiment. A one hour exposure yielded a weight change of  $-29.1\text{mg/cm}^2$  and surface and cross-sectional micrographs show a continuous borosilicate layer containing no channels, Figure 5.5.10.

Figure 5.5.11 shows the weight change versus time measurements for Mo-3Si-1B exposed at 816°C in dry air flowing at 1cm/sec. The initial rapid weight loss is followed by linear weight loss with a lesser slope. The absolute value of the slope of the linear weight loss portion of the curve is 4.6mg/cm<sup>2</sup>hr indicating that the borosilicate layer contains unsealed channels. Optical micrographs of the specimen, Figure 5.5.12, show that indeed the borosilicate layer has easily distinguishable channels through the borosilicate layer. Figure 5.5.13 shows cross-sectional micrographs depicting the channels (arrows) through the borosilicate layer which make possible the substantial continual weight loss under these conditions.

Figure 5.5.14 shows the weight change versus time measurements for Mo-3Si-1B exposed at 816°C in air + 0.1atm H<sub>2</sub>O flowing at 1cm/sec. As in the case of dry air flowing at 1cm/sec, these exposure conditions produce a rapid initial weight loss followed by a linear weight loss with a substantial absolute value of the slope of 4.5mg/cm<sup>2</sup>hr. This indicates that channels remain in the borosilicate layer making possible the substantial continual weight loss. An optical macrograph of the specimen, Figure 5.5.15, shows a surface with exposed areas of molybdenum oxide indicating that the borosilicate layer is not continuous after an hour of exposure time at 816°C in air + 0.1at H<sub>2</sub>O flowing at 1cm/sec. Cross-sectional micrographs, Figure 5.5.16, show that at a later time that the borosilicate layer does indeed have channels and is not continuous. Also, under these exposure conditions an abnormally thick MoO<sub>2</sub> layer develops under the borosilicate layer. Figure 5.5.17 shows the weight change versus time measurements for Mo-3Si-1B exposed at 816°C in dry air flowing at 10cm/sec. As was the case with slower flowing dry air, the initial rapid weight loss is followed by linear weight loss with a substantial absolute value of the slope of 6.3mg/cm<sup>2</sup>hr indicative of a non-continuous borosilicate layer. Short exposure time optical micrographs, Figure 5.5.18, show how the initial

development of the borosilicate layer (dark) is affected by the flowing gas. At longer times, the surface of the specimen has easily distinguishable channels through the borosilicate layer, Figure 5.5.19, evident from the substantial linear weight loss, Figure 5.5.17. Cross-sectional micrographs, Figure 5.5.20, confirm the presence of channels (arrows) through the borosilicate layer.

In summary, Mo-3Si-1B exposed to static air (both laboratory and dry) at 816°C develops a continuous and protective borosilicate layer containing no channels. Under these conditions, the final linear weight loss slopes both have an absolute value less than 2.2mg/cm<sup>2</sup>hr, 0.82mg/cm<sup>2</sup>hr for an exposure to static laboratory air and 1.3mg/cm<sup>2</sup>hr for an exposure to static dry air (Table 2). When Mo-3Si-1B is exposed to flowing air (both dry and with water vapor) at 816°C the channels through the borosilicate layer do not all seal. Under all three flowing gas exposure conditions (dry air flowing at 1cm/sec and 10cm/sec and air + 0.1atm H<sub>2</sub>O flowing at 1cm/sec), the final linear weight losses all have an absolute value greater than 2.2mg/cm<sup>2</sup>hr. The addition of water vapor to the exposure environment in static air conditions, in the form of laboratory air (~0.01atm H<sub>2</sub>O) versus dry bottle air, seemed to decrease the time required to develop the borosilicate layer and decrease the weight loss after the borosilicate layer had developed. In the case of flowing air, the addition of water vapor to the exposure environment had little effect on the oxidation kinetics but did affect the morphology of the scale produced on the surface of the Mo-3Si-1B specimen. Therefore, **Mo-3Si-1B exposed at 816°C in static air develops a continuous borosilicate layer free from channels while under flowing air exposure conditions the channels through the borosilicate layer do not seal. The higher gas flow rates aid in the removal of MoO<sub>3</sub> from the surface of the specimen (which is advantageous for the sealing of channels as stated in previous sections) but it also aids in**

**the removal of boron from the borosilicate glass. Removing boron from the borosilicate increases the viscosity preventing the channels from sealing and because the temperature is low (816°C) the viscosity is not reduced enough by it to counteract the effect of boron loss.**

Figure 5.5.21 shows the weight change versus time measurements for Mo-3Si-1B exposed at 900°C in dry air flowing at 1cm/sec. The initial rapid weight loss was not followed by a linear weight loss with absolute value of lesser value. This indicates that the channels through the borosilicate layer did not seal. Cross-sectional micrographs, Figure 5.5.22, confirm the presence of channels (arrows) through the borosilicate layer.

Figure 5.5.23 shows the weight change versus time measurements for Mo-3Si-1B exposed at 1000°C in static laboratory air. The initial rapid weight loss is followed by a slight linear weight loss common for an alloy that develops a continuous borosilicate layer containing no channels. Surface and cross-sectional micrographs, Figure 5.5.24, show that indeed Mo-3Si-1B exposed in static laboratory air at 1000°C develops a borosilicate layer with all the channels sealed. Figure 5.5.25 shows the weight change versus time measurements for Mo-3Si-1B exposed at 1000°C in dry air flowing at 1cm/sec. As in the case of the exposure in static laboratory air at this temperature, the weight change curve for exposures under these conditions follows the same formula for development of a continuous borosilicate layer containing no channels. Cross-sectional micrographs, Figure 5.5.26 and 5.5.27, show the development of the borosilicate layer as a function of time. As exposure time increases, it is apparent that the oxidation front is moving into the alloy leaving behind borosilicate from the oxidation of silicon and boron in the alloy as well as MoO<sub>2</sub>, Figure 5.5.27. Also, internal oxidation, Figure 5.5.28, was observed in Mo-3Si-1B exposed at 1000°C in dry air flowing at 1cm/sec. The internal oxidation was only resolved in the T2 phase, but it is expected to be present in all three phases

since the oxygen pressure in all three cases is high enough to oxidize silicon and boron. Figure 5.5.29 shows the weight change versus time measurements for Mo-3Si-1B exposed at 1000°C in dry air flowing at 10cm/sec. As was the case for the previously mentioned exposure conditions at 1000°C, the oxidation kinetics curve depicts a case where a continuous borosilicate layer containing no channels has developed. Surface and cross-sectional micrographs, Figure 5.5.30, confirm that no channels remain through the borosilicate layer when Mo-3Si-1B is exposed at 1000°C in dry air flowing at 10cm/sec. Figure 5.5.31 shows weight change versus time measurements for Mo-3Si-1B exposed at 1000°C in oxygen flowing at 10cm/sec. Once again, initial rapid weight loss is followed by slight linear weight loss indicating that the alloy has indeed formed a continuous borosilicate layer free from channels. Cross-sectional micrographs, Figure 5.5.32, confirm that no channels remain and that the borosilicate layer is continuous.

In summary, at 1000°C Mo-3Si-1B develops a continuous borosilicate layer free from channels under all gas compositions and gas flow rates studied. Under all experimental conditions, the final linear weight loss slopes have an absolute value less than 2.2mg/cm<sup>2</sup>hr (Table 2), ranging from a minimum absolute value of 0.017mg/cm<sup>2</sup>hr under dry air flowing at 1cm/sec exposure conditions to 2.2mg/cm<sup>2</sup>hr under oxygen flowing at 10cm/sec exposure conditions. The amount of time required for the channels initially present in the borosilicate to seal (i.e. the absolute value of the slope of the oxidation kinetics curve to decrease to the final linear weight loss slope) did not seem to change significantly with gas composition or gas flow rate, and the amount of initial rapid weight loss for each condition was not significantly different either. Therefore, **Mo-3Si-1B exposed at 1000°C develops a continuous borosilicate layer free from channels under all gas composition and gas flow rate conditions considered. All effects of gas composition and gas flow rate are counteracted by the decrease of the**

**viscosity of the borosilicate glass associated with the temperature increase to 1000°C permitting the sealing of the channels.**

Figure 5.5.33 shows the weight change versus time measurements for Mo-3Si-1B exposed at 1100°C in static laboratory air. Under these exposure conditions, the alloy forms a continuous borosilicate layer free from channels evident from the slight linear weight loss following the rapid initial weight loss. Cross-sectional micrographs, Figure 5.5.34, show a continuous borosilicate layer as well as substantial internal oxidation in all three phases after extended exposure at 1100°C in static laboratory air. The morphology of the internal oxidation appears to be as long stringers in the T2 intermetallic phase, similar to that observed by Hindam and Smeltzer<sup>50</sup> for Ni-Al alloys, and less elongated in the Mo<sub>3</sub>Si intermetallic phase. Figure 5.5.35 shows weight change versus time measurements for Mo-3Si-1B exposed at 1100°C in static dry air. Again, the oxidation kinetics curve produced under these conditions is typical for the development of a continuous borosilicate layer free from channels and is evident from the surface and cross-sectional micrographs, Figure 5.5.36. Figure 5.5.37 shows weight change versus time measurements for Mo-3Si-1B exposed at 1100°C in dry air flowing at 1cm/sec. As in the case of static air (dry and laboratory) the initial rapid weight loss is followed by slight linear weight loss indicative of a borosilicate layer containing no channels. Surface and cross-sectional micrographs, Figure 5.5.38, once again confirm the absence of channels through the borosilicate layer. Figure 5.5.39 shows weight change versus time measurements for Mo-3Si-1B exposed at 1100°C in air + 0.1at H<sub>2</sub>O flowing at 1cm/sec. The weight change curve is typical for the development of a borosilicate layer free from channels. Cross-sectional micrographs, Figure 5.5.40, confirm the absence of channels through the borosilicate layer as well as show substantial internal oxidation at a relatively short exposure time. Figure 5.5.41 shows weight change versus

time measurements for Mo-3Si-1B exposed at 1100°C in dry air flowing at 10cm/sec. Under these conditions, the initial rapid weight loss does not slow from channel sealing. Rather, the channels remain unsealed and the alloy continues to rapidly oxidize. Surface and cross-sectional micrographs, Figure 5.5.42, present the numerous large channels (arrows) remaining in the borosilicate layer. Figure 5.5.43 shows the weight change versus time measurements for Mo-3Si-1B exposed at 1100°C in oxygen flowing at 10cm/sec. The initial rapid weight loss again did not change slope which is indicative of a borosilicate layer containing channels. In fact, the rate of linear weight loss was the greatest observed under these conditions.

In summary, at 1100°C Mo-3Si-1B developed a continuous borosilicate layer free from channels under static air and slowly flowing (1cm/sec) air regardless of gas composition. Under these experimental conditions, the final linear weight loss slopes have an absolute value less than 2.2mg/cm<sup>2</sup>hr (Table 2), ranging from a minimum absolute value of 0.0094mg/cm<sup>2</sup>hr air + 0.1atm H<sub>2</sub>O flowing at 1cm/sec exposure conditions to 1.7mg/cm<sup>2</sup>hr under static dry air exposure conditions. By changing the gas flow rate to a more rapid condition (10cm/sec), the channels through the borosilicate layer could not seal. Under static air conditions, the addition of water vapor in the form of laboratory air versus dry bottled air, decreased the amount of initial rapid weight loss as well as decreased the amount of time required for the channels initially through the borosilicate layer to seal (Table 2). Therefore, **Mo-3Si-1B exposed at 1100°C under gas flow rates of static and 1cm/sec develops a continuous borosilicate layer free from channels regardless of considered gas compositions while under flow rate conditions of 10cm/sec the channels in the borosilicate layer do not seal regardless of gas composition. The temperature increase to 1100°C furthers the decrease in viscosity of the borosilicate glass permitting the sealing of channels. At increased gas flow rates, the loss of boron from the**

**borosilicate glass due to vaporization of  $B_2O_3$  offsets the increased temperature affect on the viscosity of the borosilicate glass preventing the channels from sealing. Also, the sum of the vapor pressures of all the vapor species produced is approaching one atmosphere at this temperature which would prevent channels through the borosilicate layer from sealing.**

In general, at 700°C a continuous borosilicate layer never forms, at 1000°C a continuous borosilicate layer always forms and at all of the other temperatures studied (816°C and 1100°C) a protective borosilicate layer may or may not form on Mo-3Si-1B. The borosilicate layer is protective when no continuous channels exist in the borosilicate layer extending from the gas interface to the alloy interface. The elimination of channels in the borosilicate layer is obtained by appropriate control of the temperature, gas compositions and gas flow conditions. From Table 2, the general trends of high temperature oxidation behavior for Mo-3Si-1B versus the gas compositions and gas flow rates considered are:

- Mo-3Si-1B exposed at 816°C in static air develops a continuous borosilicate layer free from channels while under flowing air exposure conditions the channels through the borosilicate layer do not seal. The higher gas flow rates aid in the removal of  $MoO_3$  from the surface of the specimen (which is advantageous for the sealing of channels as stated in previous sections) but it also aids in the removal of boron from the borosilicate glass. Removing boron from the borosilicate increases the viscosity preventing the channels from sealing and because the temperature is low (816°C) the viscosity is not reduced enough by it to counteract the effect of boron loss.
- Mo-3Si-1B exposed at 1000°C develops a continuous borosilicate layer free from channels under all gas composition and gas flow rate conditions considered. All effects of gas composition and gas flow rate are counteracted by the decrease of the viscosity of

the borosilicate glass associated with the temperature increase to 1000°C permitting the sealing of the channels.

- Mo-3Si-1B exposed at 1100°C under gas flow rates of static and 1cm/sec develops a continuous borosilicate layer free from channels regardless of considered gas compositions while under flow rate conditions of 10cm/sec the channels in the borosilicate layer do not seal regardless of gas composition. The temperature increase to 1100°C furthers the decrease in viscosity of the borosilicate glass permitting the sealing of channels. At increased gas flow rates, the loss of boron from the borosilicate glass due to vaporization of  $B_2O_3$  offsets the increased temperature affect on the viscosity of the borosilicate glass preventing the channels from sealing. Also, the sum of the vapor pressures of all the vapor species produced is approaching one atmosphere at this temperature which would prevent channels through the borosilicate layer from sealing.

From these statements it is clear that the question of whether the borosilicate develops continuity depends upon the rate of  $MoO_3$  vaporization from the surfaces of specimens, the viscosity of the borosilicate and factors that affect the flow of the borosilicate over the surfaces of specimens. The development of channels in the borosilicate and the sealing of channels are also important factors. All of these processes are affected by the experimental conditions in ways that are inadequately understood.

## 5.6 The Effect of Alloy Composition

The effect of alloy composition was not investigated very extensively. In discussing the effect of alloy composition on the oxidation behavior of Mo-Si-B base alloys, the as-processed microstructures for each of the alloy compositions will be presented and briefly discussed. This will be followed by comparing the oxidation kinetic data for similar compositions in order to draw conclusions on the effect of alloy composition. Alloy compositions with varying amounts of silicon (Mo-5Si-1B, Mo-7Si-1B and Mo-8.2Si-1B) and varying amounts of boron (Mo-7.4Si-2B) were supplied by Pratt & Whitney in order to study the effect of changing the volume fraction of the phases present on the high temperature oxidation behavior of this family of alloys. The remaining alloys (Mo-3Si-1B-6Ti, Mo-3Si-6Ti, Mo-3Si-1B-0.3Hf and Mo-3Si-1B-1Hf) were supplied by Pratt & Whitney because of availability. Figure 5.6.1 shows the microstructure of the base alloy (Mo-3Si-1B). The three phases, Mo(ss), Mo<sub>3</sub>Si and T2 are present with the Mo(ss) phase constituting the continuous matrix phase. Figure 5.6.2 shows the microstructure of Mo-5Si-1B. The same three phases are present as in the base alloy (Mo(ss), Mo<sub>3</sub>Si and T2) but there is no clear continuous matrix phase. Figure 5.6.3 shows the microstructure of Mo-7Si-1B. By increasing the silicon content to this point, the continuous matrix phase becomes Mo<sub>3</sub>Si. Figure 5.6.4 shows the microstructure of Mo-8.2Si-1B. The composition of this alloy is no longer in the region of the Mo-Si-B ternary phase diagram, Figure 3.1, bounded by the phases Mo(ss), Mo<sub>3</sub>Si and T2, rather it is in the region bounded by Mo<sub>3</sub>Si, Mo<sub>5</sub>Si<sub>3</sub> and T2. Therefore, this alloy contains no Mo(ss) phase, but contains a continuous matrix of Mo<sub>3</sub>Si with dispersed Mo<sub>5</sub>Si<sub>3</sub> and T2 phases. Mo-7.4Si-2B, Figure 5.6.5, also contains the phases Mo<sub>3</sub>Si, Mo<sub>5</sub>Si<sub>3</sub> and T2 meaning that its composition is in the region of the ternary phase diagram bounded by those

phases. Once again, the  $\text{Mo}_3\text{Si}$  phase seems to be the continuous matrix phase. Figure 5.6.6 shows the microstructure of Mo-3Si-1B-6Ti. By adding 6wt% titanium, the phases present in the base alloy are not affected (Mo(ss),  $\text{Mo}_3\text{Si}$  and T2) but small particles of a titanium rich phase are also present. Figure 5.6.7 shows the microstructure of Mo-3Si-6Ti. By removing the boron from the previous composition the T2 phase is removed leaving only the Mo(ss),  $\text{Mo}_3\text{Si}$  and the titanium rich phases. Figure 5.6.8 shows the microstructure of Mo-3Si-1B-0.3Hf. The three phases of the base alloy (Mo(ss),  $\text{Mo}_3\text{Si}$  and T2) are the only phases present in this alloy and the hafnium has gone into solution. By adding 1wt% hafnium to the base alloy, Figure 5.6.9, Mo-3Si-1B-1Hf also retains the three phases of the base alloy (Mo(ss),  $\text{Mo}_3\text{Si}$  and T2) but a hafnium rich phase has precipitated out at the phase boundaries.

Isothermal exposures at 816°C in dry air flowing at 1cm/sec were performed on all the available compositions for comparison. Figure 5.6.10 shows the weight change versus time measurements for the base alloy (Mo-3Si-1B) along with alloys with slightly different silicon content exposed at 816°C in dry air flowing at 1cm/sec. Under these conditions, the base alloy does not develop a protective borosilicate layer free from channels. The curves in Figure 5.6.10 indicate that Mo-5Si-1B, Mo-7Si-1B and Mo-8.2Si-1B did produce protective borosilicate layers free from channels. After further investigation, it was determined that indeed Mo-5Si-1B and Mo-8.2Si-1B developed protective borosilicate layers but Mo-7Si-1B did not. The reduction in weight loss depicted in the oxidation kinetics curve is not the result of the development of a protective scale but from the reduction of surface area of the specimen from the consumption of the alloy during the oxidation process. Figure 5.6.11 shows the weight change versus time measurements for Mo-7Si-1B and Mo-7.4Si-2B exposed at 816°C in dry air flowing at 1cm/sec. By increasing the boron content while keeping the silicon content relatively constant, the amount

of initial rapid weight loss is dramatically reduced. Figure 5.6.12 shows the weight change versus time measurements for the base alloy, Mo-3Si-1B-6Ti and Mo-3Si-6Ti exposed at 816°C in dry air flowing at 1cm/sec. Initially, the addition of 6wt% titanium helped develop a protective borosilicate layer but at later times the protection of the layer broke down and rapid oxidation followed. In the case of Mo-3Si-6Ti oxidation, no signs of protective oxide development were observed. Figure 5.6.13 shows the weight change versus time measurements for the base alloy, Mo-3Si-1B-0.3Hf and Mo-3Si-1B-1Hf exposed at 816°C in dry air flowing at 1cm/sec. The addition of small amounts of hafnium to the base alloy composition seems to only affect the amount of initial rapid weight loss. Although, reproducibility studies under these conditions, discussed in further sections, lead to the conclusion that this amount of data spread can be accommodated by the inherent error of the measurements at this temperature under these conditions. All of these results suggest that the development of the borosilicate layer is influenced by the silicon and boron content of the Mo-Si-1B base alloys.

## 6.0 CONCLUDING REMARKS

The critical factor in developing oxidation resistance in Mo-3Si-1B is the development of the borosilicate layer. At 700°C the loss of MoO<sub>3</sub> via vaporization is not rapid enough to permit a borosilicate layer to be formed. At temperatures from 816°C to 1100°C a protective borosilicate layer may or may not form on Mo-3Si-1B. The borosilicate layer is protective when no continuous channels exist in the borosilicate layer extending from the gas interface to the alloy interface. The elimination of channels in the borosilicate layer is obtained by appropriate control of the temperature and gas flow conditions whereby MoO<sub>3</sub> is removed via vaporization while the borosilicate viscosity is not increased due to loss of B<sub>2</sub>O<sub>3</sub>. Once the borosilicate layer is continuous and free of channels, subsequent oxidation occurs by inward diffusion of oxygen and the outward diffusion of molybdenum through this layer with vaporization of MoO<sub>3</sub> at the gas borosilicate layer interface and the formation of MoO<sub>2</sub> and additional borosilicate at the alloy MoO<sub>2</sub> interface. The rates of these processes are small but need further investigation.

Development of the borosilicate layer is affected by other conditions such as the fabrication techniques used to prepare the alloys as well as surface preparation of specimens. These factors can affect how the borosilicate flows over the surface of the specimen and rates at which MoO<sub>3</sub> is removed from the surface of the alloy. Further research is required to:

- Understand in more detail the borosilicate layer development in static gas environments.
- Better definition of pores (not channels) in the borosilicate layer.
- Obtain more detailed understanding of the oxidation kinetics of Mo-3Si-1B with protective layers of borosilicate.

- Understand how the microstructure of the alloy affects the development of the borosilicate layer. More specifically, how the distribution of the phases and size of the grains affect channel sealing and borosilicate formation.
- Better understand factors such as specimen surface conditions in regards to the number of channels that develop in the borosilicate layer formed on Mo-3Si-1B

**Table 1: Tabulation of selected properties of molybdenum at room temperature.**

Density	10.22 g/cm <sup>3</sup>
Young's modulus, E	324 GPa
Yield strength <sup>1,2</sup>	690 MPa
Tensile strength <sup>2</sup>	835 MPa
Elongation <sup>2</sup>	12 %
Hardness <sup>2</sup>	240 HV
Coefficient of thermal expansion	4.9 X 10 <sup>-6</sup> /°C
Thermal conductivity	135 W/(m K)
Specific heat	0.27 J/(kg K)
Electrical resistivity	0.06 μΩ m

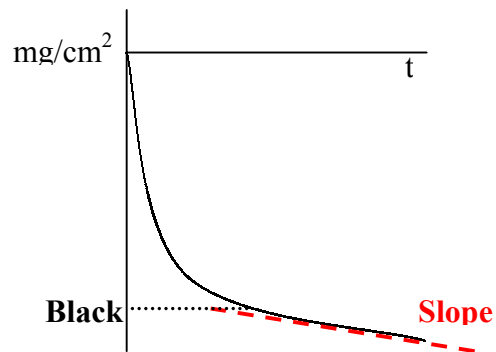
1. 0.2% offset, 2. Material reduced ~80% [2].

**Table 2: Comparison of the effects of temperature and gas environment on the development of a protective borosilicate layer (C), or a borosilicate layer containing channels (X).**

Gas Environment	700°C	816°C	1000°C	1100°C
Static laboratory air	No borosilicate layer evident	C -63mg/cm <sup>2</sup> -0.82mg/cm <sup>2</sup> hr	C -16mg/cm <sup>2</sup> -1.1mg/cm <sup>2</sup> hr	C -41mg/cm <sup>2</sup> -1.1mg/cm <sup>2</sup> hr
Static dry air		C -91mg/cm <sup>2</sup> -1.3mg/cm <sup>2</sup> hr		C -70mg/cm <sup>2</sup> -1.7mg/cm <sup>2</sup> hr
Dry air flowing at 1cm/sec		X -46mg/cm <sup>2</sup> -4.6mg/cm <sup>2</sup> hr	C -35mg/cm <sup>2</sup> -0.017mg/cm <sup>2</sup> hr	C -11mg/cm <sup>2</sup> -0.23mg/cm <sup>2</sup> hr
Air + 0.1atm H <sub>2</sub> O flowing at 1cm/sec		X -70mg/cm <sup>2</sup> -4.5mg/cm <sup>2</sup> hr		C -31mg/cm <sup>2</sup> -0.094mg/cm <sup>2</sup> hr
Dry air flowing at 10cm/sec		X -30mg/cm <sup>2</sup> -6.3mg/cm <sup>2</sup> hr	C -21mg/cm <sup>2</sup> -2.1mg/cm <sup>2</sup> hr	X -50mg/cm <sup>2</sup> hr
Oxygen flowing at 10cm/sec	↓		C -12mg/cm <sup>2</sup> -2.2mg/cm <sup>2</sup> hr	X -350mg/cm <sup>2</sup> hr

C = continuous borosilicate layer

X = borosilicate layer with unsealed channels



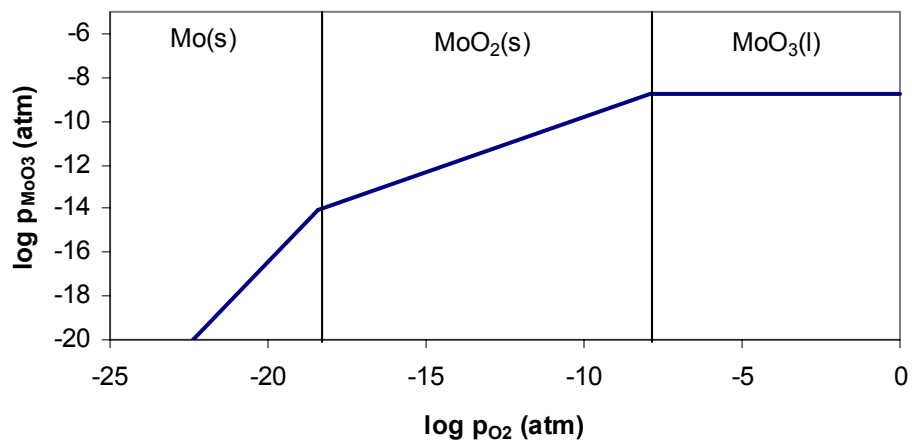


Figure 2.3.1: Volatile species diagram for molybdenum at 1100K.

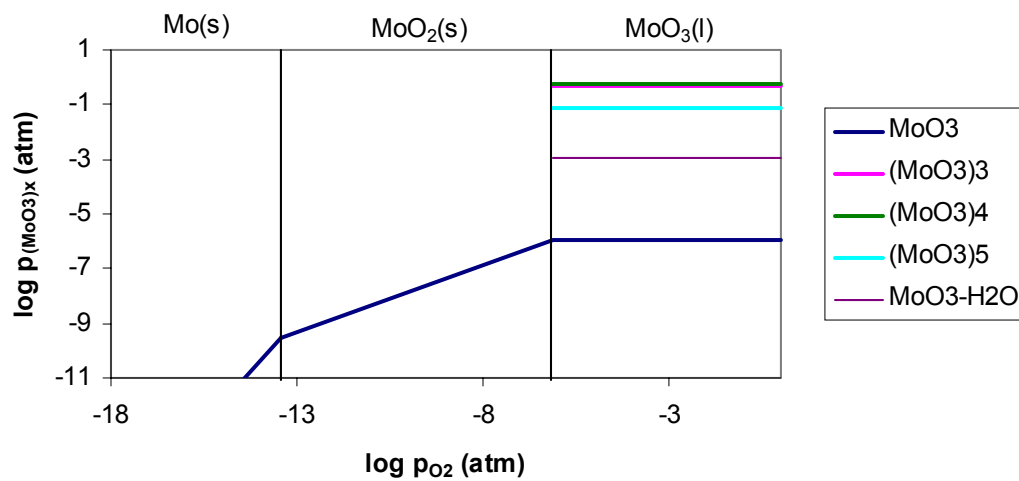


Figure 2.3.2: Volatile species diagram for molybdenum at 1350K ( $p_{\text{H}_2\text{O}} = 0.1\text{atm}$ ).

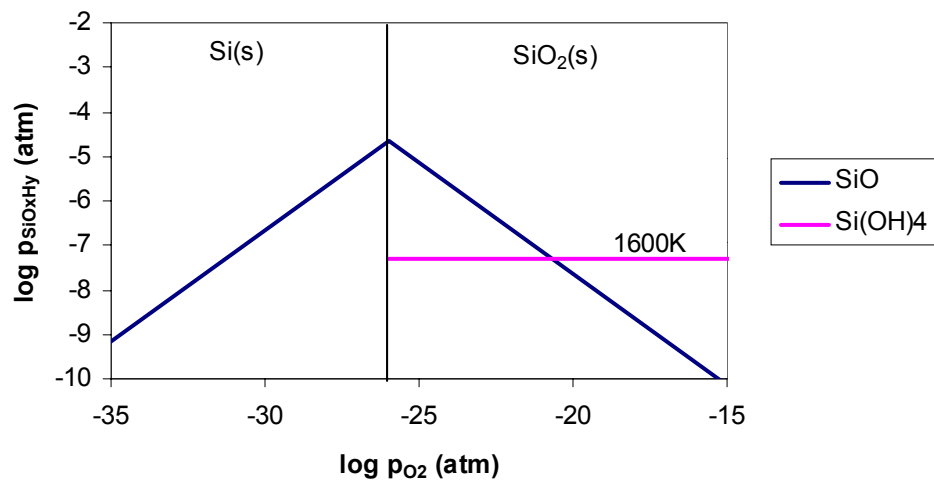


Figure 2.4.1: Volatile species diagram for silicon at 1350K ( $p_{\text{H}_2\text{O}} = 0.1\text{atm}$ ).

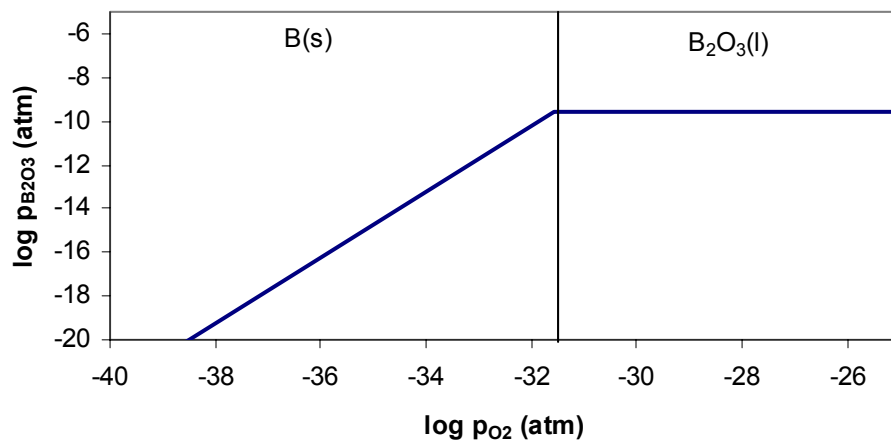


Figure 2.5.1: Volatile species diagram for boron at 1100K.

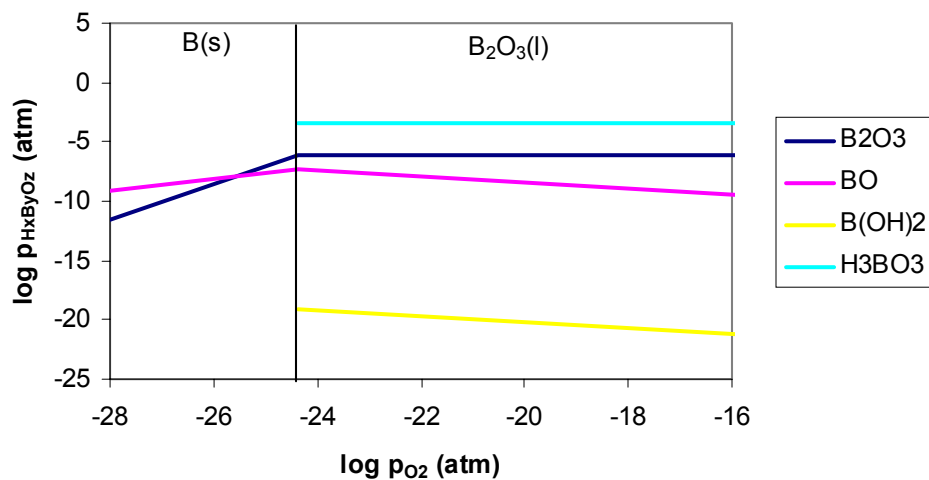


Figure 2.5.2: Volatile species diagram for boron at 1350K ( $p_{H_2O} = 0.1\text{atm}$ ).

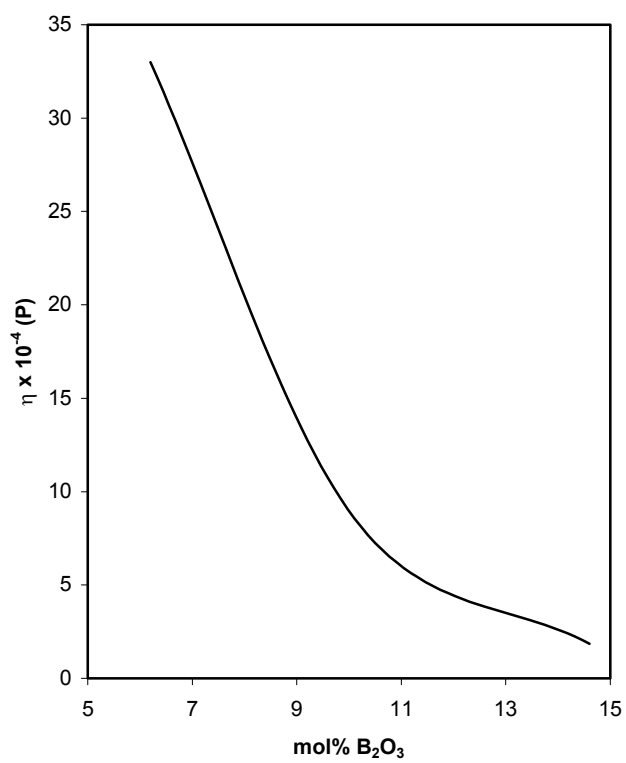


Figure 2.8.1: Borosilicate glass viscosity as a function of composition at  $\sim 1760^\circ\text{C}^{51}$ .

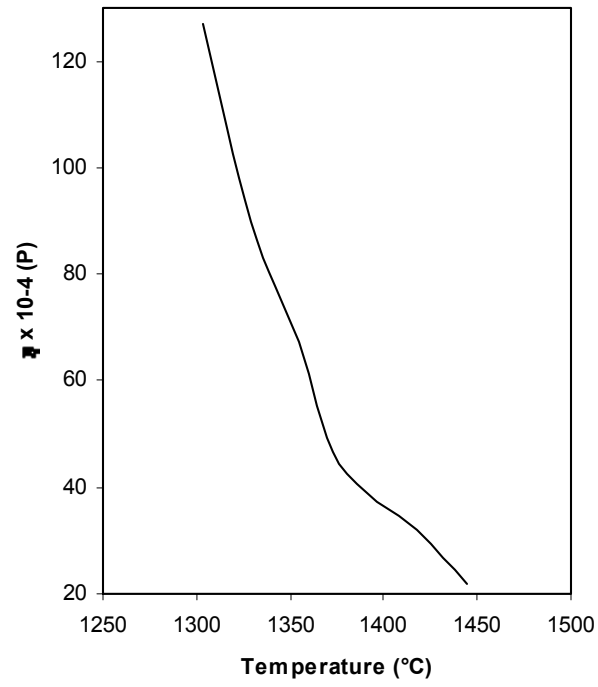


Figure 2.8.2: Borosilicate glass (25 mol% B<sub>2</sub>O<sub>3</sub>) viscosity as a function of temperature<sup>51</sup>.

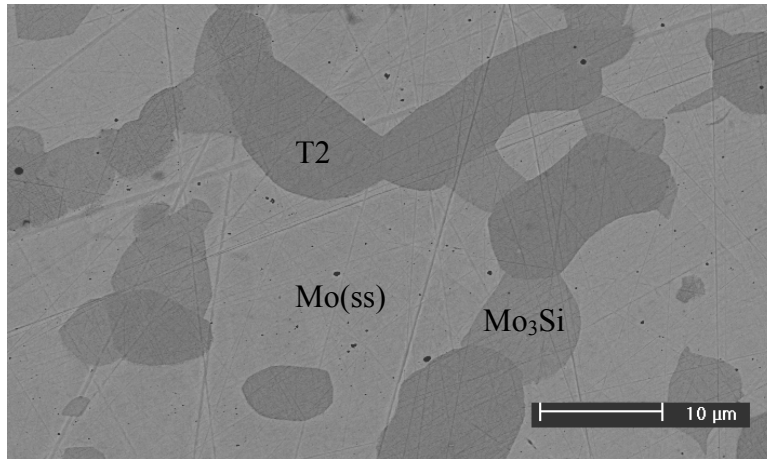


Figure 4.1: Micrograph showing the three phases in Mo-3Si-1B

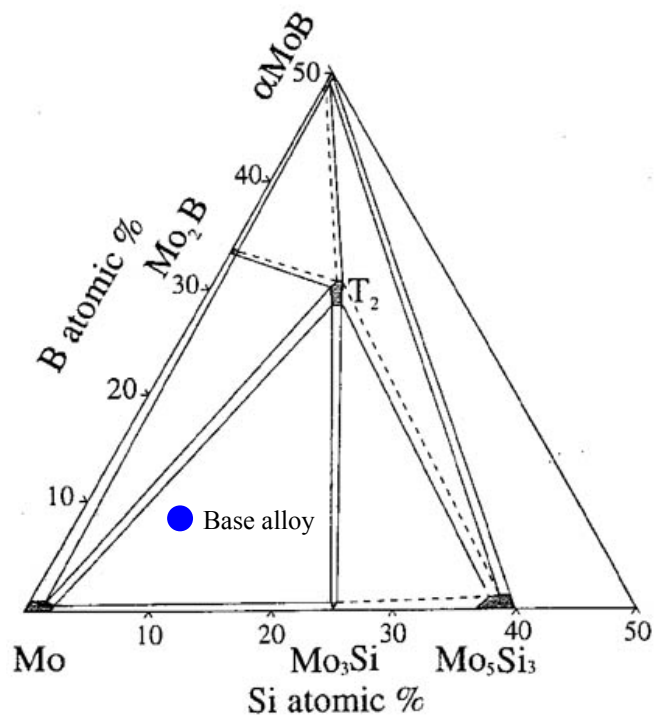


Figure 4.2: Molybdenum rich corner of the Mo-Si-B isothermal ternary phase diagram at 1600°C with Mo-3Si-1B composition identified<sup>36</sup>.

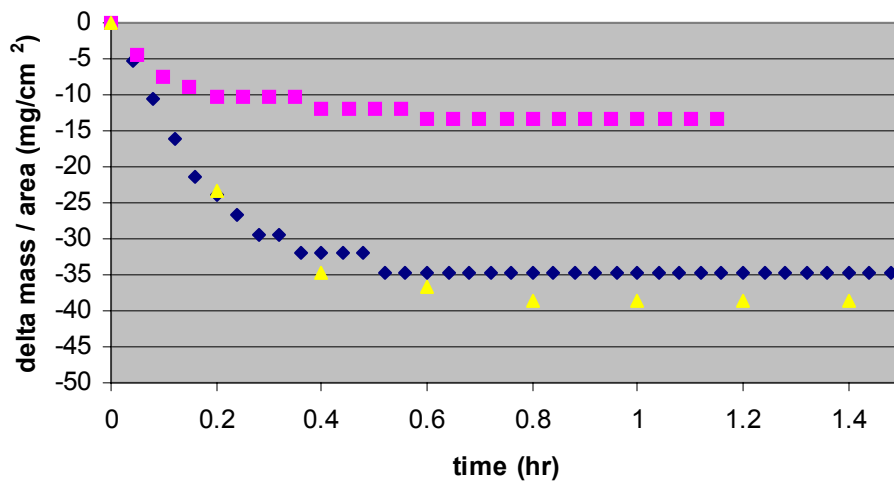


Figure 5.1: Three Mo-3Si-1B specimens exposed at 1000°C in dry air flowing at 1cm/sec.

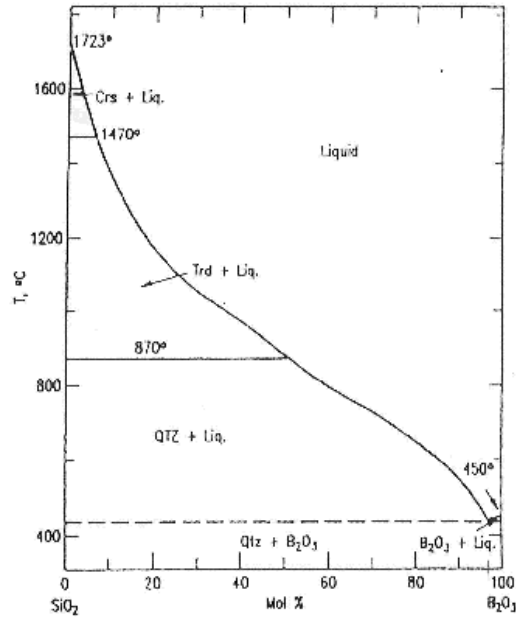


Figure 5.1.1: SiO<sub>2</sub>-B<sub>2</sub>O<sub>3</sub> phase diagram<sup>52</sup>.

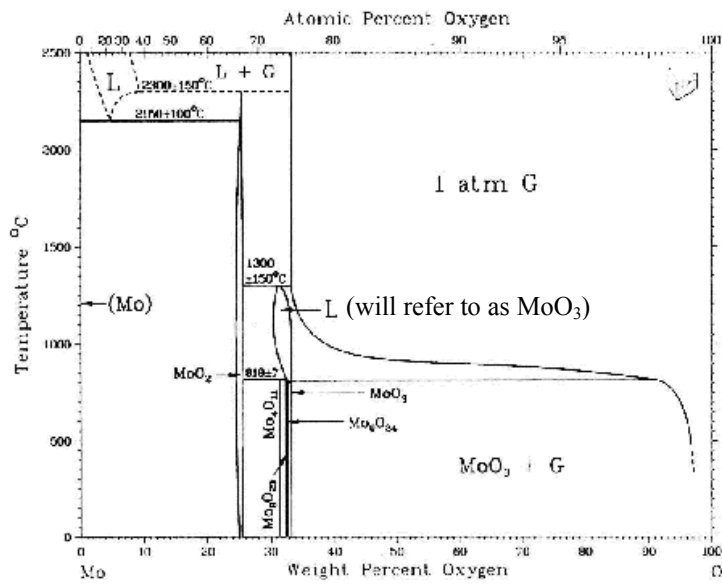


Figure 5.1.2: Mo-O phase diagram (the sequence of phases should be Mo<sub>9</sub>O<sub>24</sub>, Mo<sub>4</sub>O<sub>11</sub>, Mo<sub>8</sub>O<sub>23</sub>, MoO<sub>3</sub> rather than as indicated in this diagram)<sup>53</sup>.

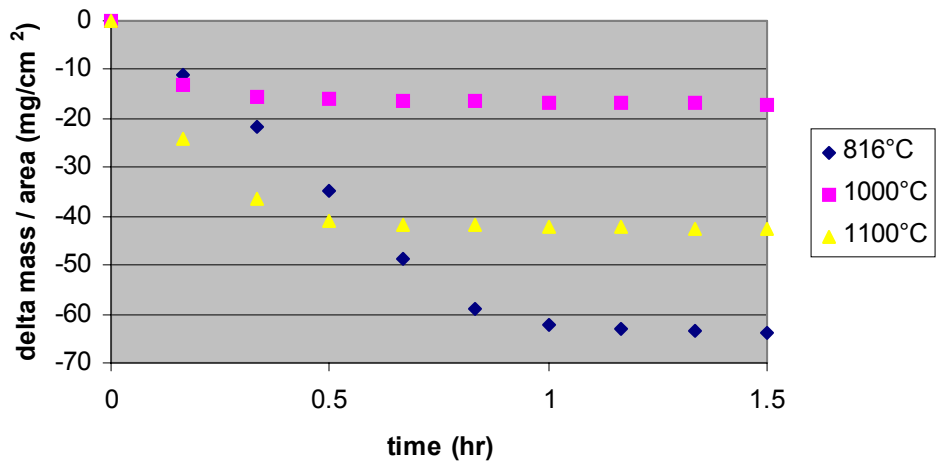


Figure 5.2.1: Weight change versus time data for the oxidation of Mo-3Si-1B exposed in static laboratory air at the temperature indicated (continuous borosilicate layer free from channels).

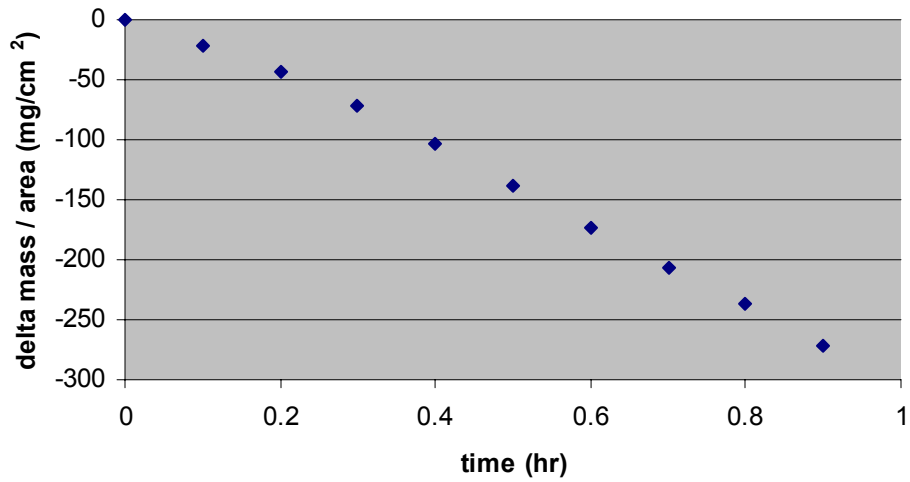
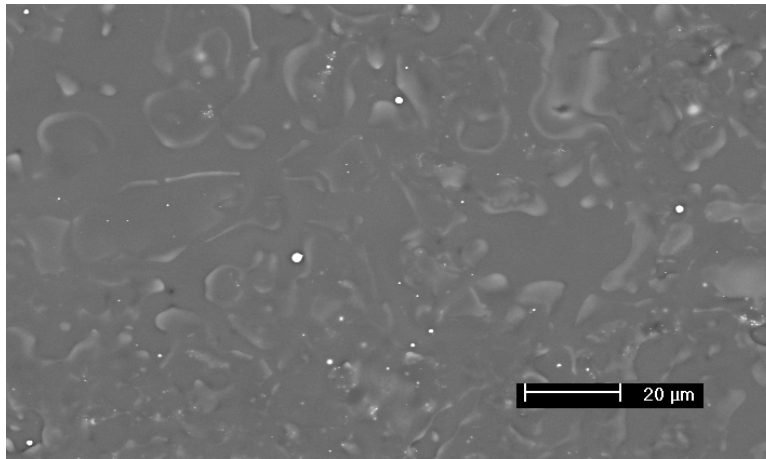
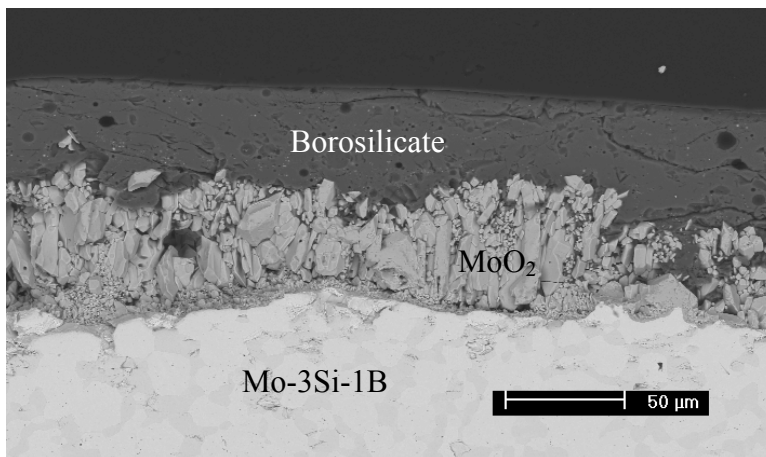


Figure 5.2.2: Weight change versus time data for the oxidation of Mo-3Si-1B exposed at 1100°C in dry air flowing at 10cm/sec (borosilicate layer containing unsealed channels).



**Figure 5.2.3:** Backscattered electron micrograph showing the surface of the borosilicate layer on Mo-3Si-1B after five hours exposure at 816°C in static laboratory air.



**Figure 5.2.4:** Backscattered electron micrograph showing the cross-sectional view of the specimen described in Figure 5.2.3. The borosilicate layer is continuous and a layer of MoO<sub>2</sub> is evident on the alloy beneath the borosilicate layer.

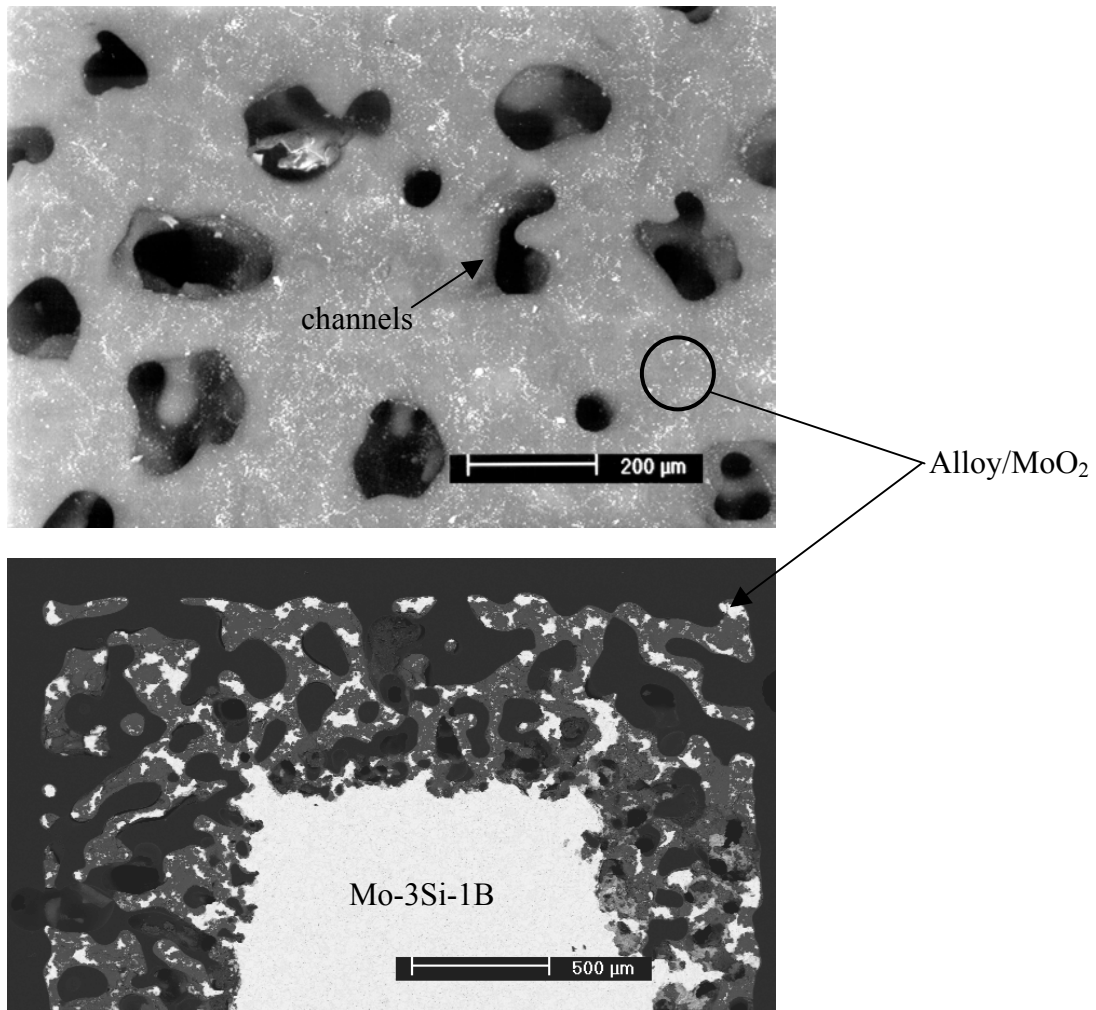


**Figure 5.2.5: Surface micrograph and cross-section of Mo-3Si-1B alloy exposed at 1100°C in dry air flowing at 10cm/sec for one hour. Channels exist within the borosilicate layer.**

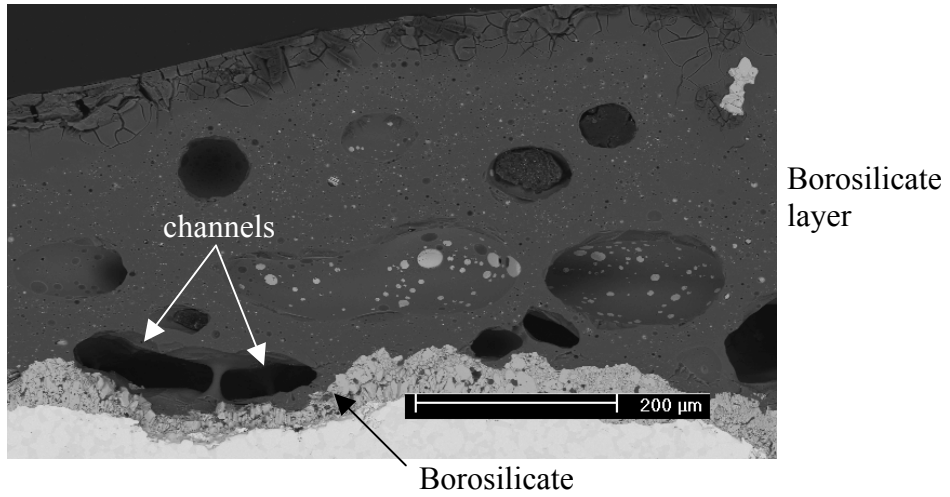
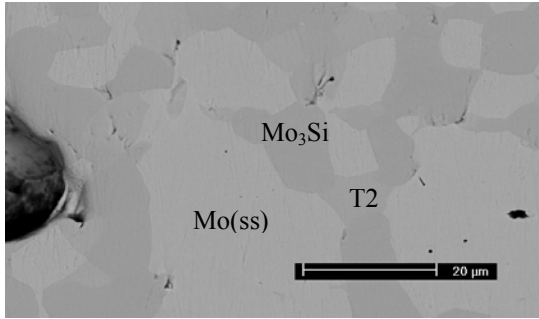
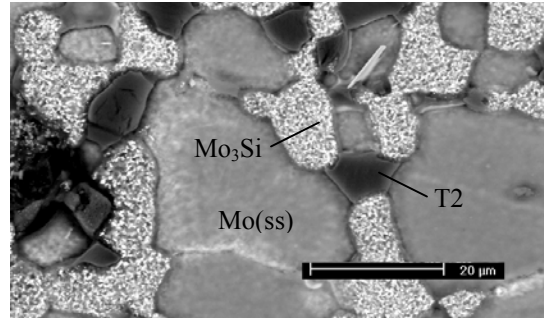


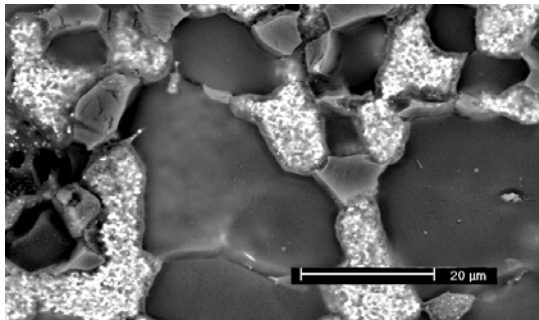
**Figure 5.2.6: Backscattered electron micrograph showing the cross-section of Mo-3Si-1B specimen exposed at 816°C in dry air flowing at 1cm/sec for one hour. Channels in the borosilicate are evident and the walls of these channels contain balls of liquid  $\text{MoO}_3$ .**



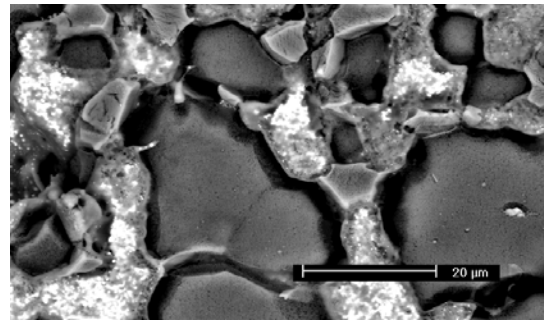
(a) as-processed



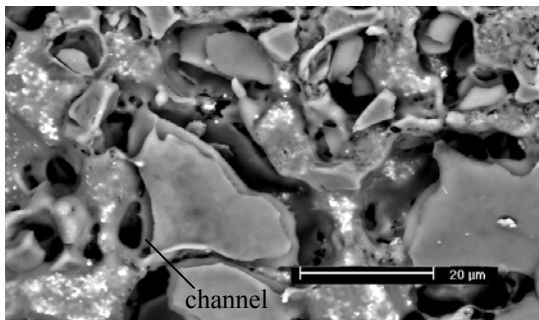
(b) 1 minute exposure



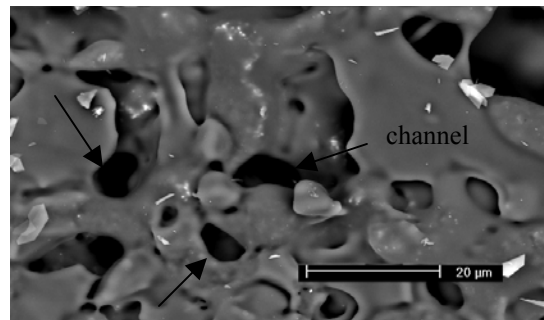
(c) 2 minute exposure



(d) 4 minute exposure

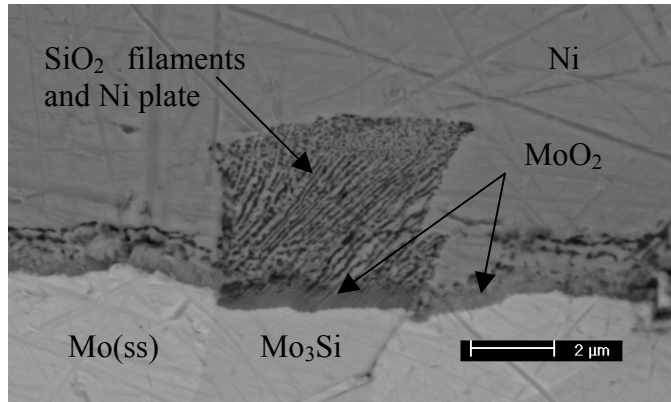


(e) 10 minute exposure

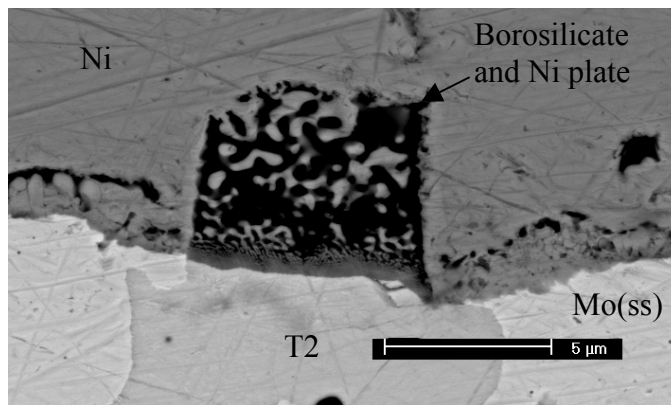


(f) 30 minute exposure

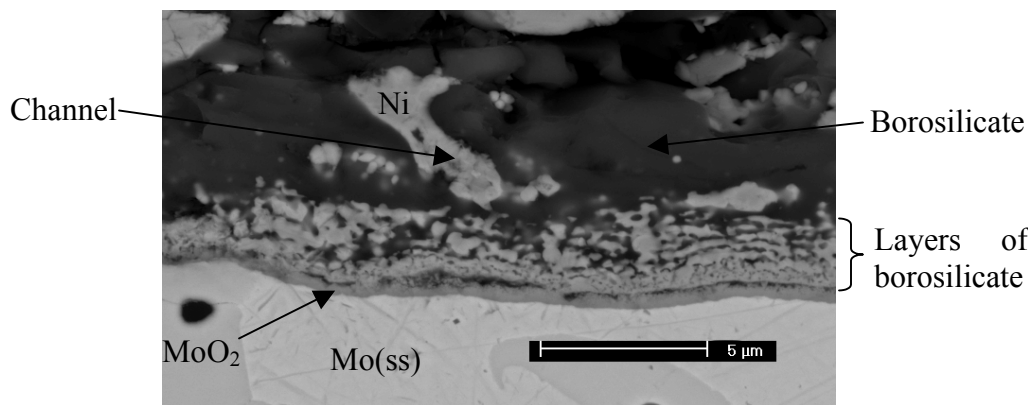
**Figure 5.2.7: Backscattered electron micrographs that show the borosilicate layer development on Mo-3Si-1B as a function of time after exposure at 1000°C in static laboratory air.**



(a) 1 minute exposure

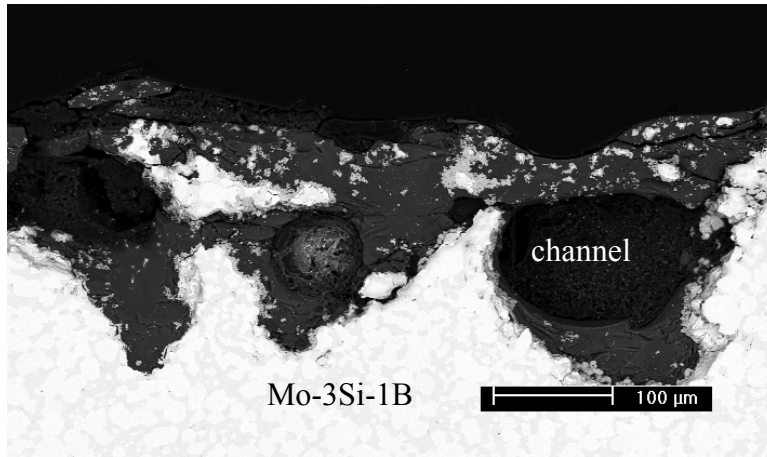


(b) 1 minute exposure

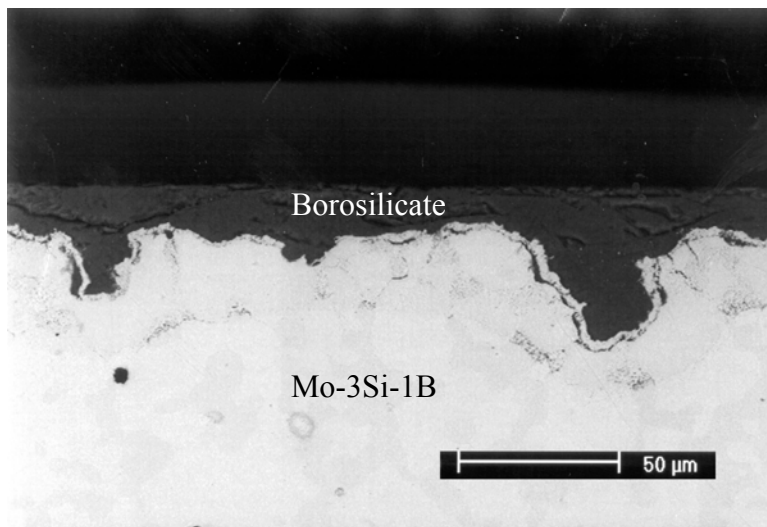


(c) 4 minute exposure

**Figure 5.2.8: Backscattered electron micrographs showing the cross-sectional views of Mo-3Si-1B exposed at 1000°C in static laboratory air as a function of exposure time. These specimens were plated with nickel prior to metallographic preparation.**



(a) Mo-3Si-1B exposed at 1100°C in static dry air for 3 hours.



(b) Mo-3Si-1B exposed at 1100°C in static laboratory air for 100 hours.

**Figure 5.2.9:** Backscattered electron micrographs that show characteristics of the borosilicate layer formed on Mo-3Si-1B. In (a), channels exist in the borosilicate layer and the attack of the alloy is more extensive in the vicinity of these channels. In (b), all of the channels have sealed but the borosilicate layer is thicker in those areas where the channels had caused more extensive attack.

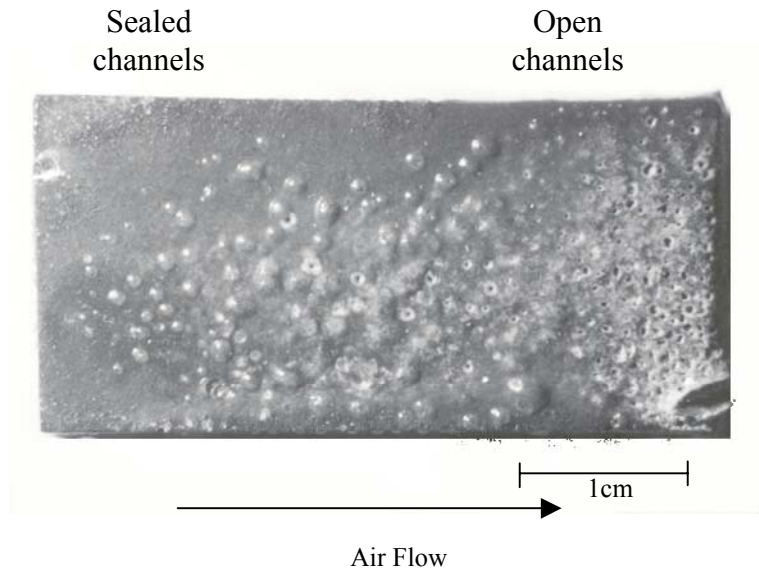
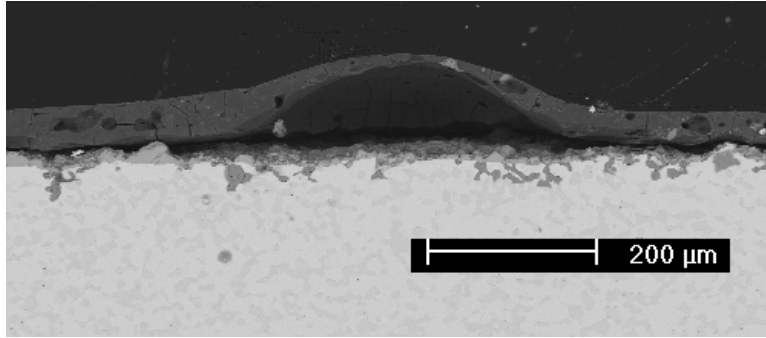


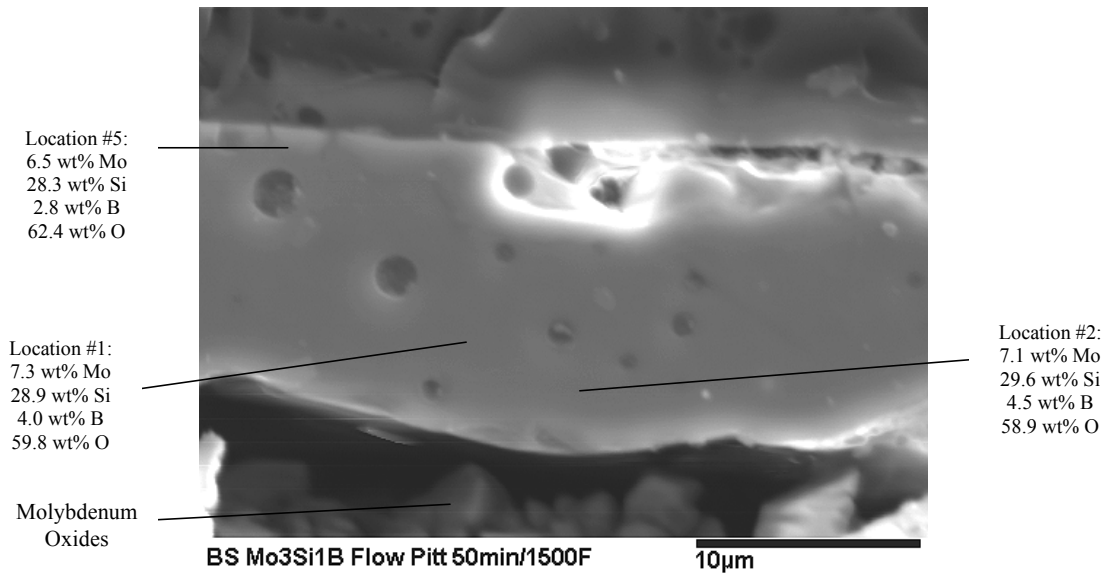
**Figure 5.2.10: Mo-3Si-1B exposed at 816°C in dry air flowing at 1cm/sec. Open channels are evident at the trailing edge of the specimen whereas the channels are sealed near the center of the specimen. (Ref. Shiela Woodard)**



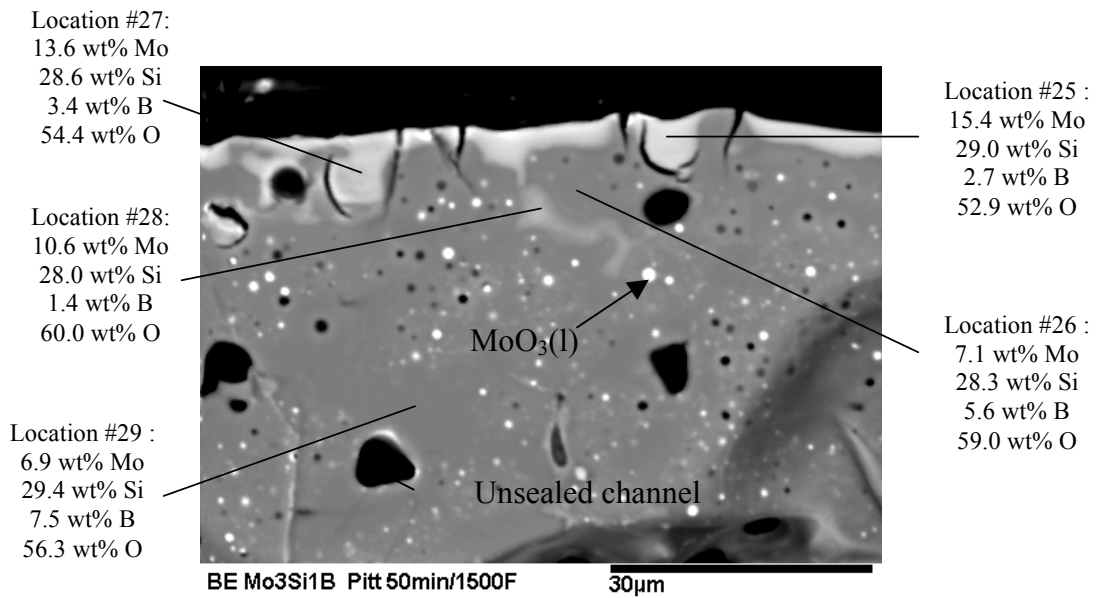
a) center of specimen.

Mo is soluble in the borosilicate

Mo is at higher concentrations at the trailing edge



b) leading edge.



c) trailing edge

**Figure 5.2.11: Cross-sectional views of the specimen described in Figure 5.2.10. (a) buckle in the borosilicate layer near the center of the specimen. (b) a section near the leading edge of the specimen showing spherical pores. (c) a cross-section near the trailing edge showing unsealed channels, spherical pores, and balls of MoO<sub>3</sub>.**

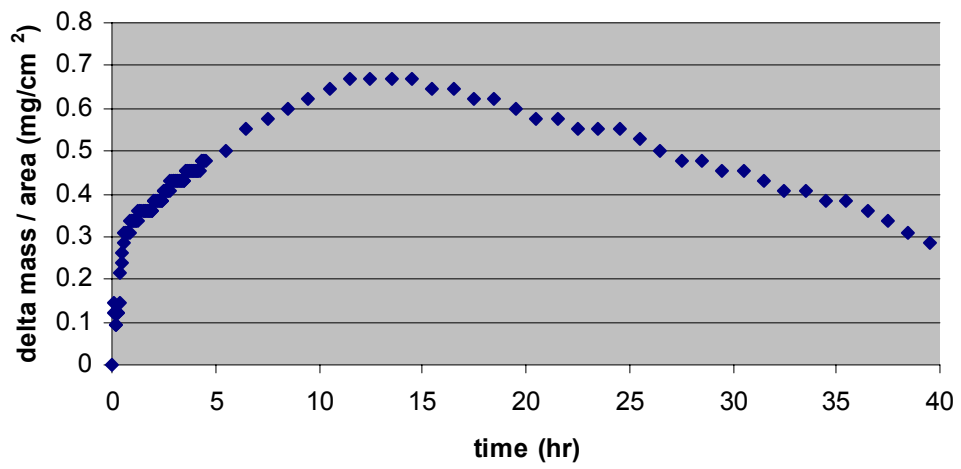
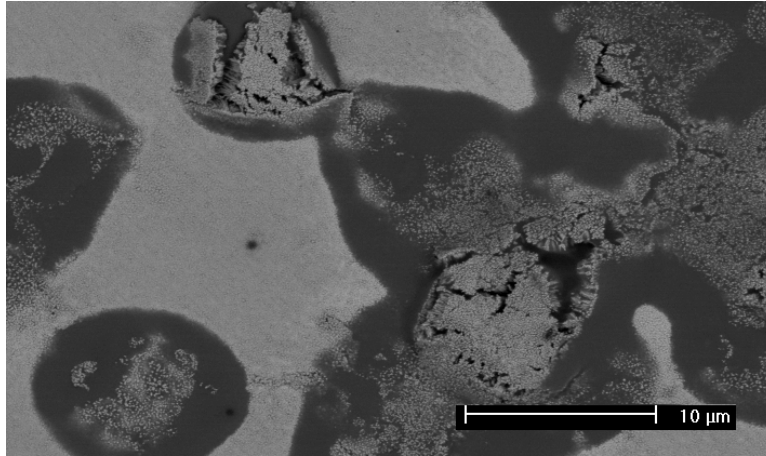
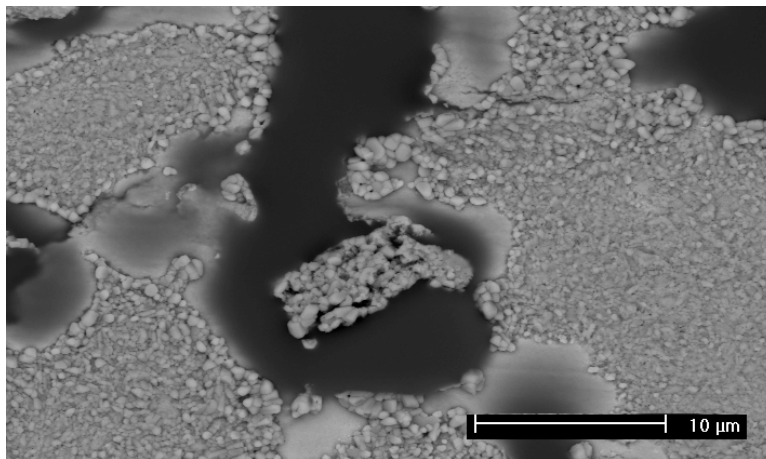


Figure 5.2.12: Weight change versus time data for the oxidation of Mo-3Si-1B exposed at 1000°C in argon flowing at 10cm/sec.



(a)



(b)

**Figure 5.2.13: Backscattered electron micrographs of Mo-3Si-1B exposed at 1000°C in argon flowing at 10cm/sec for (a) 2 hours and (b) 18 hours.**

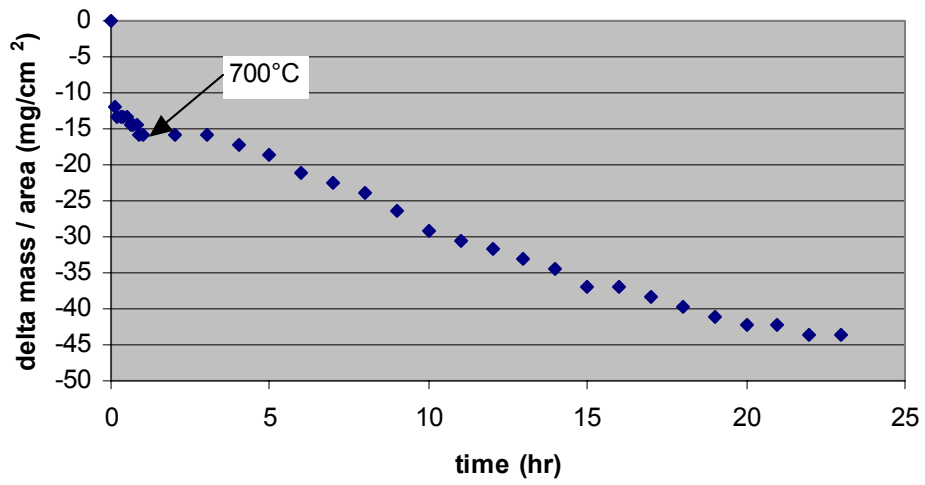
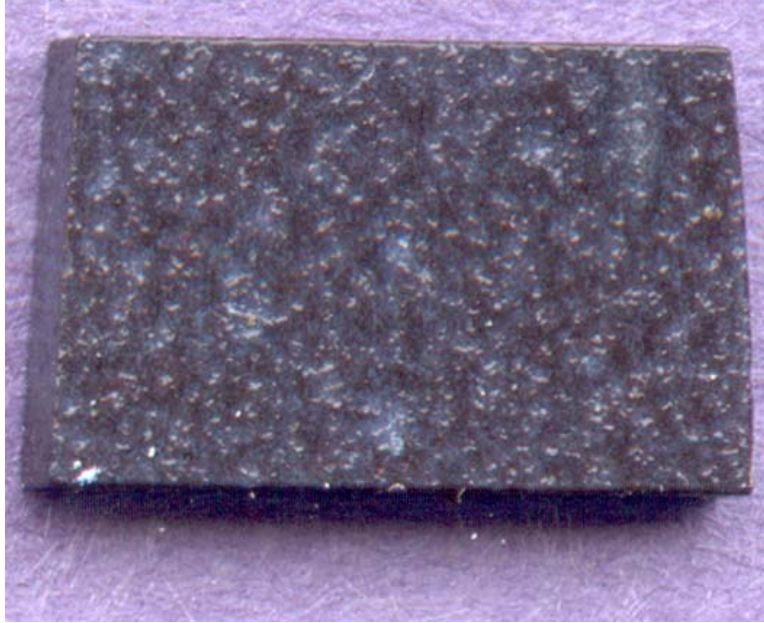


Figure 5.2.14: Weight change versus time data for Mo-3Si-1B exposed at 1000°C in dry air flowing at 1cm/sec for one hour followed by an exposure at 700°C in dry air flowing at 1cm/sec for an additional 20 hours with the specimen remaining in situ.

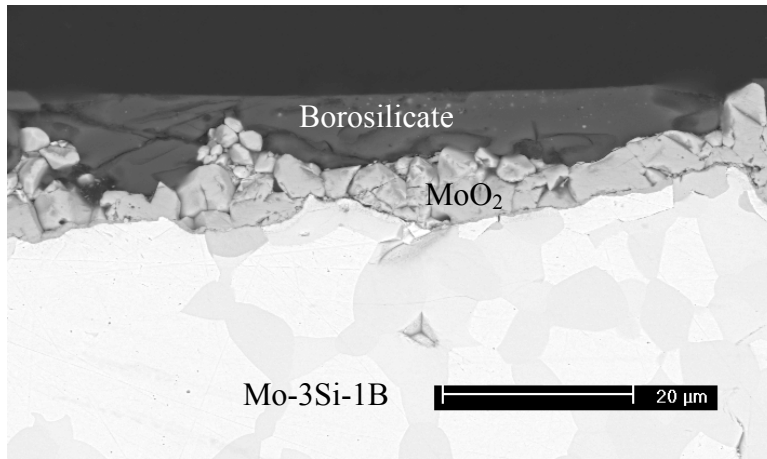


(a)

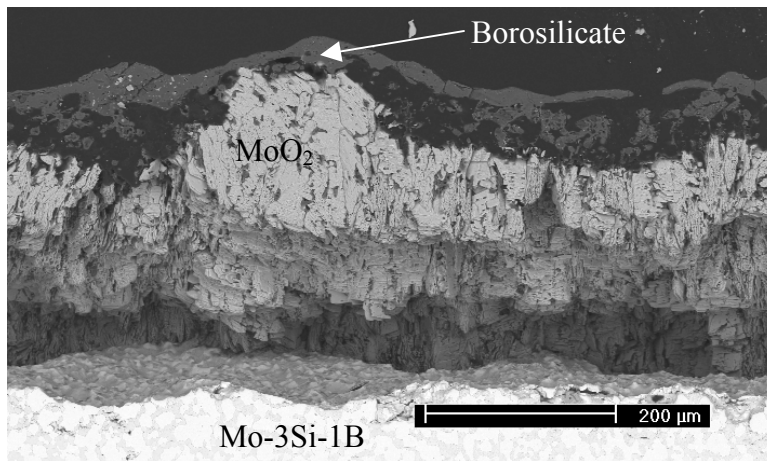


(b)

**Figure 5.2.15: Surface photographs of Mo-3Si-1B exposed at (a) 1000°C in dry air flowing at 1cm/sec for one hour (pretreatment) and (b) 1000°C in dry air flowing at 1cm/sec for one hour (pretreatment) followed by an exposure at 700°C in dry air flowing at 1cm/sec for 20 hours with the specimen in situ.**

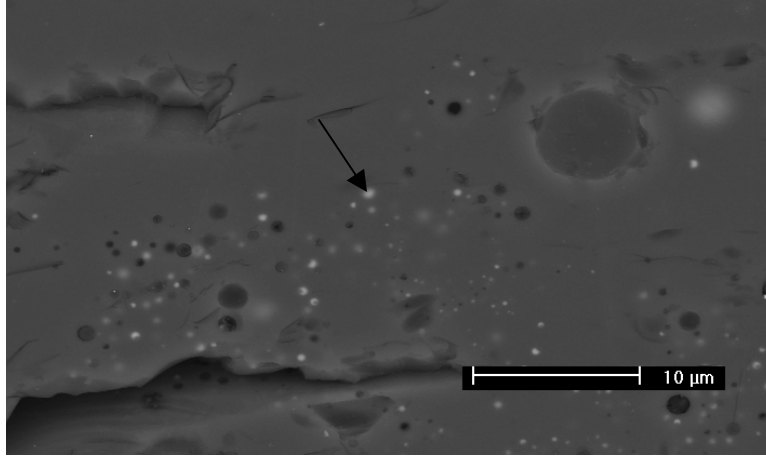


(a)

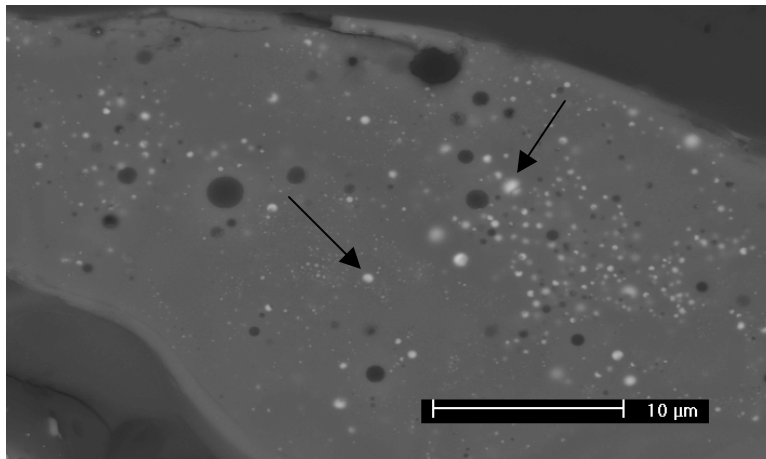


(b)

**Figure 5.2.16: Backscattered electron micrographs of Mo-3Si-1B exposed at (a) 1000°C in dry air flowing at 1cm/sec for one hour (pretreatment) and (b) 1000°C in dry air flowing at 1cm/sec for one hour (pretreatment) followed by an exposure at 700°C in dry air flowing at 1cm/sec for 20 hours with the specimen in situ.**



(a)



(b)

**Figure 5.2.17: Backscattered electron micrograph of the borosilicate layer on Mo-3Si-1B exposed at (a) 1000°C in dry air flowing at 1cm/sec for 20 hours and (b) 1000°C in dry air flowing at 1cm/sec for one hour (pretreatment) followed by an exposure at 700°C in dry air flowing at 1cm/sec for 20 hours with the specimen in situ.**

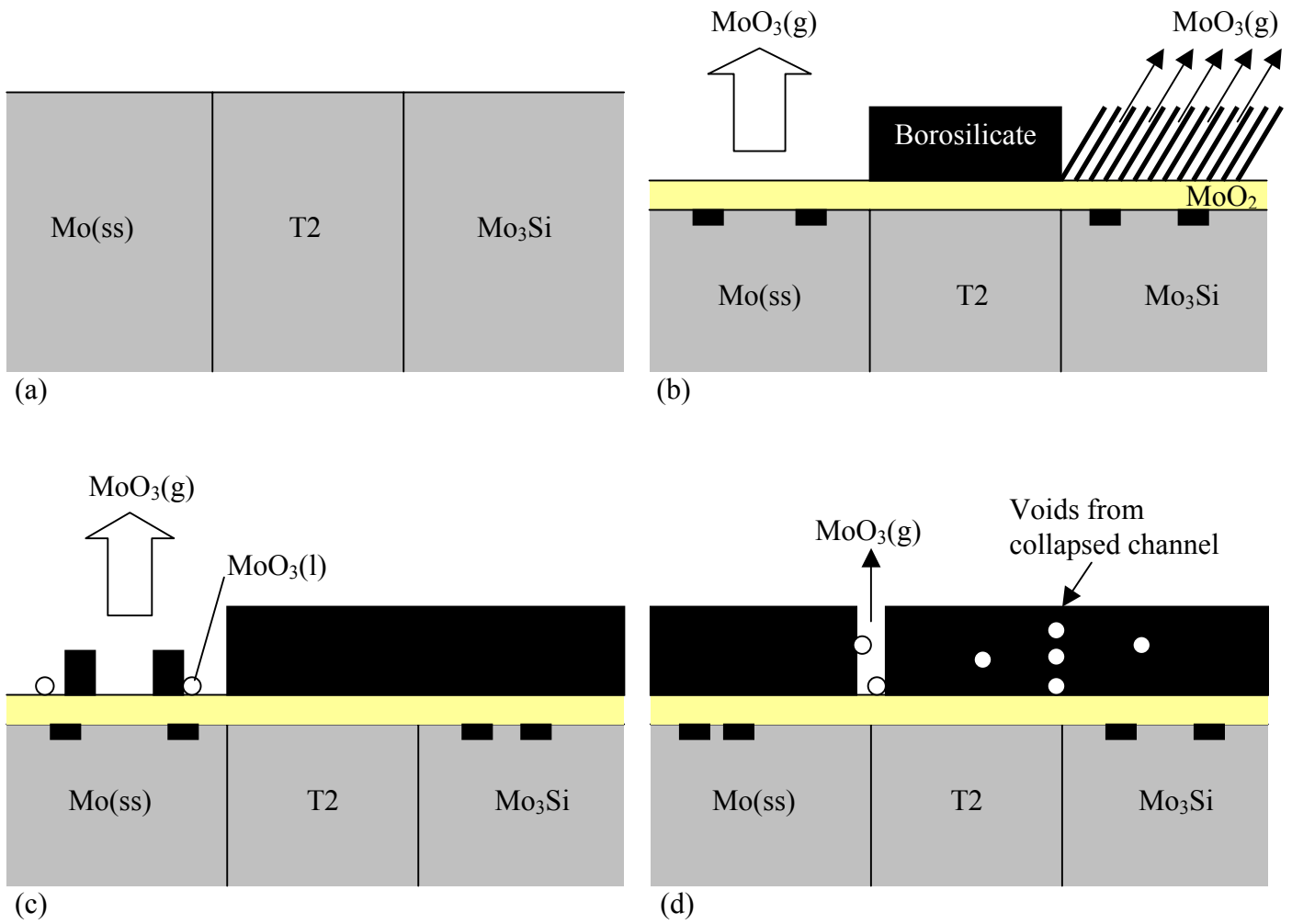


**Figure 5.2.18: Sketches illustrating schematically the development of the borosilicate layer on the three phases in the Mo-3Si-1B upon exposure to air at temperatures of 816°C and higher**

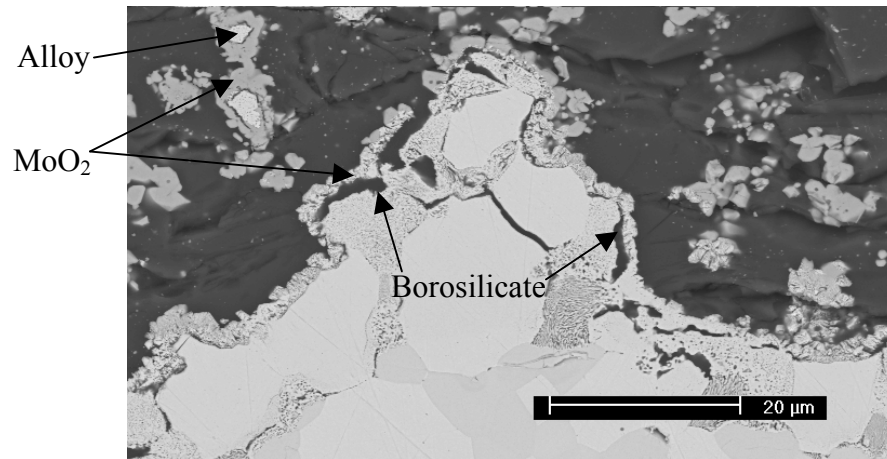


**Figure 5.2.19: Backscattered electron micrograph showing the Mo-3Si-1B alloy after seven days in static laboratory air at 1000°C. Particles of alloy covered with MoO<sub>2</sub> are evident in the borosilicate and borosilicate can be seen to have developed beneath the layer of MoO<sub>2</sub>.**

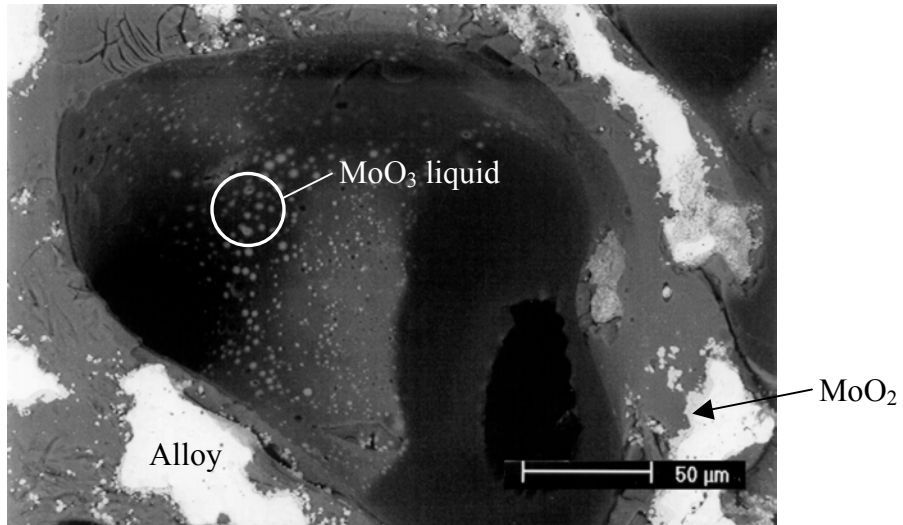


**Figure 5.3.1:** Backscattered electron cross-sectional micrograph taken through a channel in a layer of the borosilicate. Spheres of MoO<sub>3</sub> can be seen on the walls of the channel. In the borosilicate adjacent to the channel, only MoO<sub>2</sub> on particles of the alloy are evident.

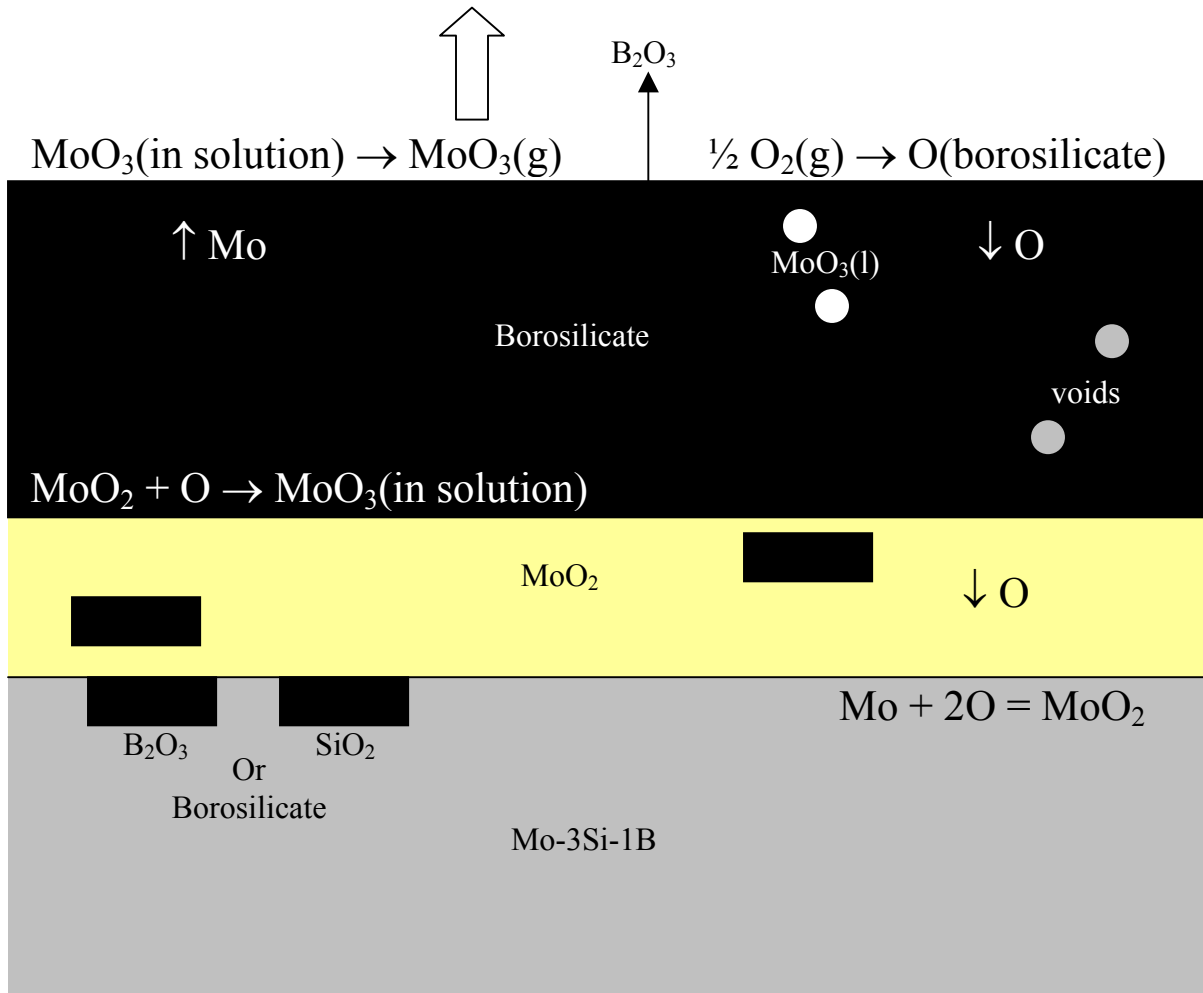
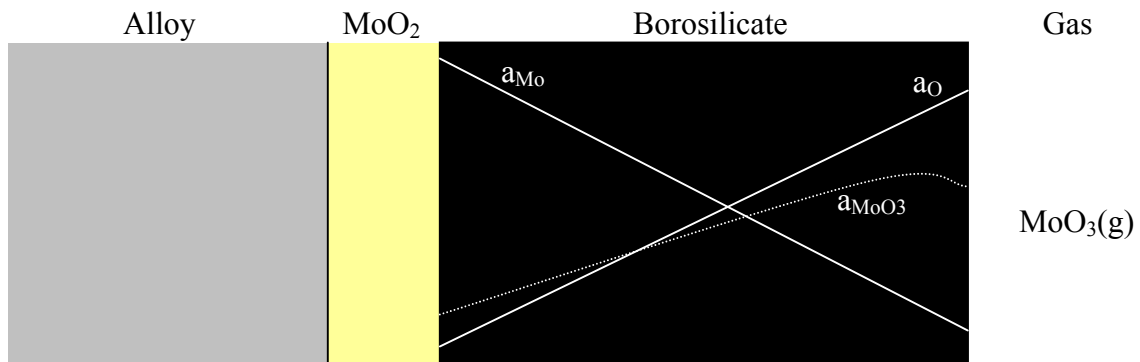
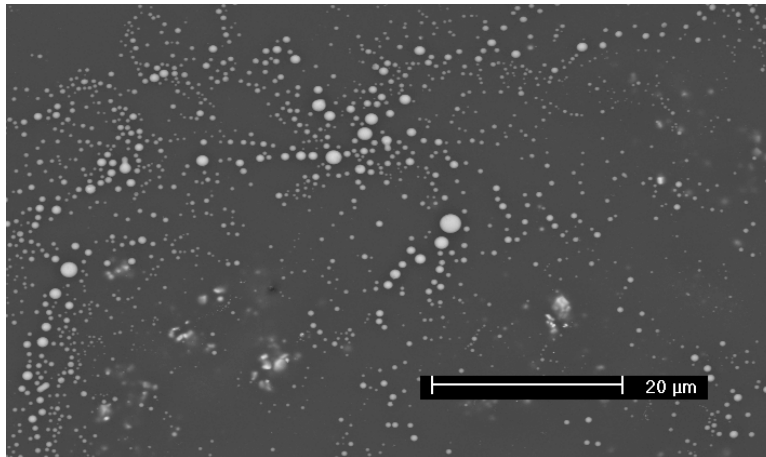


Figure 5.3.2: Schematic diagram to show a possible mechanism for transport through the borosilicate layer on Mo-3Si-1B along with formation of MoO<sub>2</sub> and vaporization of MoO<sub>3</sub> and B<sub>2</sub>O<sub>3</sub>.



**Figure 5.3.3:** Schematic showing the variation of the activity of molybdenum, and the activity of oxygen across a borosilicate layer on Mo-3Si-1B assuming that the activity of MoO<sub>2</sub> throughout the borosilicate layer is constant.



**Figure 5.3.4: Backscattered electron micrograph of the surface of a borosilicate layer formed upon Mo-3Si-1B after one hour in dry flowing air (10cm/sec) at 1100°C. Spheres of MoO<sub>3</sub> are present in the borosilicate just beneath the borosilicate-gas interface.**

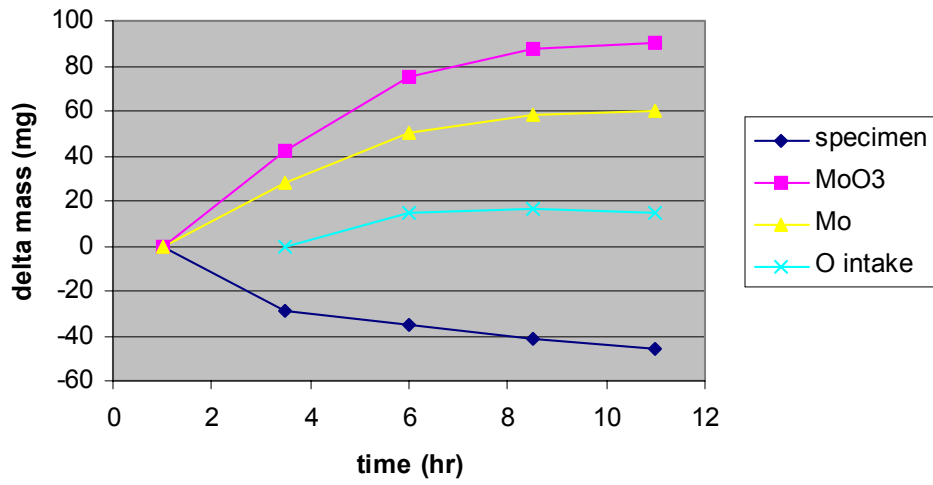


Figure 5.3.5: Mo-3Si-1B pretreated at 1000°C in dry air flowing at 1cm/sec for one hour followed by additional exposures under the same conditions, along with the weight of the MoO<sub>3</sub> deposition and the calculated Mo weight associated with additional exposures.

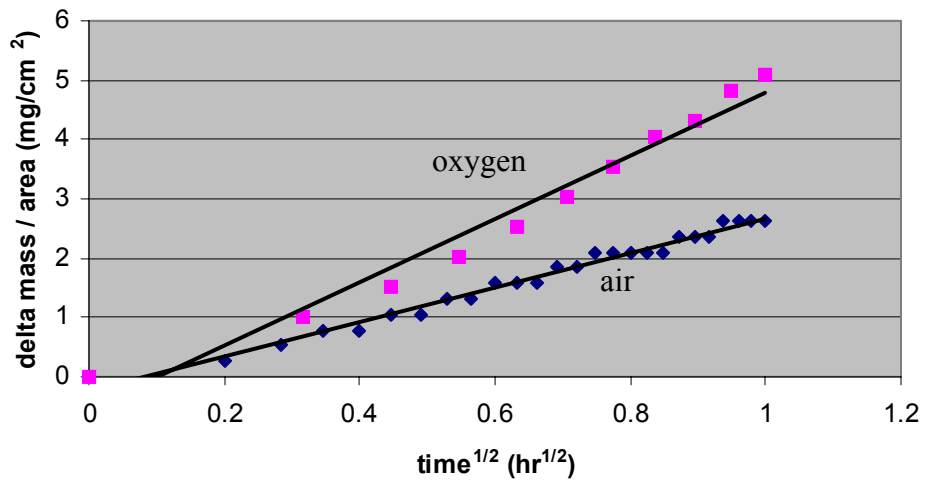
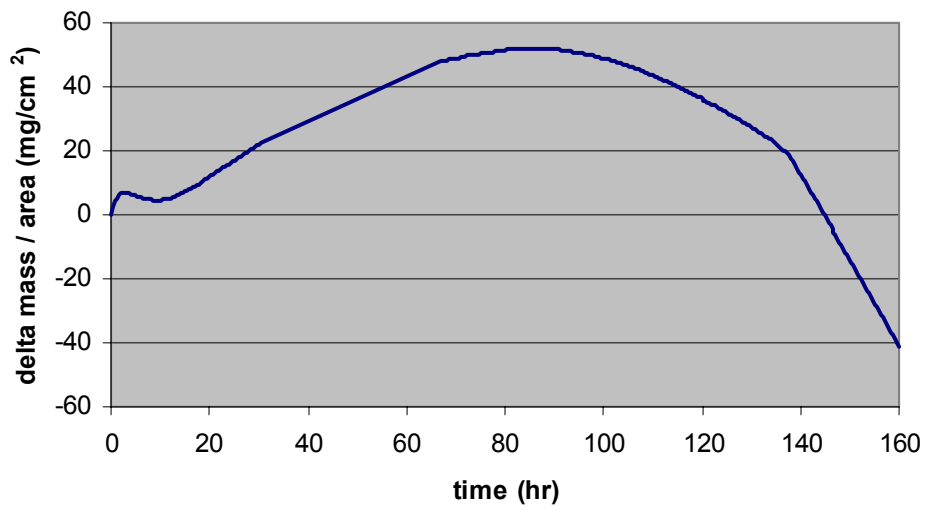


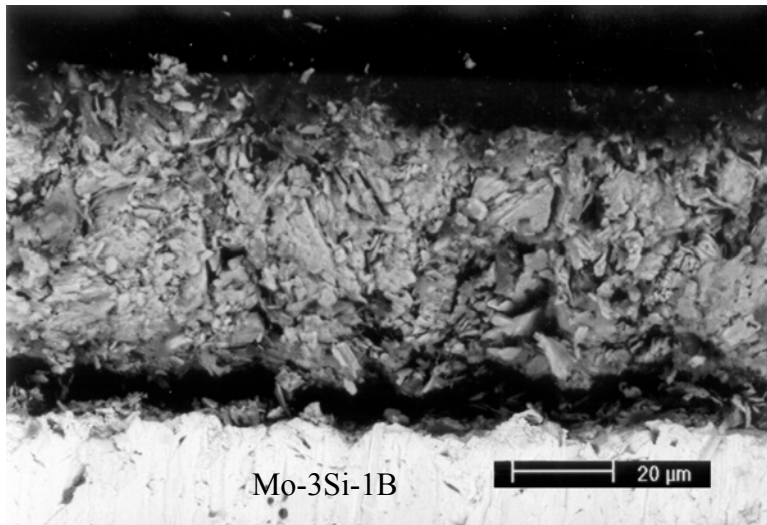
Figure 5.4.1: Weight change versus the square root of time data for the oxidation of Mo-3Si-1B exposed at 700°C in dry air flowing at 1cm/sec and oxygen flowing at 10cm/sec. The results show that these data conform to a parabolic rate law and weight gains rather than weight losses are observed.



**Figure 5.4.2: Weight change versus time data for the oxidation of Mo-3Si-1B exposed at 700°C in dry air flowing at 1cm/sec. For these long oxidation times, weight losses eventually occur.**



**Figure 5.4.3: Optical macrograph of Mo-3Si-1B specimen after 160 hours of oxidation where the weight change versus time data are presented in Figure 5.4.2.**



Mo oxide  
~42 $\mu\text{m}$   
From weight gain  
 $x = 16.5\mu\text{m}$ .

**Figure 5.4.4:** Backscattered electron micrograph of the oxide scale formed on Mo-3Si-1B after exposure at 700°C for one hour in dry air flowing at 1cm/sec. Calculation of the thickness of the oxide using the weight change data in Figure 5.4.1 gives an oxide thickness of 16.5 $\mu\text{m}$  whereas the actual thickness is 42 $\mu\text{m}$ . There must have been a weight loss of 3.83mg/cm<sup>2</sup>.

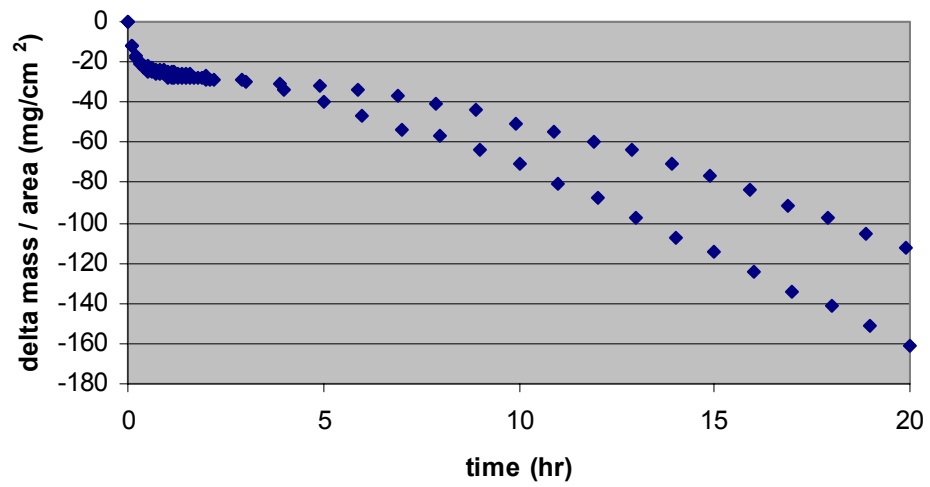


Figure 5.5.1: Weight change versus time data for the oxidation of two specimens of Mo-3Si-1B exposed to identical conditions (816°C in dry air flowing at 10cm/sec).

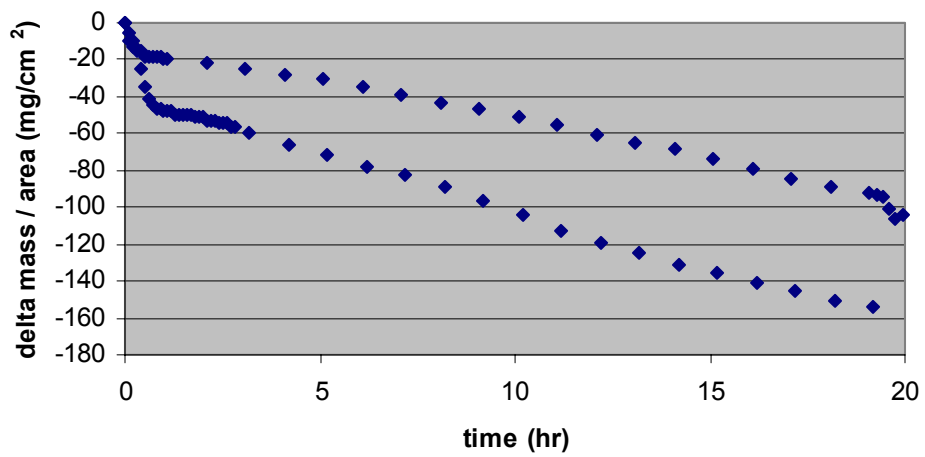


Figure 5.5.2: Weight change versus time data for the oxidation of two specimens of Mo-3Si-1B exposed to identical conditions (816°C in dry air flowing at 1cm/sec).

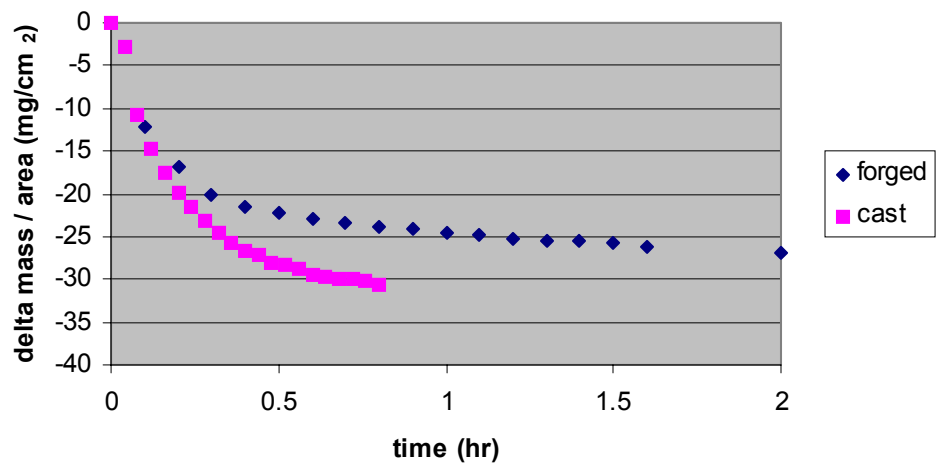


Figure 5.5.3: Comparison of weight change versus time data for the oxidation of forged and cast specimens exposed to identical conditions (816°C in dry air flowing at 10cm/sec).

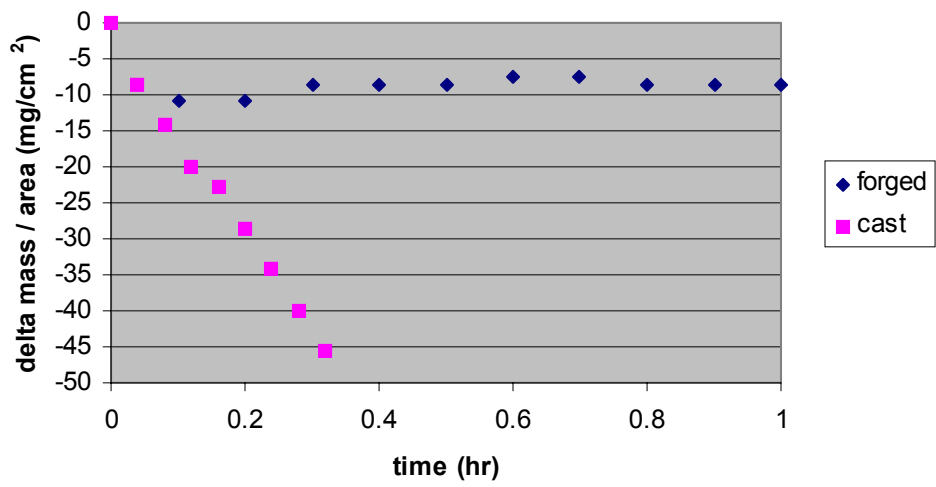


Figure 5.5.4: Comparison of weight change versus time data for the oxidation of forged and cast specimens exposed to identical conditions (1100°C in dry air flowing at 1cm/sec).

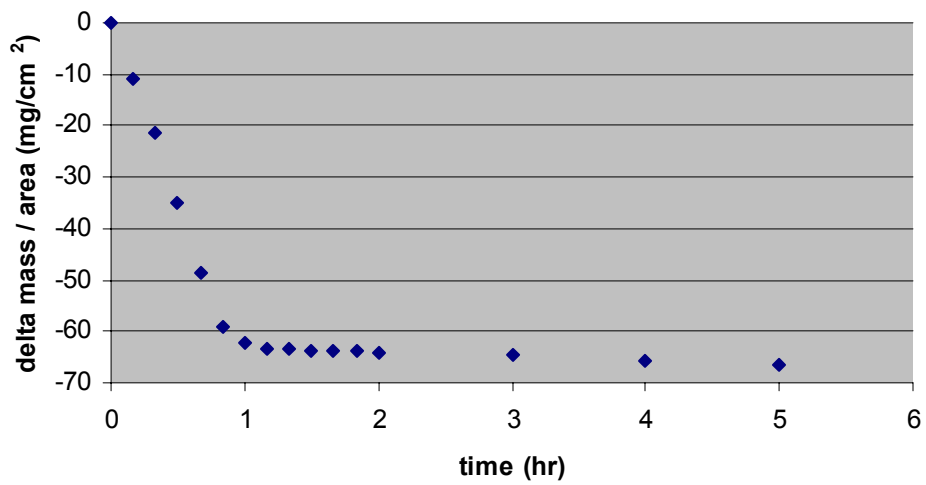
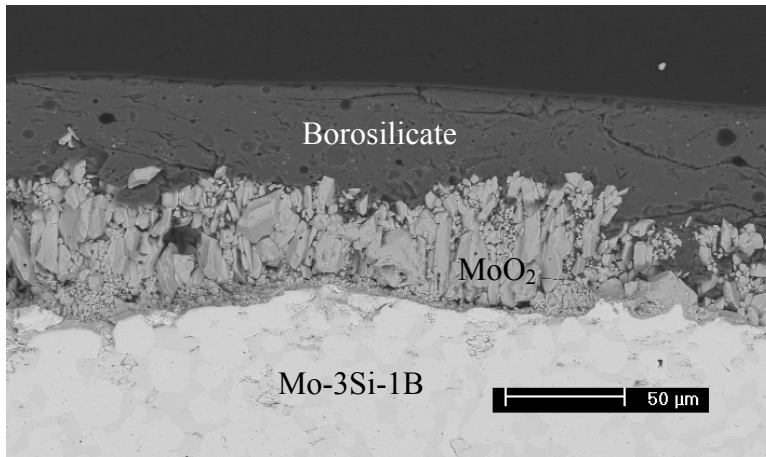
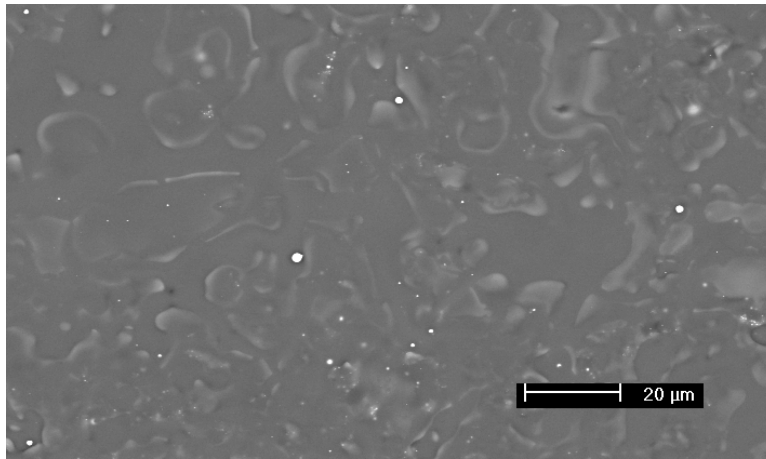


Figure 5.5.5: Weight change versus time data for the oxidation of Mo-3Si-1B exposed at 816°C in static laboratory air.



**Figure 5.5.6: Backscattered electron micrographs of the surface and cross-section of Mo-3Si-1B exposed at 816°C in static laboratory air for 5 hours.**

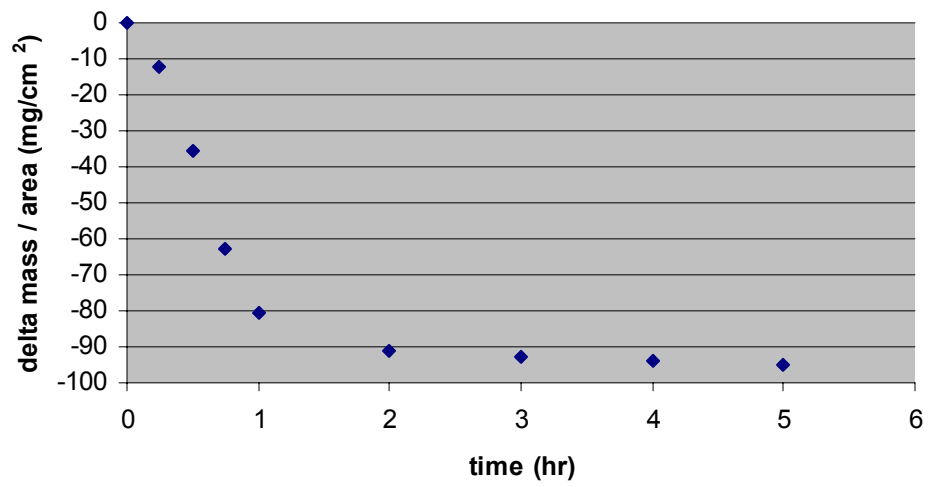
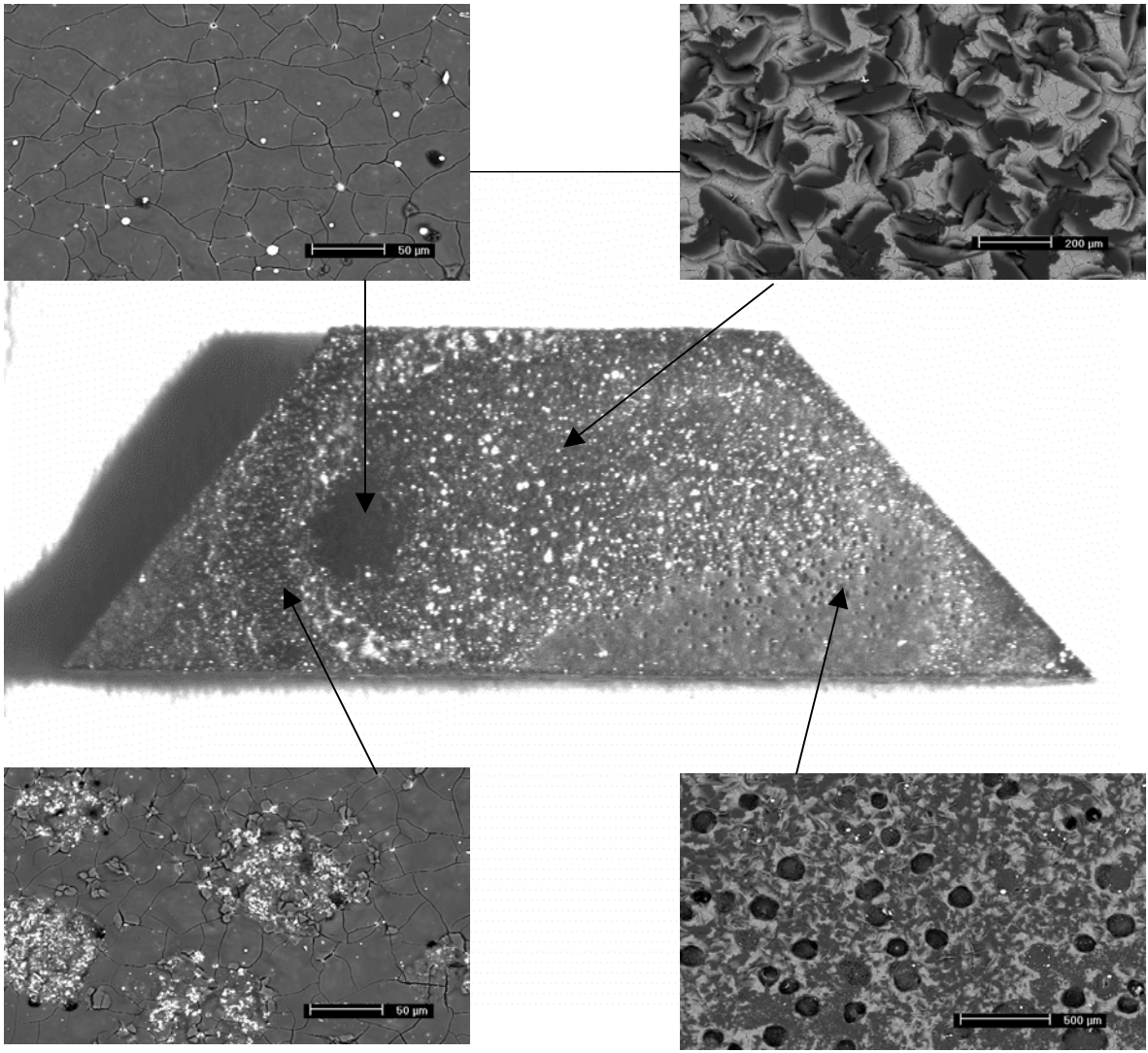
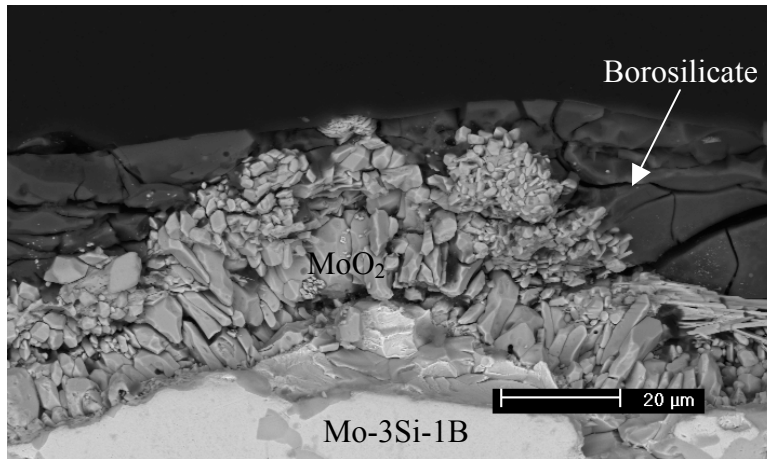
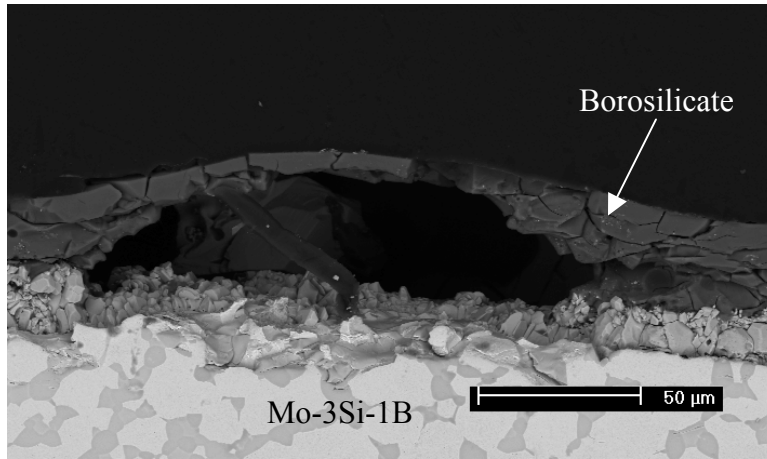


Figure 5.5.7: Weight change versus time data for the oxidation of Mo-3Si-1B exposed at 816°C in static dry air.



(a)



(b)

**Figure 5.5.8: (a) Optical and (b) backscattered electron micrographs of Mo-3Si-1B exposed at 816°C in static dry air for 1 hour.**

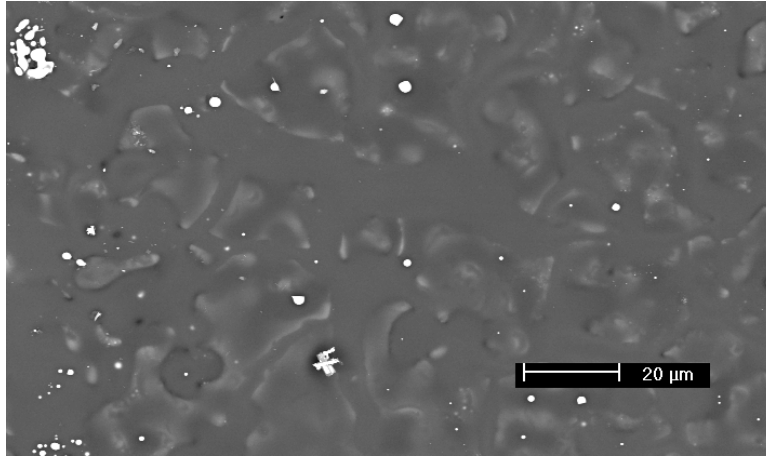


**Figure 5.5.9: Backscattered electron micrograph of the surface of Mo-3Si-1B exposed at 816°C in static dry air for 5 hours.**

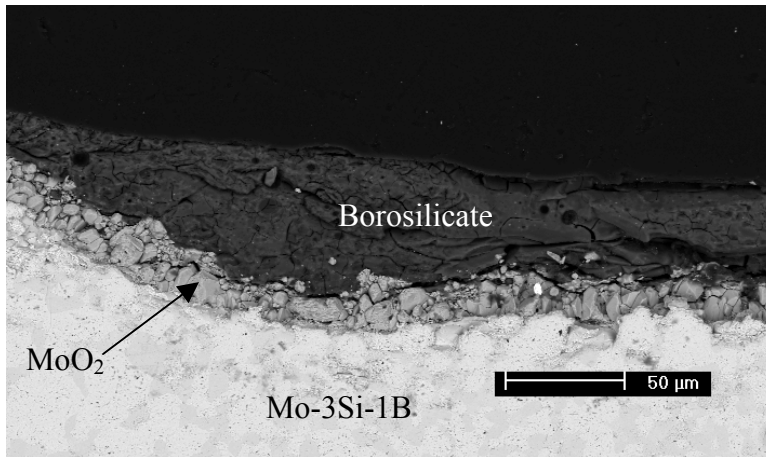
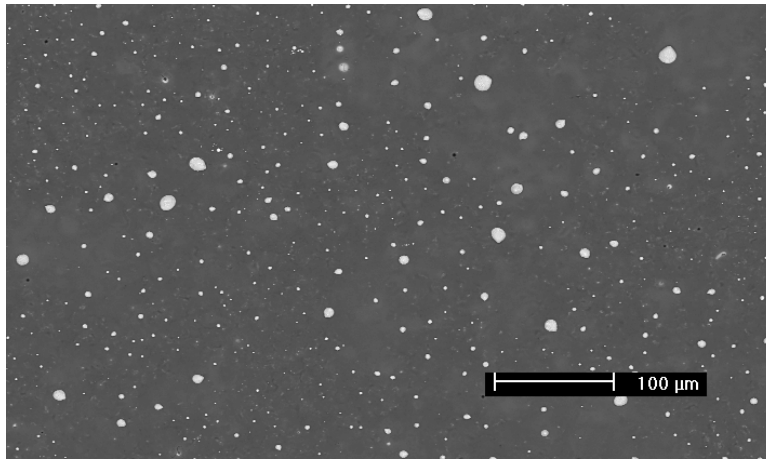


**Figure 5.5.10: Backscattered electron micrographs of the surface and cross-section of Mo-3Si-1B exposed at 816°C in static oxygen for 1 hour.**

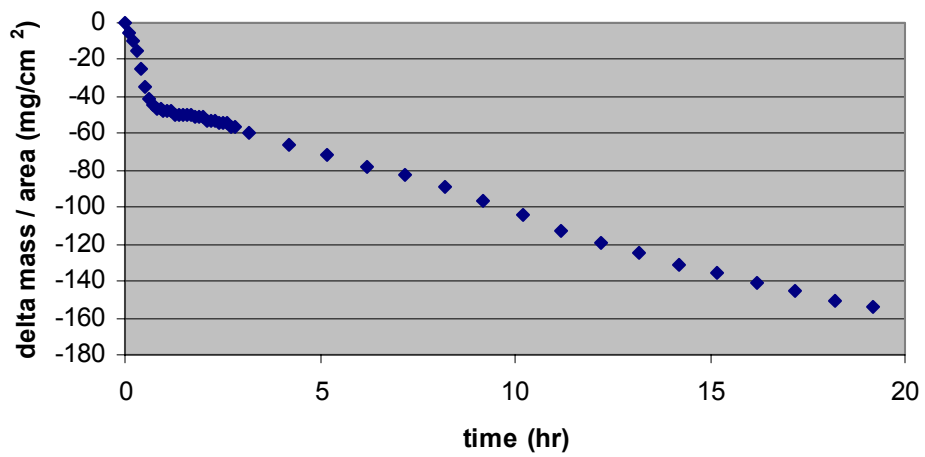
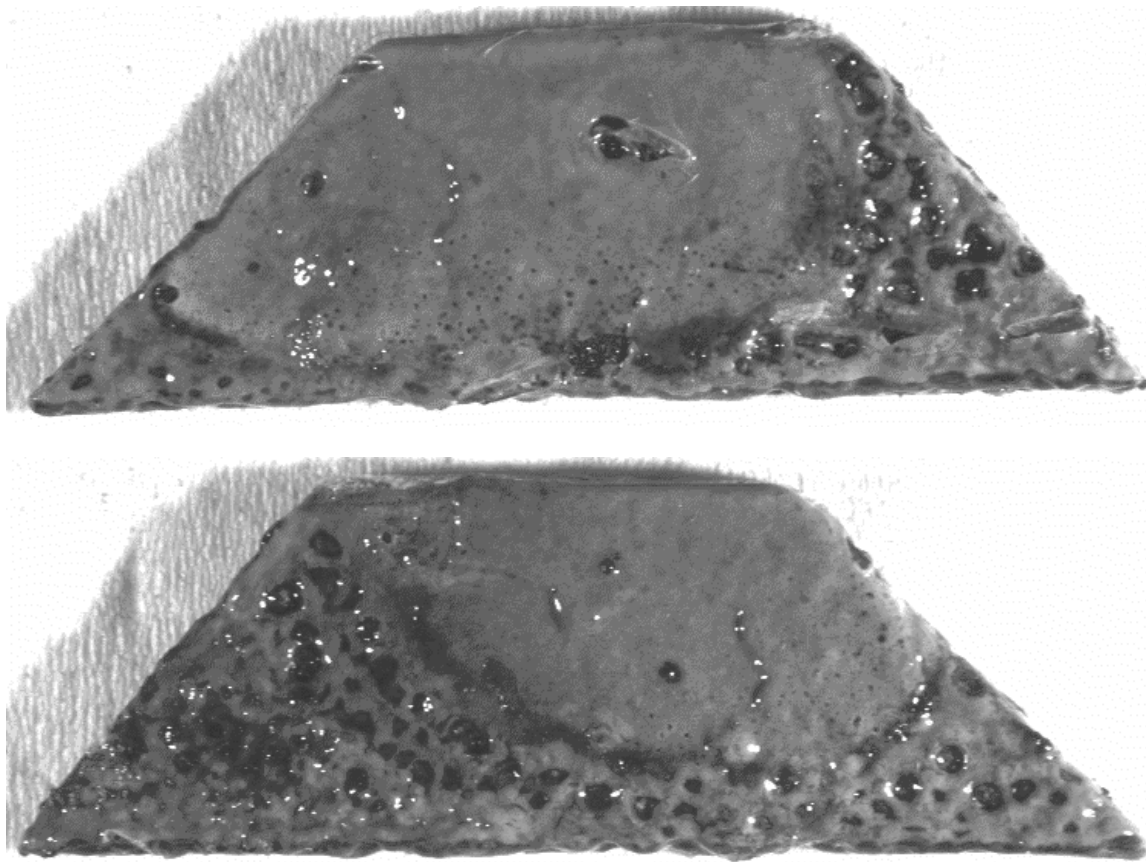


Figure 5.5.11: Weight change versus time data for the oxidation of Mo-3Si-1B exposed at 816°C in dry air flowing at 1cm/sec.



**Figure 5.5.12: Optical macrographs of Mo-3Si-1B exposed at 816°C in dry air flowing at 1cm/sec for 20 hours.**

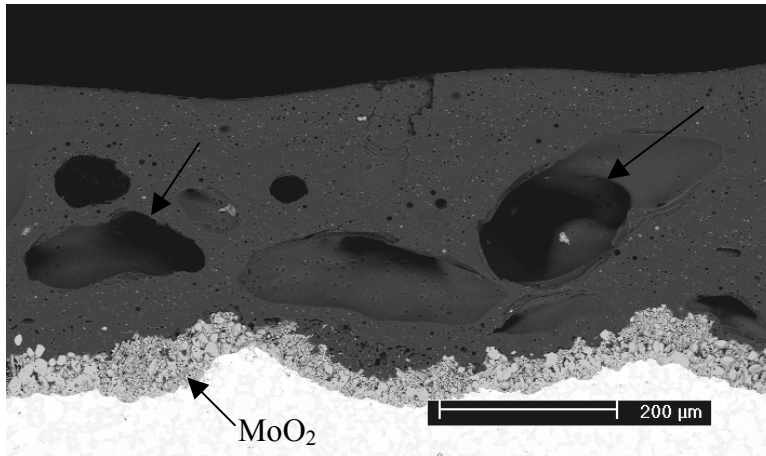
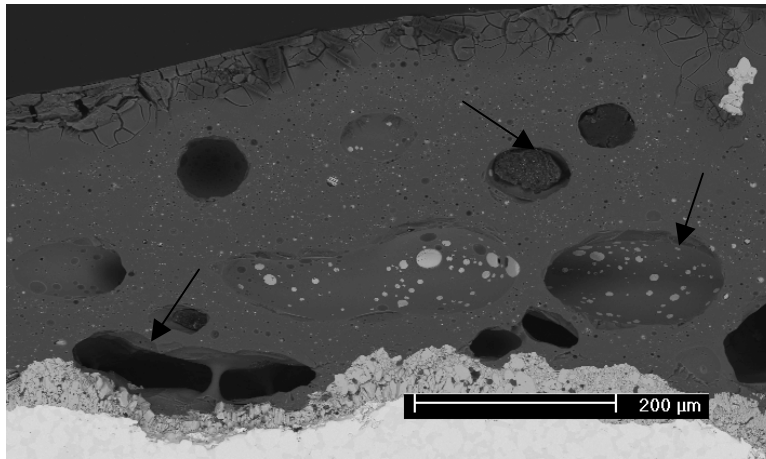


Figure 5.5.13: Backscattered electron micrographs of the cross-section of Mo-3Si-1B exposed at 816°C in slowly flowing dry air for 20 hours.

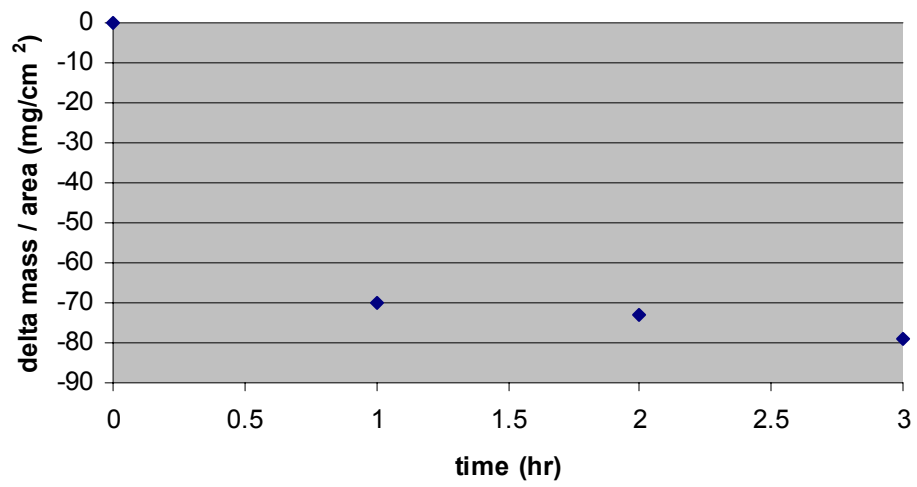
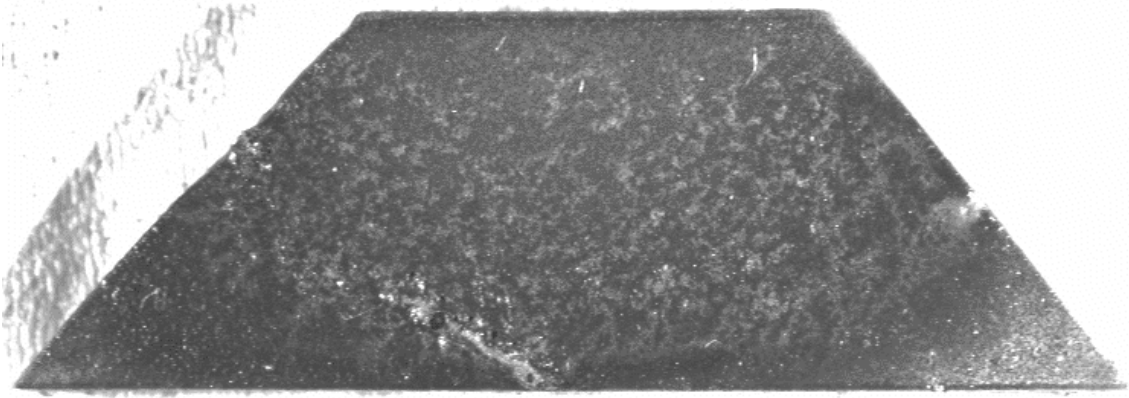
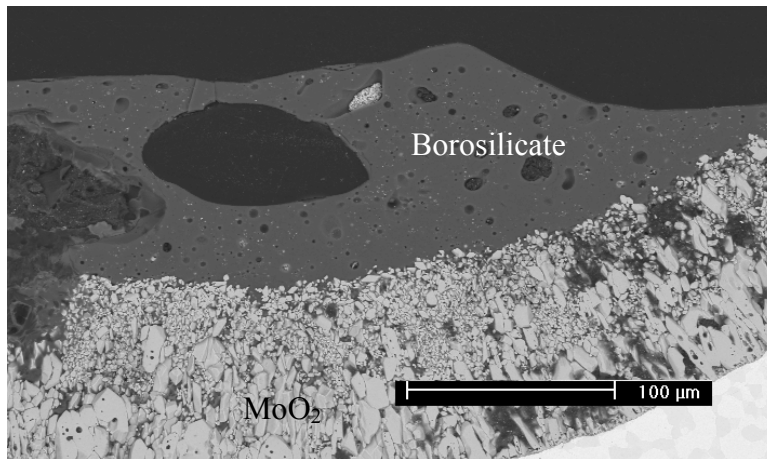
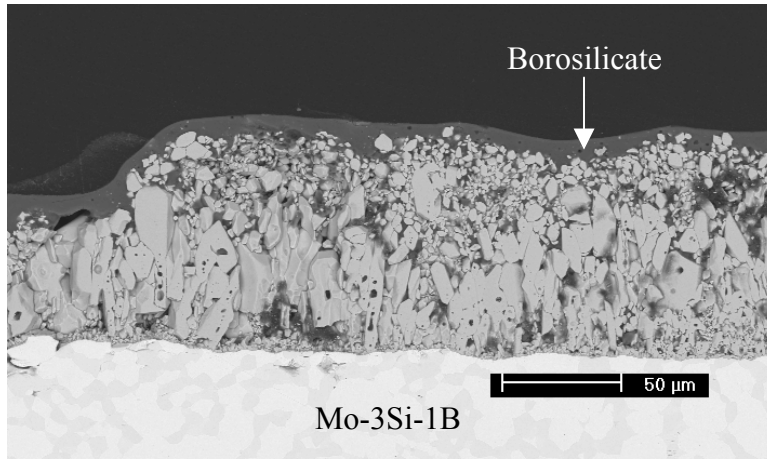


Figure 5.5.14: Weight change versus time data for the oxidation of Mo-3Si-1B exposed at 816°C in air + 0.1atm of H<sub>2</sub>O flowing at 1cm/sec.



**Figure 5.5.15: Optical macrograph of Mo-3Si-1B exposed at 816°C in air + 0.1atm of H<sub>2</sub>O flowing at 1cm/sec for 1 hour.**



**Figure 5.5.16: Backscattered electron micrographs of Mo-3Si-1B exposed at 816°C in air + 0.1atm H<sub>2</sub>O flowing at 1cm/sec for 3 hours.**

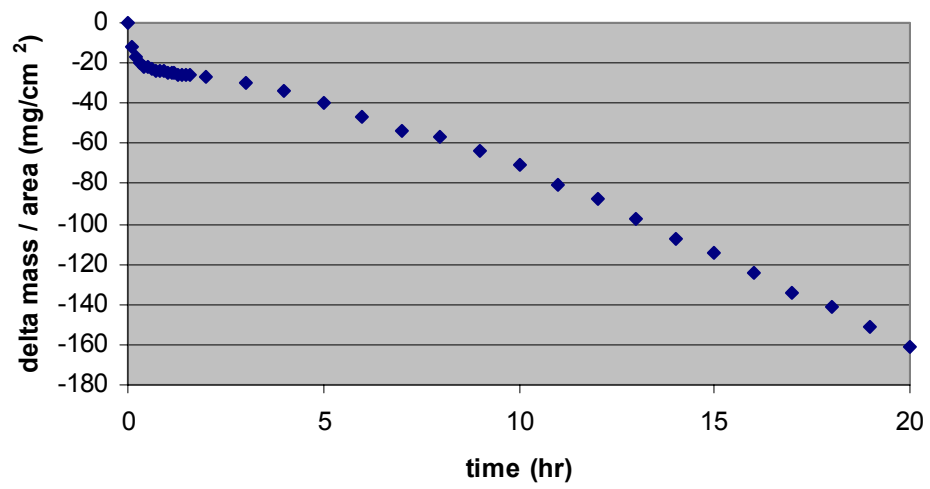


Figure 5.5.17: Weight change versus time data for the oxidation of Mo-3Si-1B exposed at 816°C in dry air flowing at 10cm/sec.

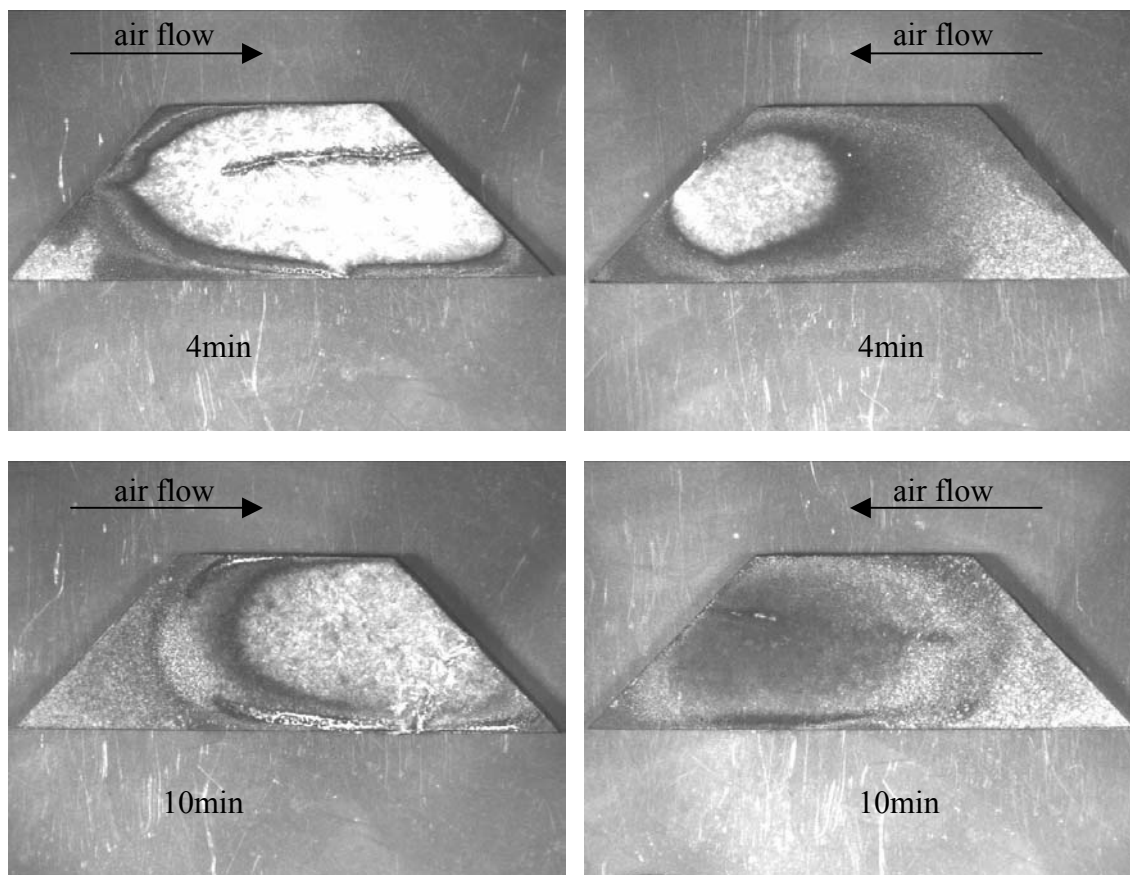
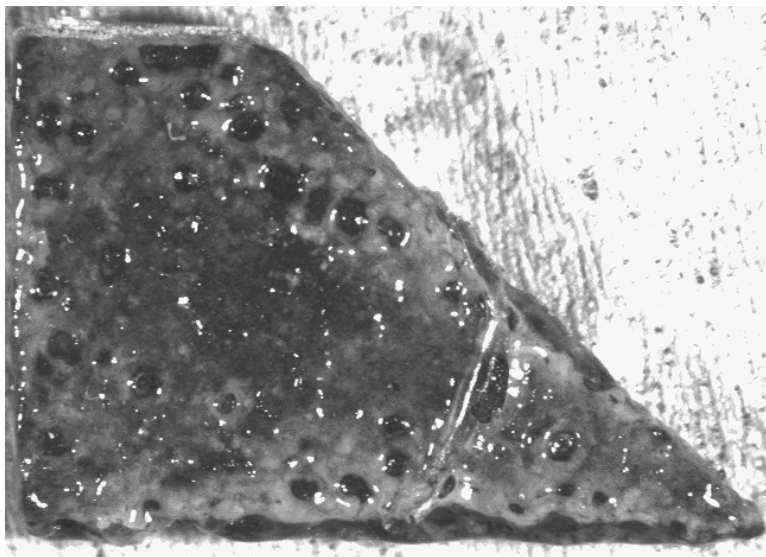
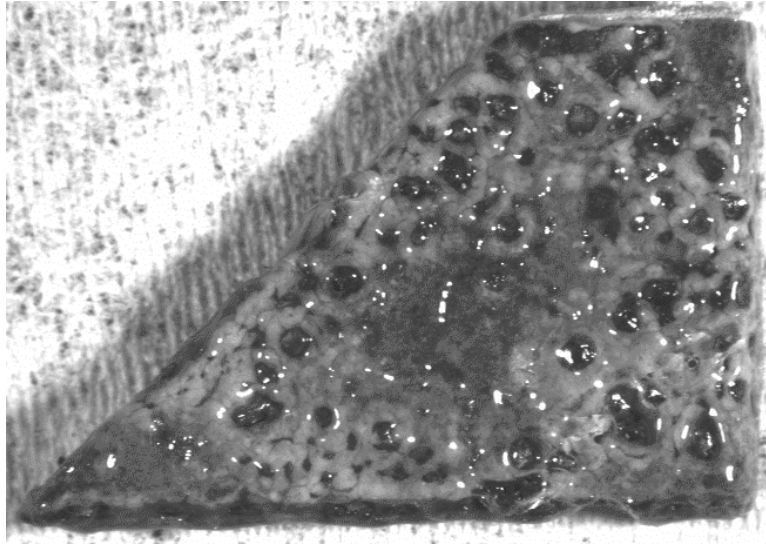
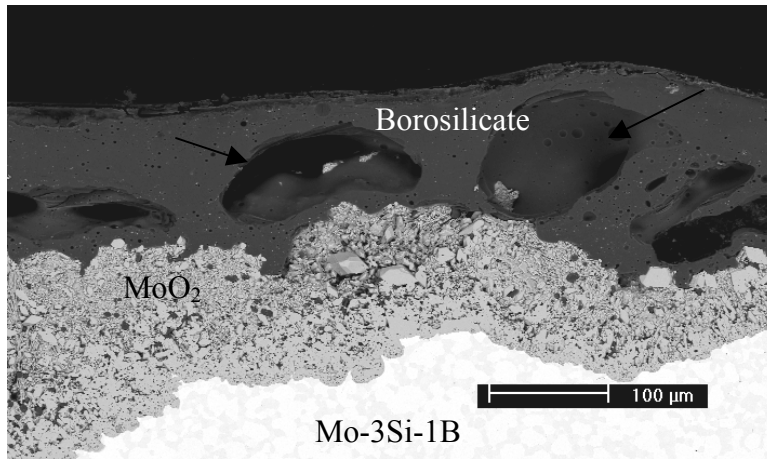
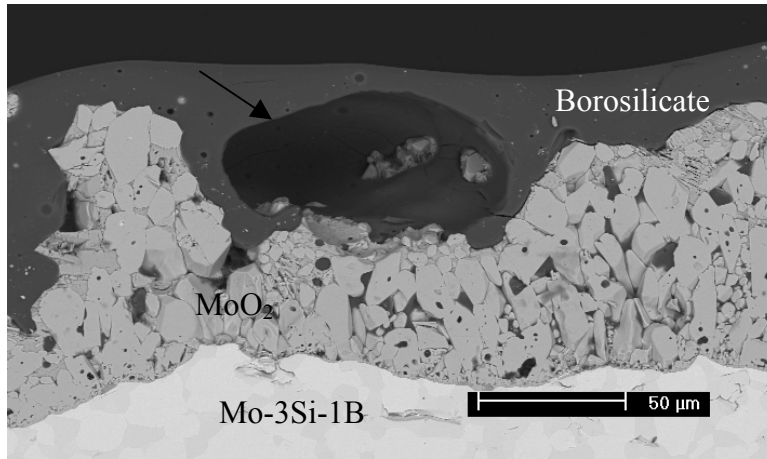


Figure 5.5.18: Optical macrographs of Mo-3Si-1B exposed at 816°C in dry air flowing at 10cm/sec.



**Figure 5.5.19: Optical macrographs of Mo-3Si-1B exposed at 816°C in dry air flowing at 10cm/sec for 20 hours.**



**Figure 5.5.20: Backscattered electron micrographs of Mo-3Si-1B exposed at 816°C in dry air flowing at 10cm/sec for 20 hours.**

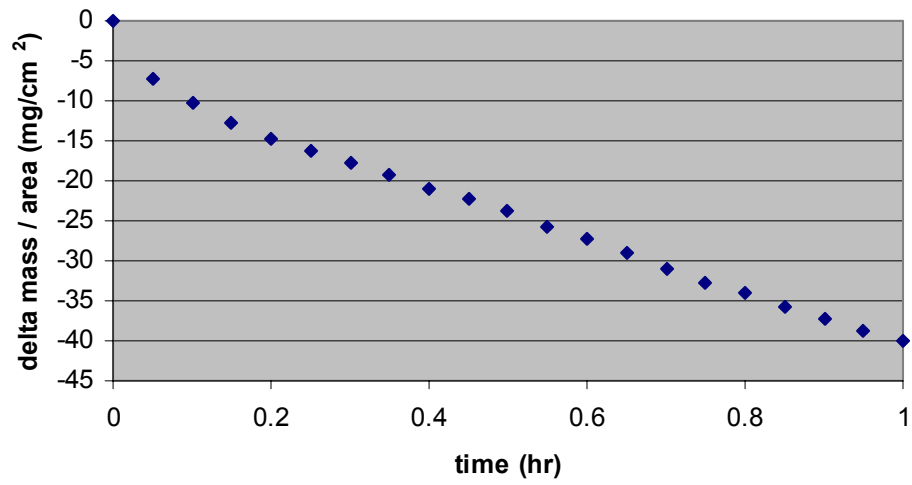
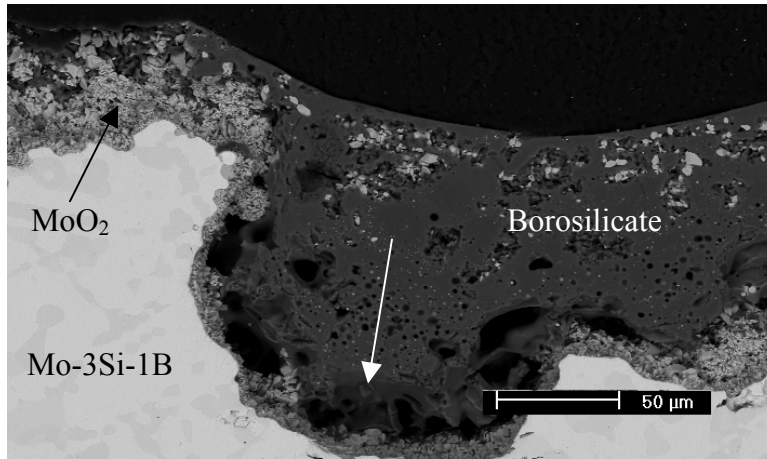


Figure 5.5.21: Weight change versus time for the oxidation of Mo-3Si-1B exposed at 900°C in dry air flowing at 1cm/sec.



**Figure 5.5.22: Backscattered electron micrograph of the cross-section of Mo-3Si-1B exposed at 900°C in dry air flowing at 1cm/sec for 1 hour.**

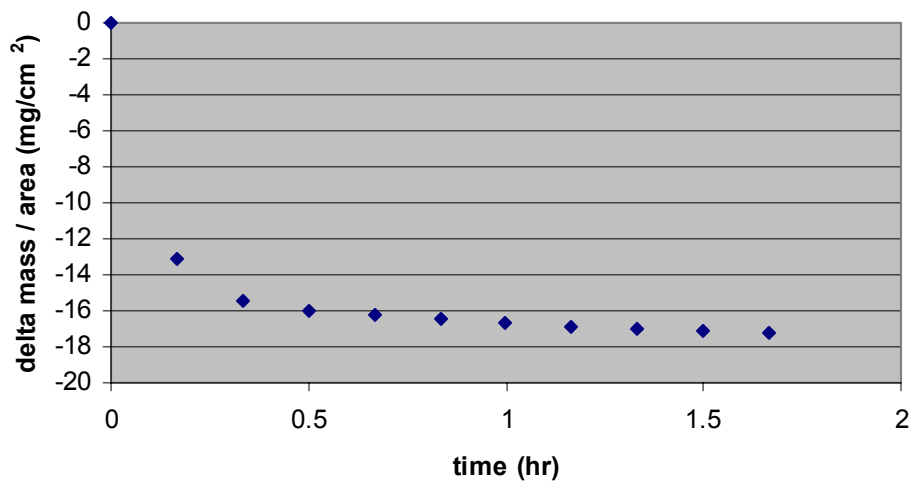
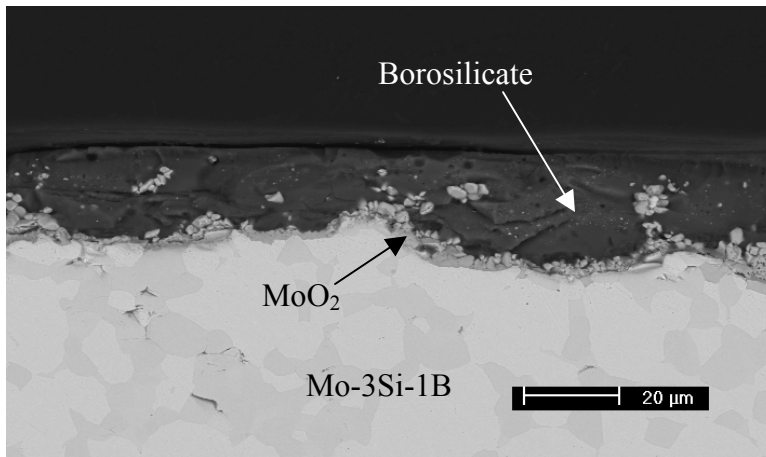
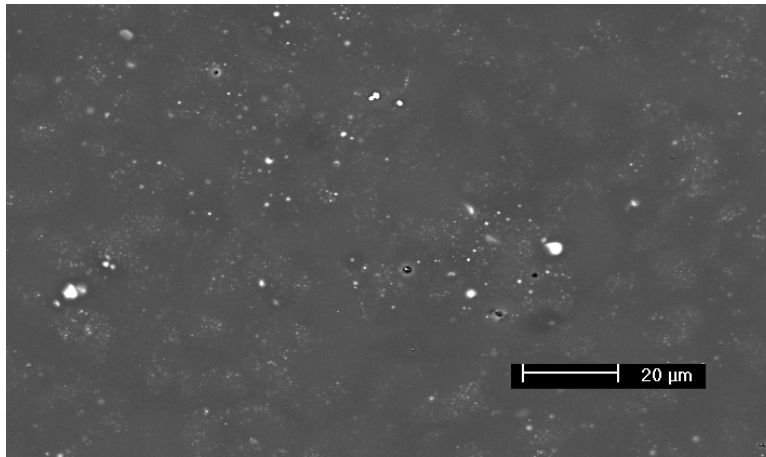


Figure 5.5.23: Weight change versus time for the oxidation of Mo-3Si-1B exposed at 1000°C in static laboratory air.



**Figure 5.5.24: Backscattered electron micrograph of Mo-3Si-1B exposed at 1000°C in static laboratory air for 110 minutes.**

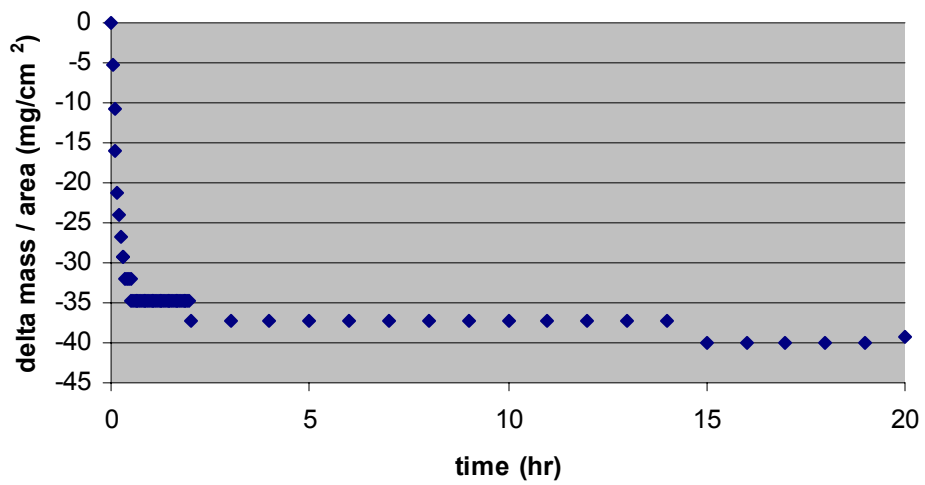
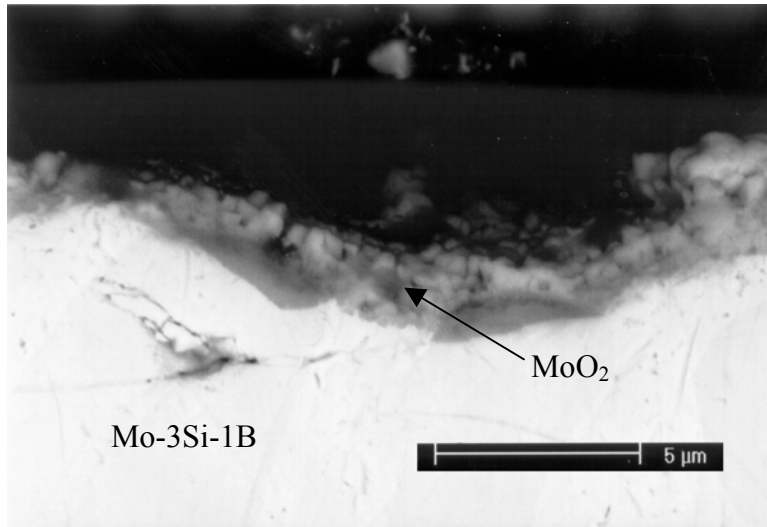
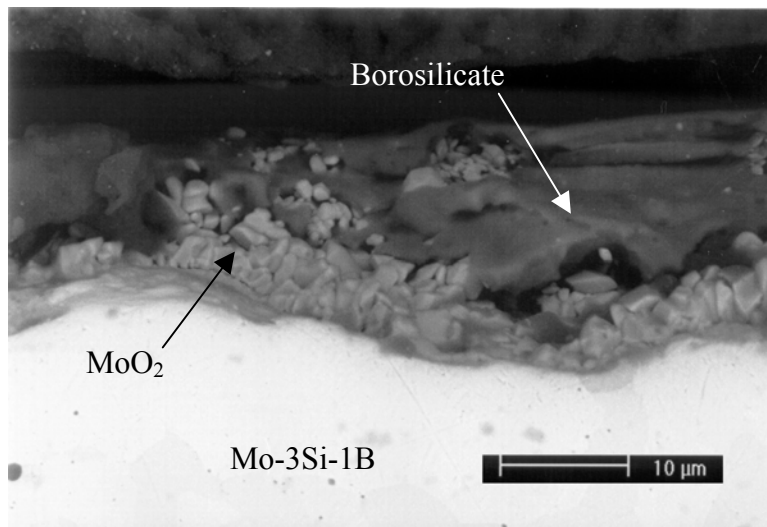


Figure 5.5.25: Change of weight versus time for the oxidation of Mo-3Si-1B exposed at 1000°C in dry air flowing at 1cm/sec.

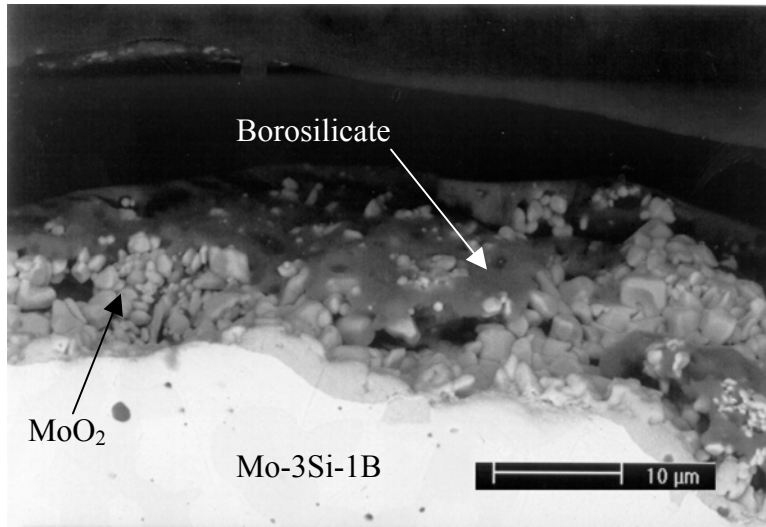


(a)

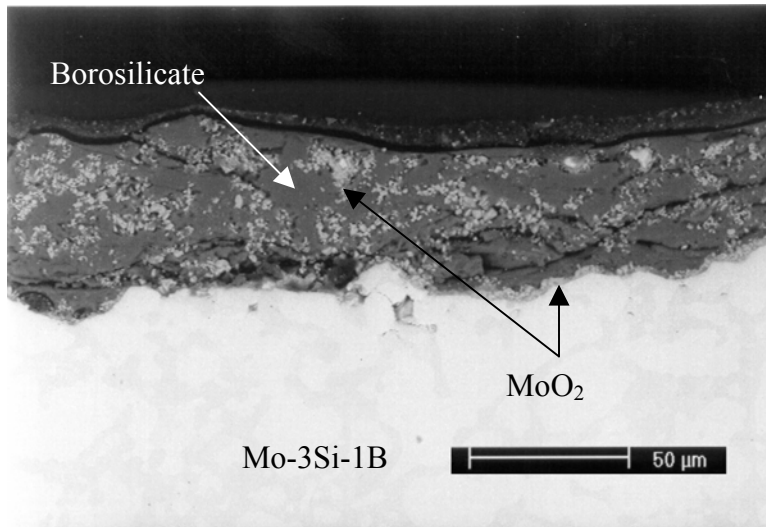


(b)

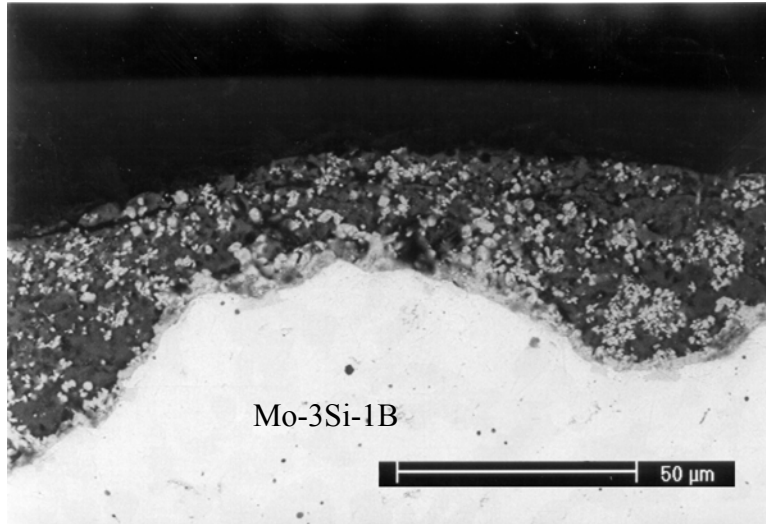
**Figure 5.5.26: Backscattered electron micrograph of the cross-section of Mo-3Si-1B exposed at 1000°C in dry air flowing at 1cm/sec for (a) 2 minutes and (b) 10 minutes.**



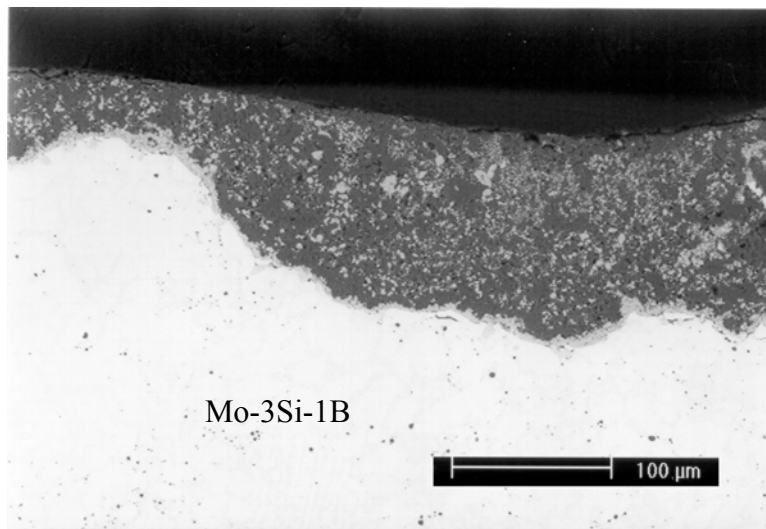
(a)



(b)



(c)



(d)

**Figure 5.5.27: Backscattered electron micrograph of the cross-section of Mo-3Si-1B exposed at 1000°C in dry air flowing at 1cm/sec for (a) 20 minutes, (b) 30 minutes, (c) 1 hour, and (d) 20 hours.**

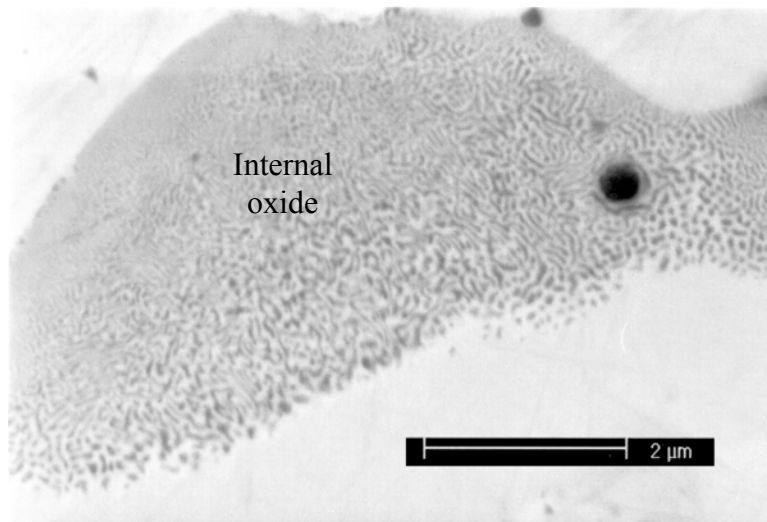
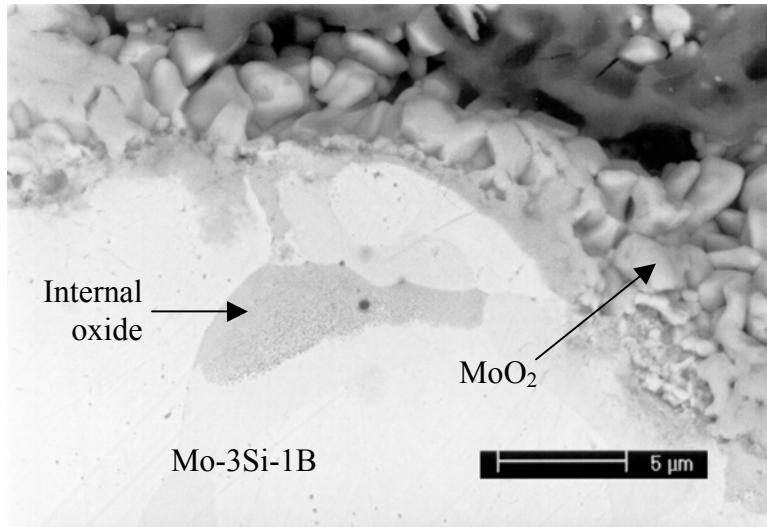


**Figure 5.5.28: Backscattered electron micrographs of internal oxidation in Mo-3Si-1B exposed at 1000°C in dry air flowing at 1cm/sec for 20 minutes.**

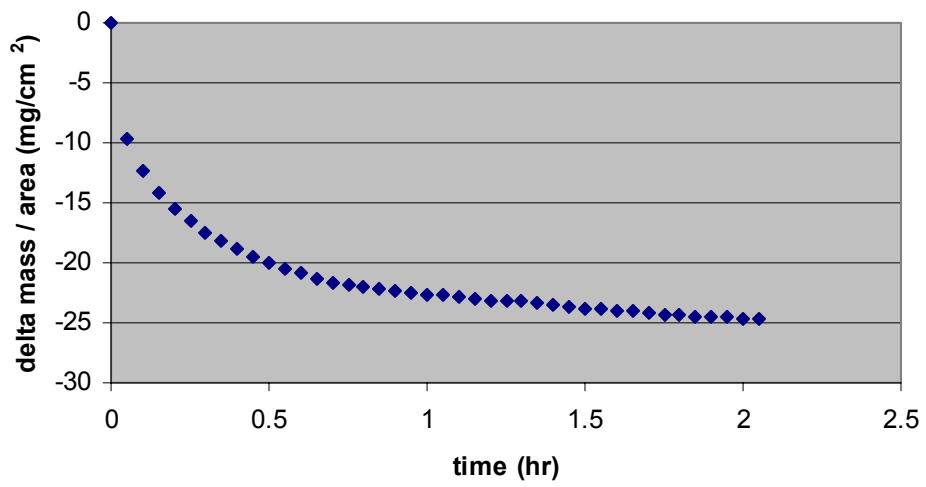
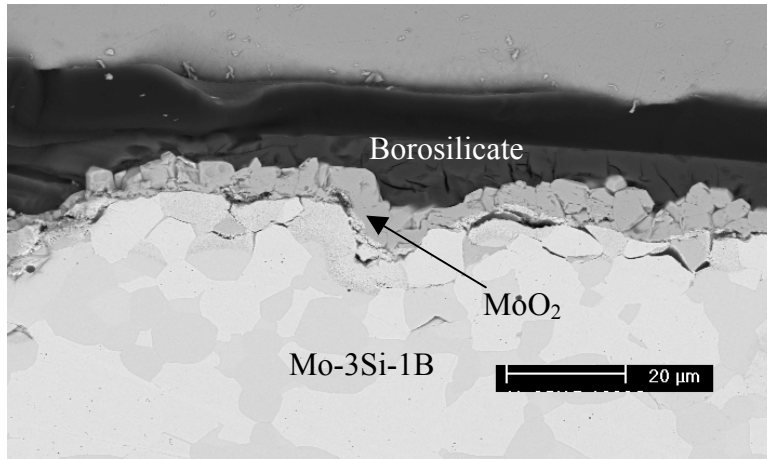


Figure 5.5.29: Weight change versus time for the oxidation of Mo-3Si-1B exposed at 1000°C in dry air flowing at 10cm/sec.



**Figure 5.5.30: Backscattered electron micrographs of Mo-3Si-1B exposed at 1000°C in dry air flowing at 10cm/sec.**

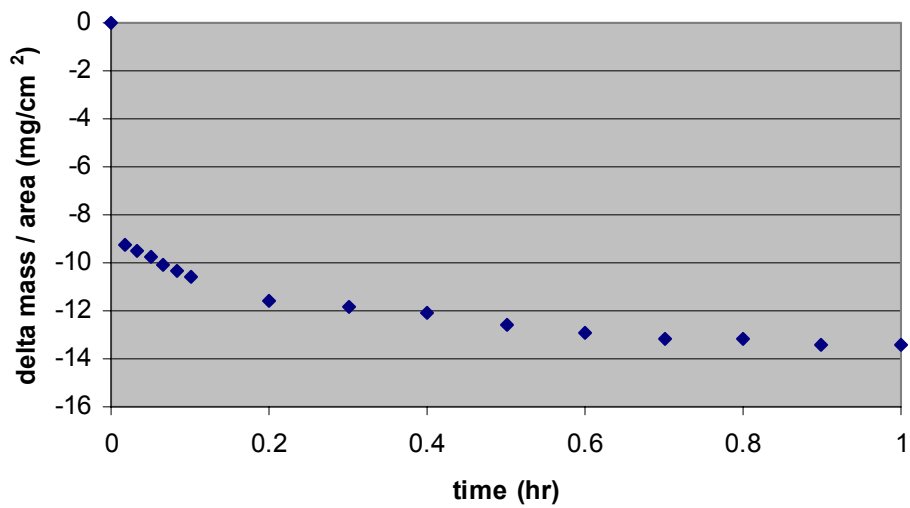
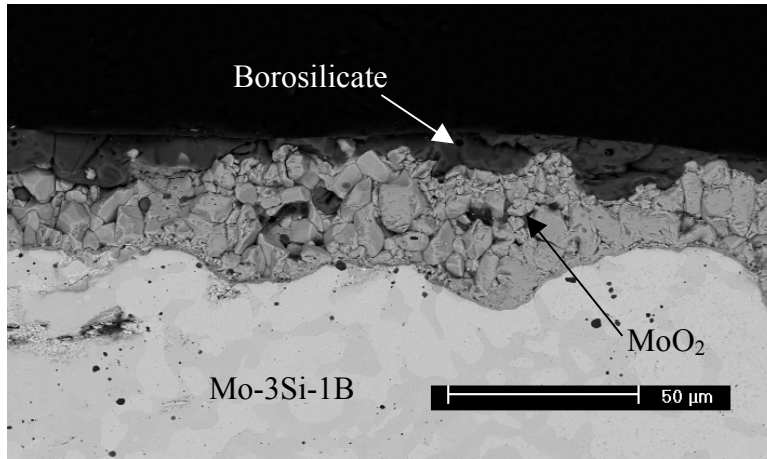


Figure 5.5.31: Weight change versus time for the oxidation of Mo-3Si-1B exposed at 1000°C in oxygen flowing at 10cm/sec.



**Figure 5.5.32: Backscattered micrograph of the cross-section of Mo-3Si-1B exposed at 1000°C in oxygen flowing at 10cm/sec for one hour.**

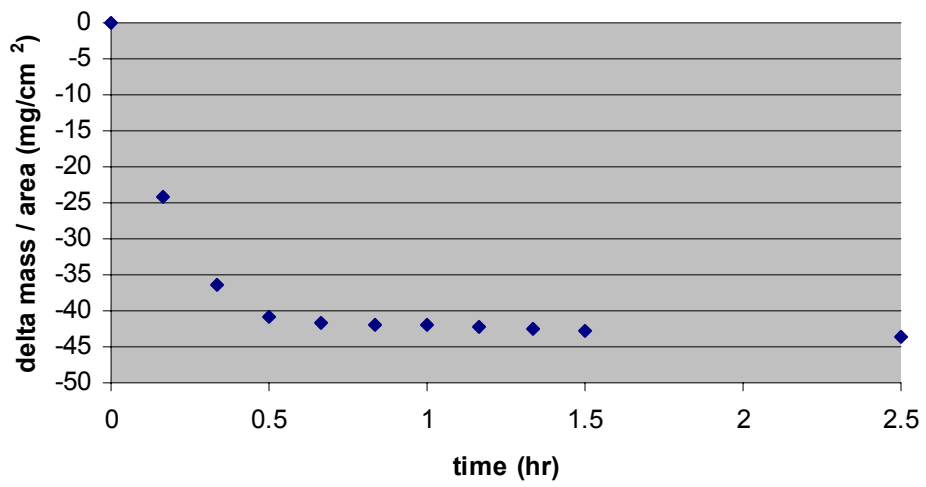
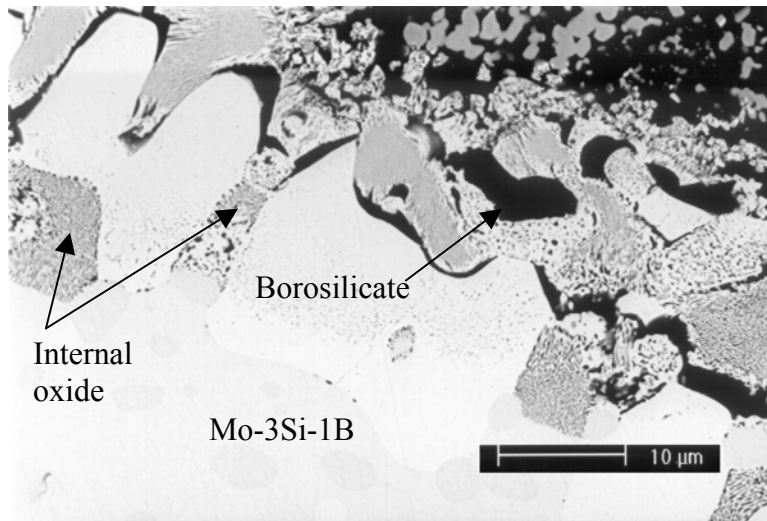
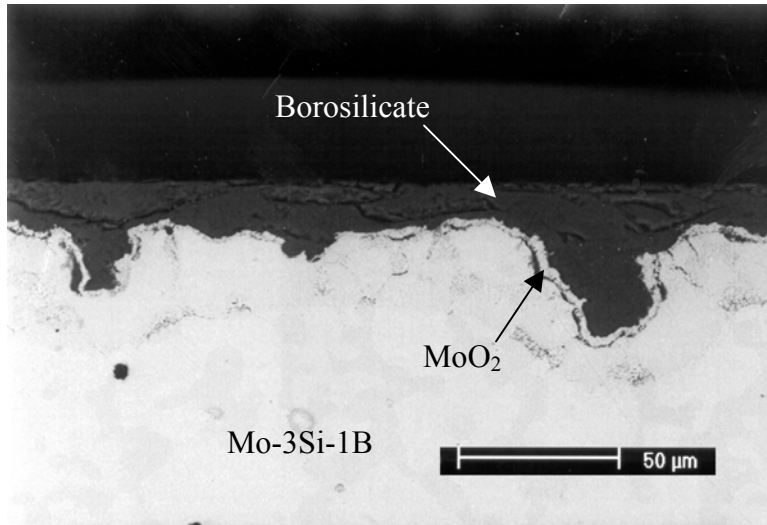


Figure 5.5.33: Weight change versus time for the oxidation of Mo-3Si-1B exposed at 1100°C in static laboratory air.



**Figure 5.5.34:** Backscattered electron micrograph of Mo-3Si-1B exposed at 1100°C in static laboratory air for 100 hours.

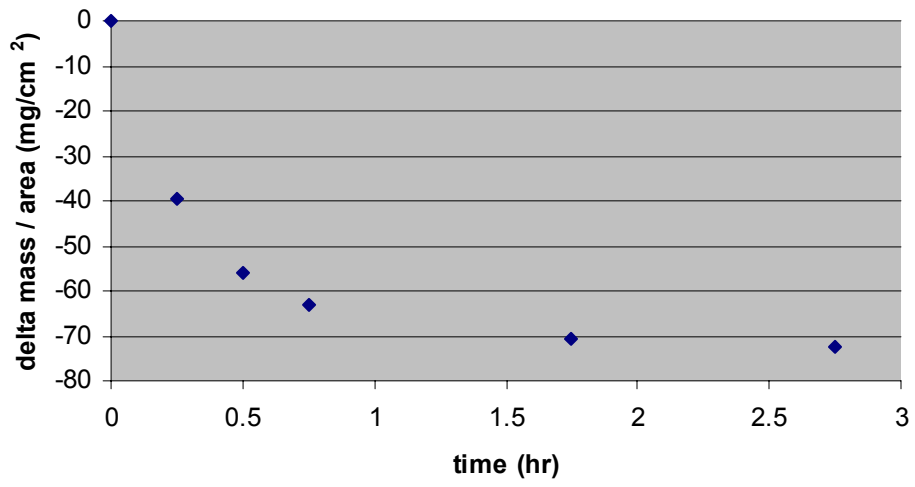
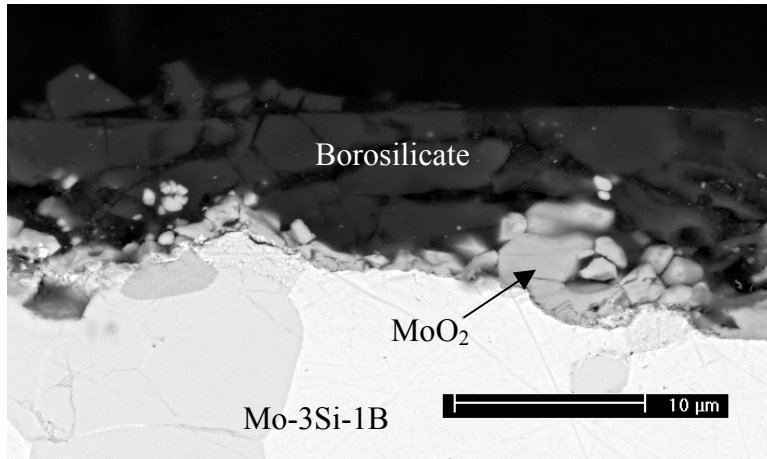


Figure 5.5.35: Weight change versus time for the oxidation of Mo-3Si-1B exposed at 1100°C in static dry air.



**Figure 5.5.36:** Backscattered electron micrographs of Mo-3Si-1B exposed at 1100°C in static dry air for 3 hours.

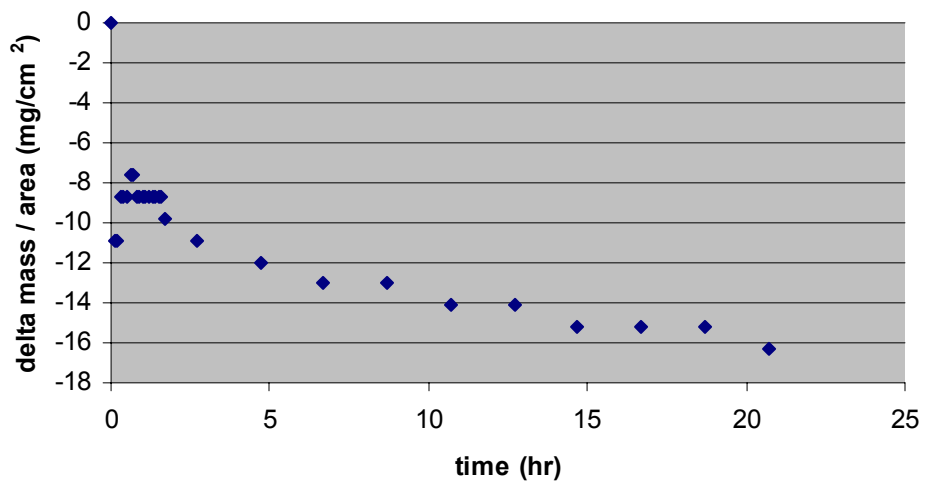


Figure 5.5.37: Weight change versus time for the oxidation of Mo-3Si-1B exposed at 1100°C in dry air flowing at 1cm/sec.

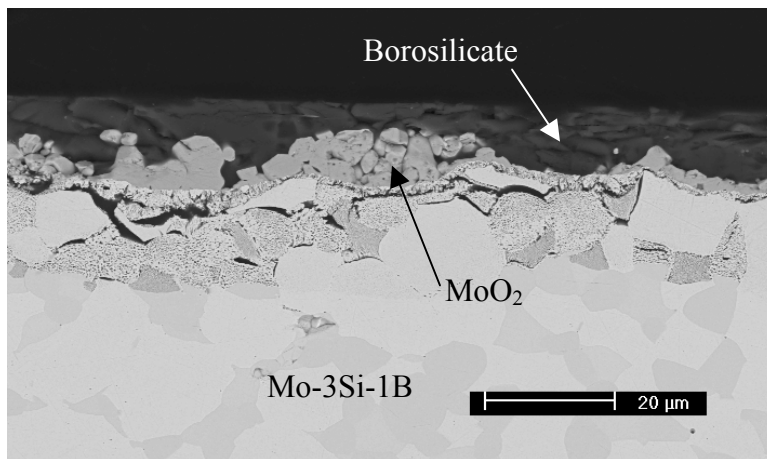
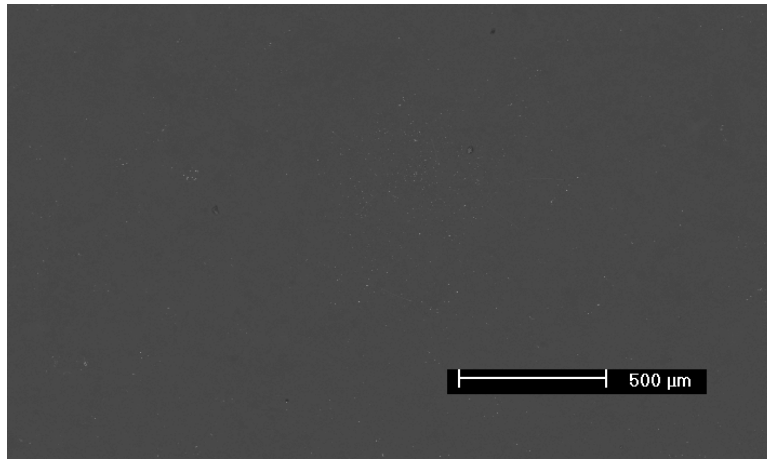


Figure 5.5.38: Backscattered electron micrograph of Mo-3Si-1B exposed at 1100°C in dry air flowing at 1cm/sec for 20 hours.

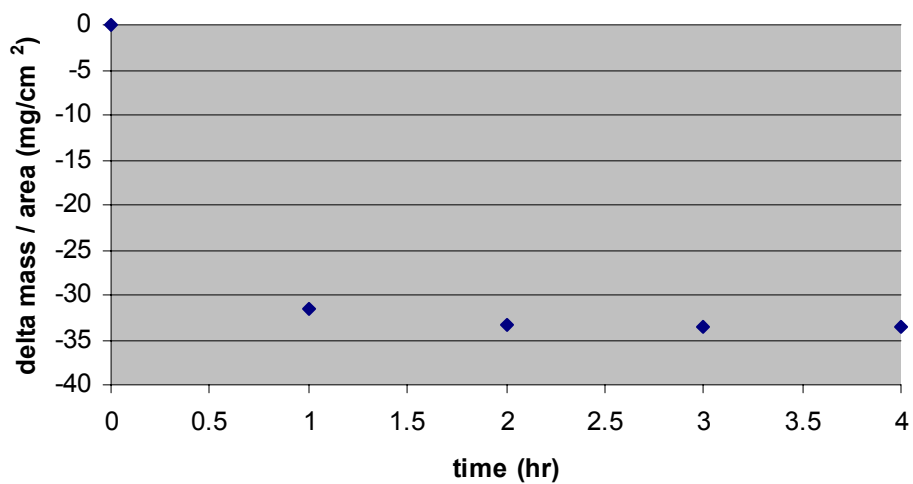
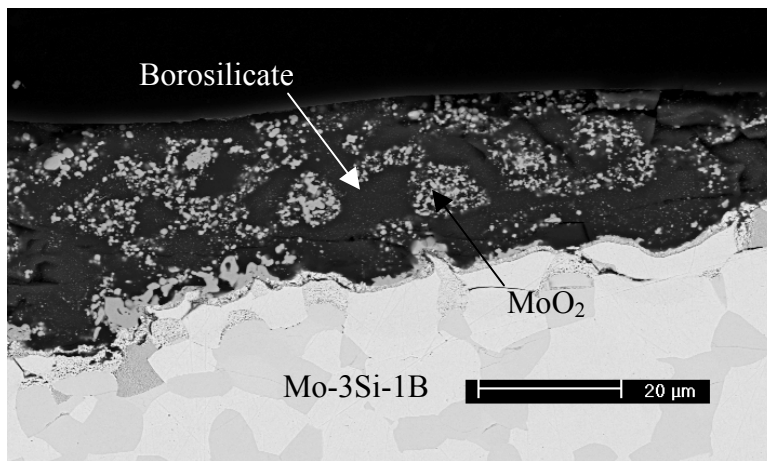
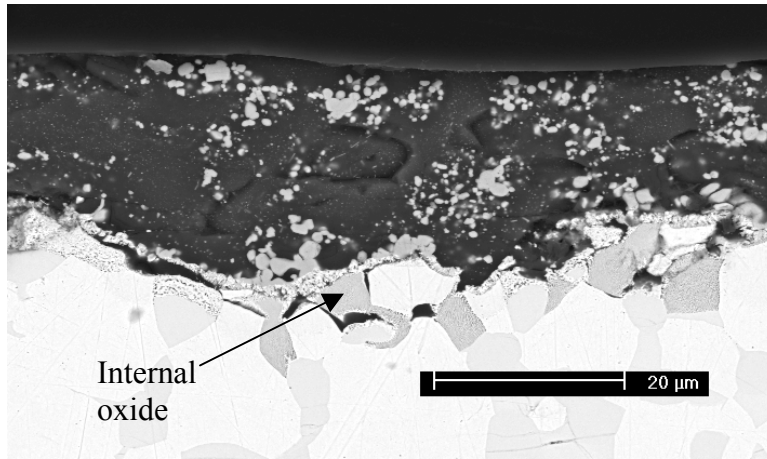


Figure 5.5.39: Weight change versus time for the oxidation of Mo-3Si-1B exposed at 1100°C in air + 0.1atm H<sub>2</sub>O flowing at 1cm/sec.



**Figure 5.5.40: Backscattered electron micrographs of Mo-3Si-1B exposed at 1100°C in air + 0.1atm H<sub>2</sub>O flowing at 1cm/sec for 4 hours.**

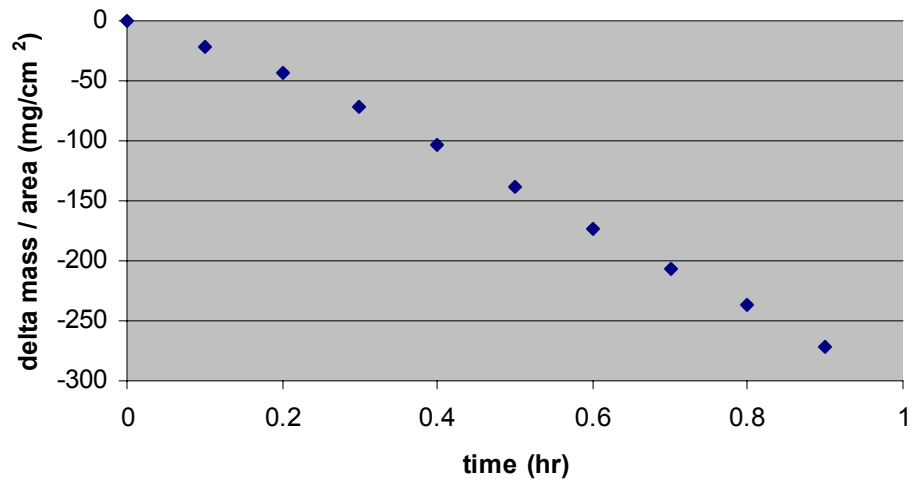
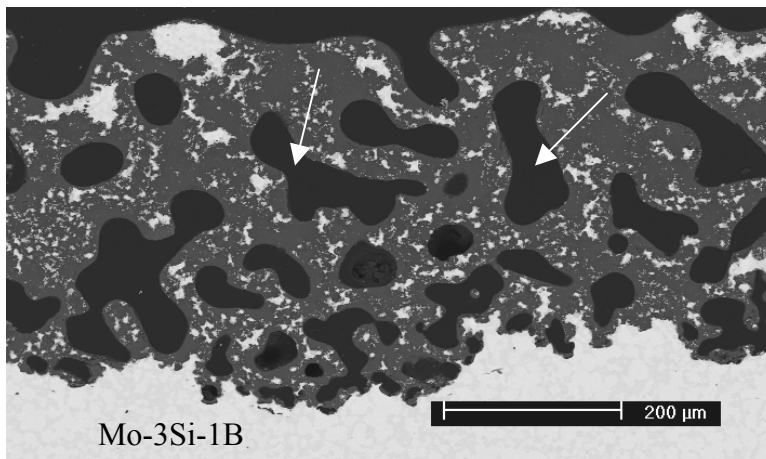
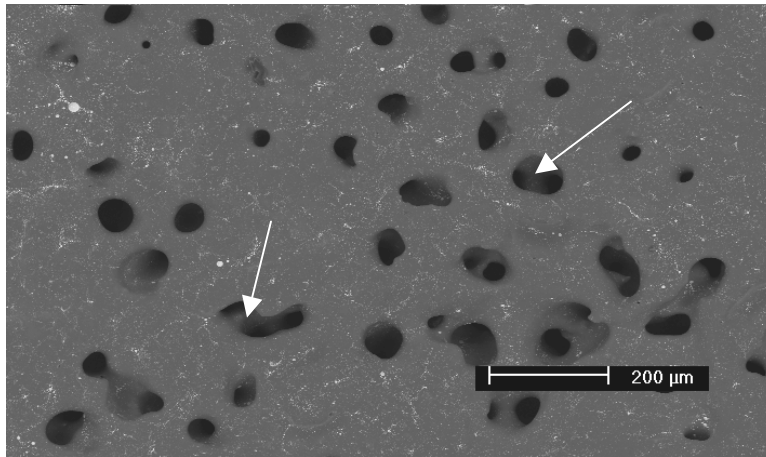
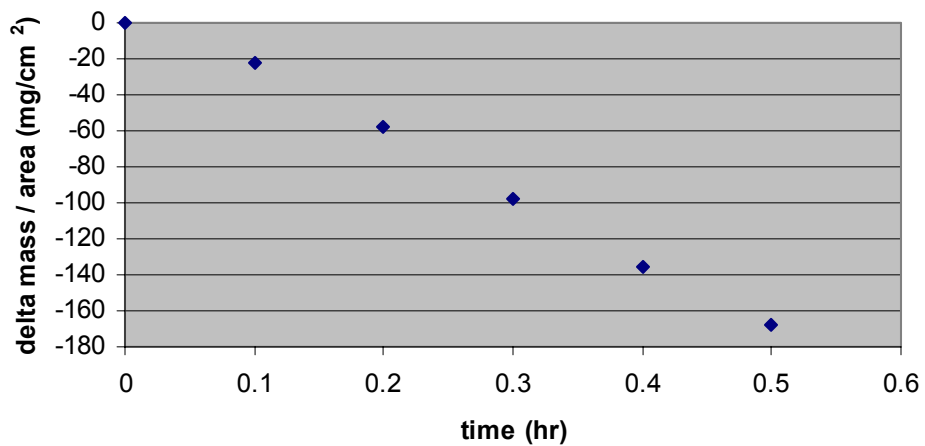


Figure 5.5.41: Weight change versus time for the oxidation of Mo-3Si-1B exposed at 1100°C in dry air flowing at 10cm/sec.



**Figure 5.5.42: Backscattered electron micrographs of Mo-3Si-1B exposed at 1100°C in dry air flowing at 10cm/sec for one hour.**



**Figure 5.5.43: Weight change versus time data for the oxidation of Mo-3Si-1B exposed at 1100°C in oxygen flowing at 10cm/sec.**

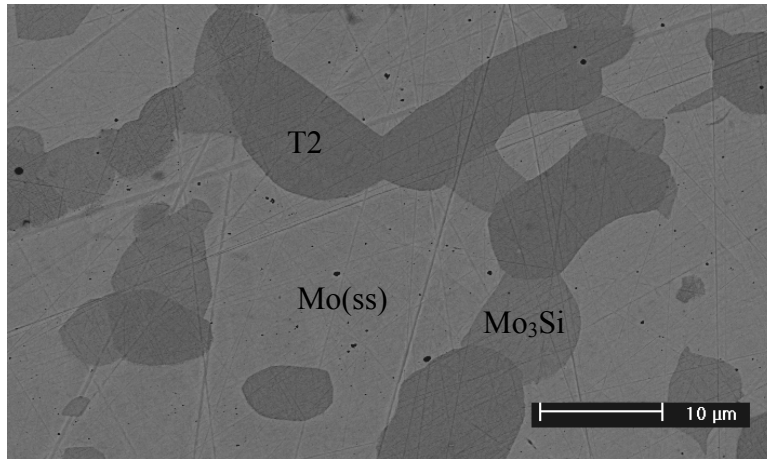


**Figure 5.6.1: Backscattered electron micrograph of as-processed Mo-3Si-1B.**

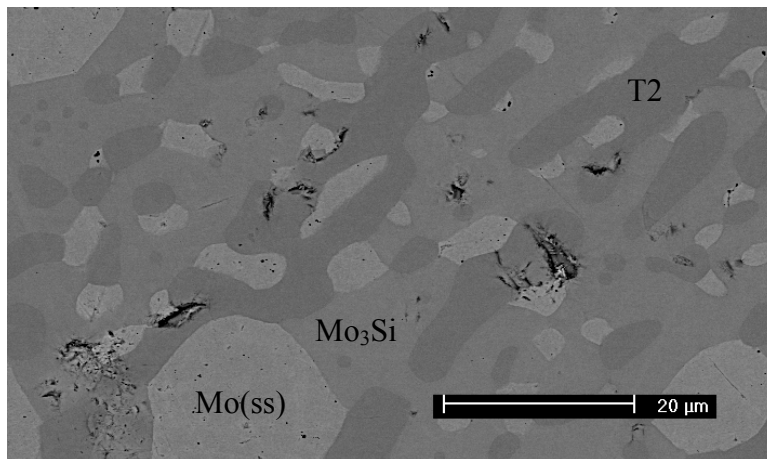


**Figure 5.6.2: Backscattered electron micrograph of as-processed Mo-5Si-1B.**

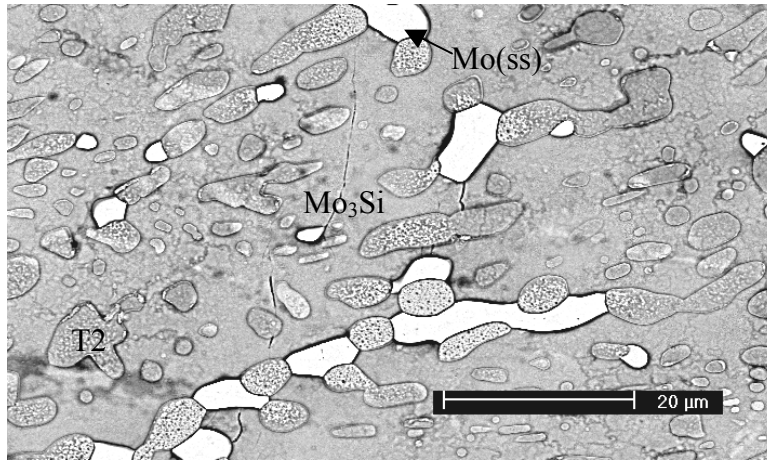


Figure 5.6.3: Backscattered electron micrograph of as-processed Mo-7Si-1B.

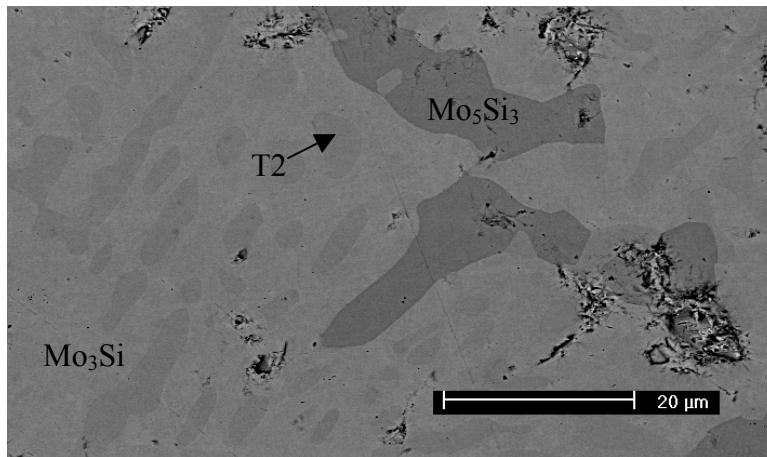


Figure 5.6.4: Backscattered electron micrograph of as-processed Mo-8.2Si-1B.

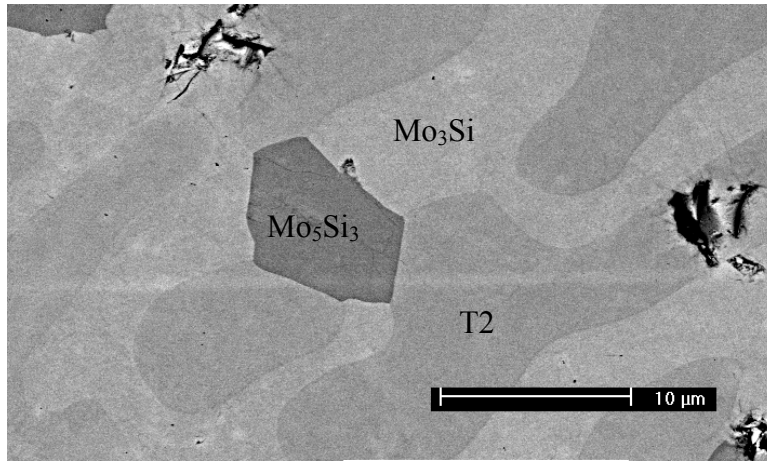


Figure 5.6.5: Backscattered electron micrograph of as-processed Mo-7.4Si-2B.

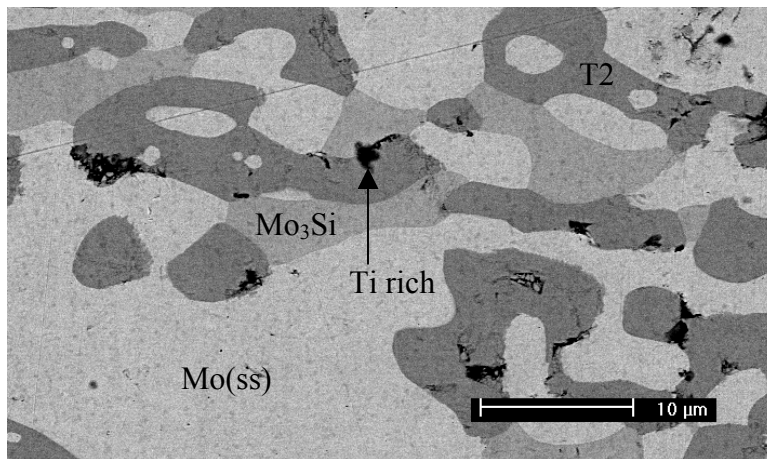
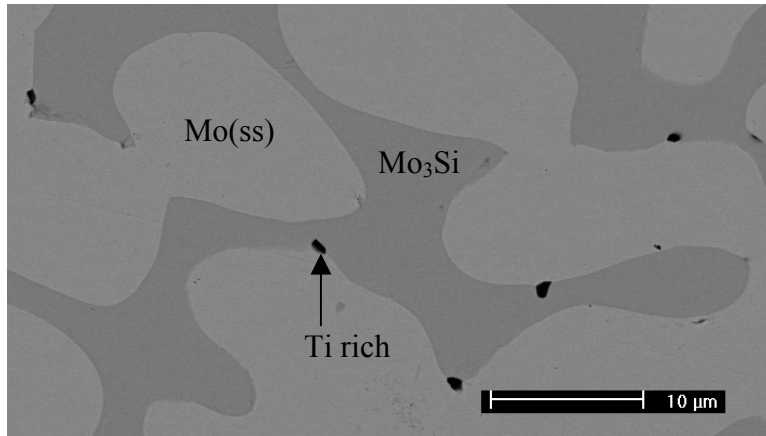
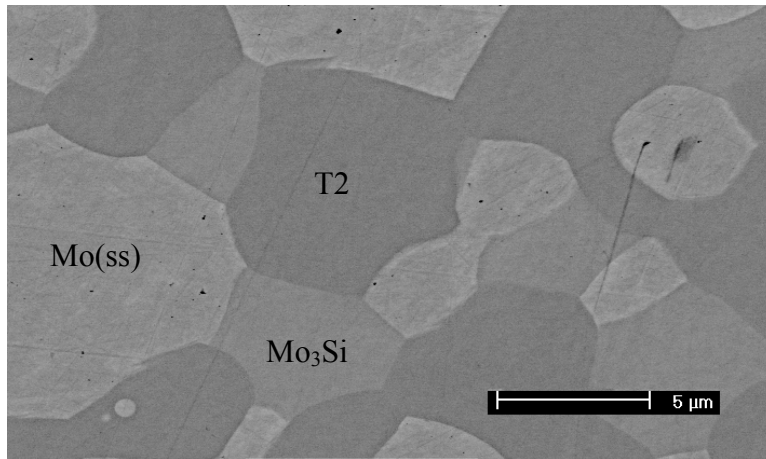


Figure 5.6.6: Backscattered electron micrograph of as-processed Mo-3Si-1B-6Ti.



**Figure 5.6.7: Backscattered electron micrograph of as-processed Mo-3Si-6Ti.**



**Figure 5.6.8: Backscattered electron micrograph of as-processed Mo-3Si-1B-0.3Hf.**

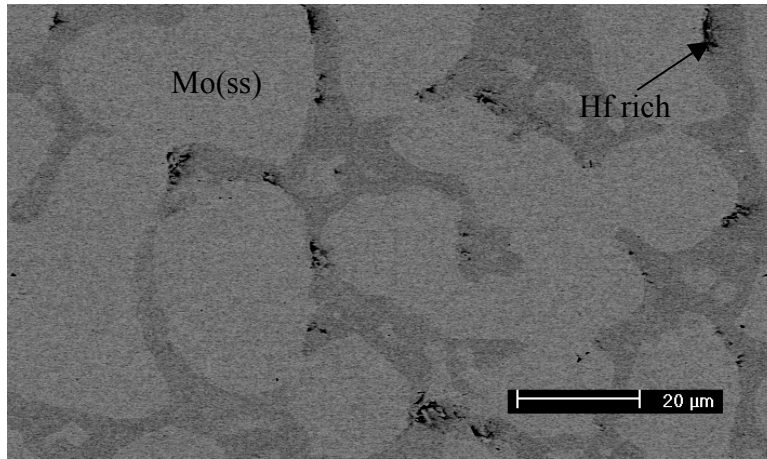


**Figure 5.6.9: Backscattered electron micrograph of as-processed Mo-3Si-1B-1Hf.**

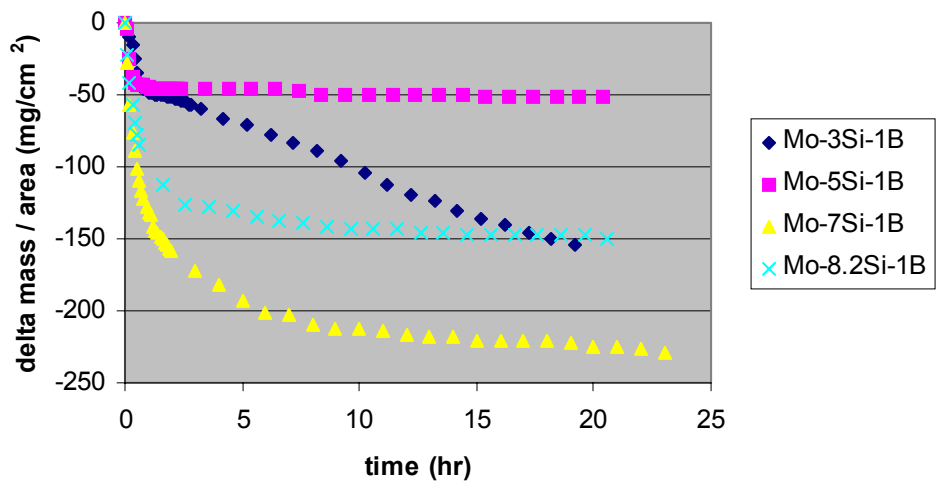


Figure 5.6.10: Weight change versus time data for the oxidation of alloys exposed at 816°C in dry air flowing at 1cm/sec.

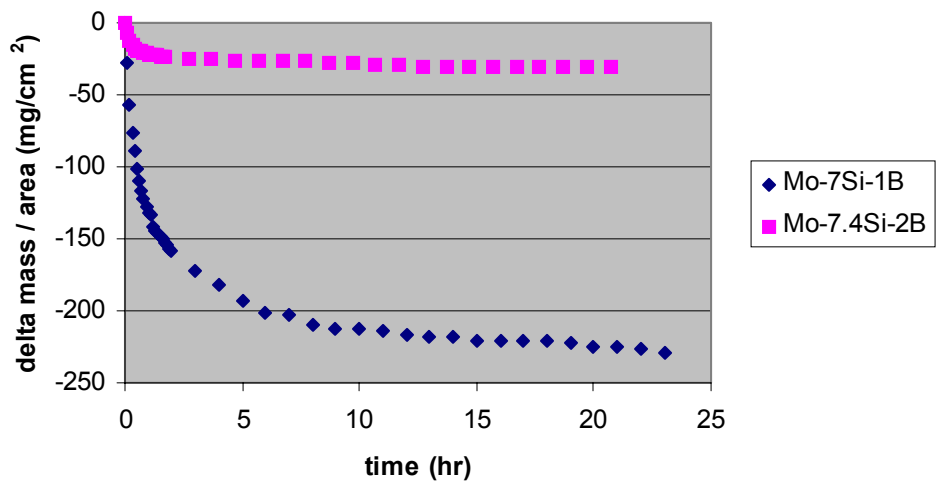


Figure 5.6.11: Weight change versus time data for the oxidation of alloys exposed at 816°C in dry air flowing at 1cm/sec.

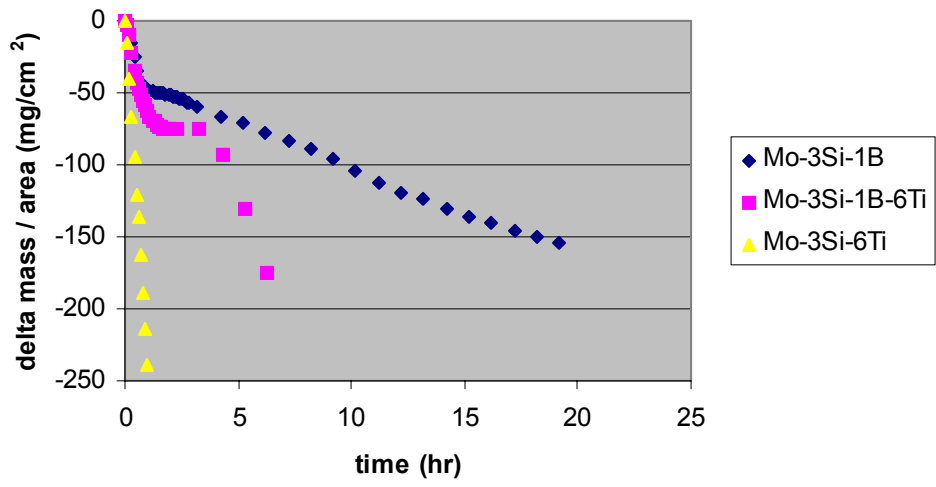


Figure 5.6.12: Weight change versus time data for the oxidation of alloys exposed at 816°C in dry air flowing at 1cm/sec.

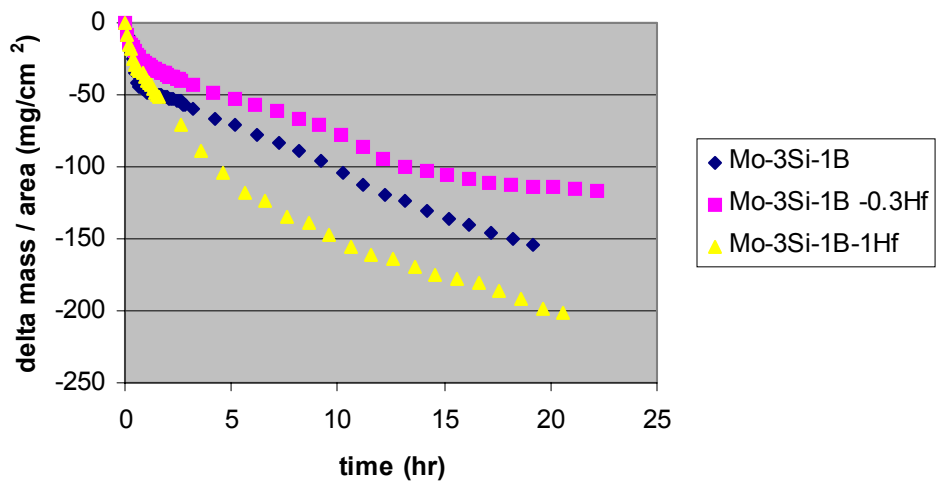


Figure 5.6.13: Weight change versus time data for the oxidation of alloys exposed at 816°C in dry air flowing at 1cm/sec.

## BIBLIOGRAPHY

1. N. Birks, G. H. Meier, Introduction to high temperature oxidation of metals, Edward Arnold Ltd., 1983.
2. J. A. Shields Jr., *Advanced Mat. & Proc.*, 10/92, 1992, p.28.
3. J. W. Semmel Jr., "Refractory metals and alloys", Interscience New York-London, 1960, p.146.
4. M. W. Chase Jr., C. A. Davies, J. R. Downey Jr., D. J. Frurip, R. A. McDonald and A. N. Syverud, JANF Thermochemical Tables Third Edition, Journal of Physical and Chemical Reference Data, Vol. 14, 1985.
5. Y. A. Gerasimov, A. N. Krestovnikov and A. S. Shakhov, Chemical Thermodynamics in Nonferrous Metallurgy, Vol. III, Gosudarstvennoe Nauchno-Tekhnicheskoe Izdatel'stvo Literaturny po Chernoi i Tsvetnoi Metallurgii Moskva, 1963.
6. J. F. Elliott and M. Gleiser, Thermochemistry for Steelmaking, Vol. 1, The American Iron and Steel Institute, Addison-Wesley Publishing Company, Inc., 1960.
7. P. J. Meschter, *Metall. Trans. A*, 23A, 6, June 1992, p.1763.
8. G. R. Belton and A. S. Jordan, *J. Phys. Chem.*, 69, 6, June 1965, p.2065.
9. E. A. Gulbransen, K. F. Andrew and F. A. Brassart, *J. Electrochem. Soc.*, 110, 1963, p.952.
10. E. A. Gulbransen and W. S. Wysong, *AIME*, 175, 1948, p.628.
11. E. S. Bartlett and D. N. Williams, *Trans. AIME*, 212, 1958, p.280.
12. E. S. Jones, J. F. Mosher, R. Speiser and J. W. Spretnak, *Corrosion*, 14, 1958, p.2t.
13. B. Lustman, *Met. Prog.*, 57, 1950, p.629.
14. E. A. Gulbransen, K. F. Andrew and F. A. Brassart, *J. Electrochem. Soc.*, 110, 1963, p.242.
15. E. F. Fialko, A. V. Kikhtenko, V. B. Goncharov and K. I. Zamaraev, *J. Phys. Chem. A*, 101, 1997, p.8607.

16. J. Berkowitz and M. G. Inghram, *J. Chem. Phys.*, 26, 1957, p.842.
17. C. Wagner, *Corrosion Sci.*, 5, 1965, p.751.
18. E. A. Gulbransen, K. F. Andrew and F. A. Brassart, *J. Electrochem. Soc.*, 113, 1966, p.834.
19. A. Hashimoto, *Geochimica et Cosmochimica Acta*, 56, 1992, p.511.
20. E. J. Opila, J. L. Smialek, R. C. Robinson, D. S. Fox and N. S. Jacobson, *J. Am. Ceram. Soc.*, 82, 7, 1999, p. 1826.
21. J. L. Smialek, R. C. Robinson, E. J. Opila, D. S. Fox and N. S. Jacobson, *Adv. Composite Mater.*, 8, 1, 1999, p.33.
22. L. Shaw and R. Abbaschian, *J. Mat. Sci.*, 30, 1995, p.5272.
23. D. A. Berztiss, R. R. Cerchiara, E. A. Gulbransen, F. S. Pettit and G. H. Meier, *Mat. Sci. Engr.*, A155, 1992, p.165.
24. H. J. Grabke and G. H. Meier, *Oxid. Met.*, 44, 1995, p.147.
25. J. B. Berkowitz-Mattuck, P. E. Blackburn and E. J. Felten, *Trans. AIME*, 233, 1965, p.1093.
26. M. K. Meyer and M. Akinc, *J. Am. Ceram. Soc.*, 79, 1996, p.938.
27. M. K. Meyer, A. J. Thom and M. Akinc, *Intermetallics*, 7, 1999, p.153.
28. E. Summers, A. J. Thom, B. Cook and M. Akinc, *Intermetallics*, 8, 2000, p.1169.
29. M. F. Yan, J. B. Macchesney, S. R. Nagel and W. W. Rhodes, *J. Mat. Sci.*, 15, 1980, p.1371.
30. G. W. Scherer, *J. Am. Cer. Soc.*, 60, 1977, p.236.
31. G. W. Scherer and D. L. Bachman, *J. Am. Cer. Soc.*, 60, 1977, p.239.
32. J. K. Mackenzie and R. Shuttleworth, *Proc. Phys. Soc. London*, 62B, 1949, p.832.
33. R. H. Doremus, "Glass Science", Wiley New York, 1973, p.105.
34. T. A. Parthasarathy, M. G. Mendiratta and D. M Dimiduk, *Acta Mat.*, 50, 2002, p. 1857.
35. Private Communication, Rafael Raban, Pratt & Whitney, East Hartford, CT, 2001.
36. J. S. Park, R. Sakidja and J. H. Perepezko, *Scripta Mat.*, 46, 2002, p. 765.

37. D. M. Berczik, U. S. Patent number: 5,595,616, Jan. 21, 1997.
38. J. H. Perepezko, "Phase stability and microstructure control in high temperature (Mo, Nb)-Si-B alloys", AFOSR contract number: F49620-00-1-0077, 1999.
39. X. Fan, K. Hack and T. Ishigaki, *Mat. Sci. Engr.*, A278, 2000, p.26.
40. J. H. Perepezko, R. Sakidja, S. Kim, Z. Dong and J. S. Park, *Structural Intermetallics 2001*, The Minerals, Metals & Materials Society, 2001, p. 505.
41. R. Sakidja, H. Sieber and J. H. Perepezko, *Molybdenum and Molybdenum Alloys*, The Minerals, Metals & Materials Society, 1998, p. 99.
42. J. H. Schneibel, M. J. Kramer and D. S. Easton, *Scripta Mat.*, 46, 2002, p. 217.
43. J. H. Schneibel, C. T. Liu, D. S. Easton and C. A. Carmichael, *Mater. Sci. Eng.*, A261, 1999, p. 78.
44. M. Akinc, M. K. Meyer, M. J. Kramer, A. J. Thom, J. J. Huebsch and B. Cook, *Mater. Sci. Eng.*, A261, 1999, p. 16.
45. K. J. Leonard and V. K. Vasudevan, "Microstructure effects on the creep behavior of the next generation of refractory alloys for very high temperature applications", AFOSR grant number: F49620-00-1-0080, 1999.
46. D. M. Dimiduk, "High temperature materials & nanophase aluminum alloy technology 2306AW1,2606AW4", Air Force Research Laboratory, Materials & Manufacturing Directorate, 1999.
47. S. Woodard, Results of Microprobe Analysis of Mo-3Si-1B, Pratt and Whitney, June 2001.
48. G. T. Bayer, MS Thesis, University of Pittsburgh, 1992.
49. W. J. Quadraekers, A. Elschner, H. Holsbrecher, K. Schmidt, W. Speier and H. Nickel, *Mekrochemia Acta*, 107, 1992, p. 197.
50. H. M. Hindam and W. W. Smeltzer, *J. Electrochem. Soc.*, 127, 1980, p.1622.
51. N. P. Bansal and R. H. Doremus, *Handbook of Glass Properties*, Academic Press, Inc., 1986, p. 243.
52. T. J. Rockett and W. R. Foster, *J. Am. Ceram. Soc.*, 48, 2, 1965, p.78.
53. T. B. Massalski Editor-in-Chief, *Binary Phase Diagrams*, Vol. 2, ASM, 1986, p.1613.